Thermodynamic Characteristics of Lithium Chloride in Rotary Heat and Mass Exchangers

by

Justus Johannes Rau

A thesis submitted in partial fulfillment

of the requirements for the degree

Master of Science

in

Chemical Engineering

at the

University of Wisconsin - Madison

1989

Abstract

Thermodynamic Characteristics of Lithium Chloride in Rotary Heat and Mass Exchangers

The interaction of moist air with the sorbent determines the performance of rotary dehumidifiers and the entire desiccant cooling system. The behavior of the air-water vapor-desiccant system is therefore of central interest for modeling rotary heat and mass exchangers. Lithium Chloride is commonly used as desiccant in commercial systems, especially because of the low humidities that can be obtained. This thesis provides relationships to describe the sorption equilibria of the air-water vapor-LiCl system.

Rotary heat and mass exchangers are described by two conservation laws and two transfer equations. They form a system of two coupled non-linear hyperbolic partial differential equations and two ordinary differential equations. Since the isotherms and isopiestics of LiCl exhibit discontinuities, conventional numerical methods that solve this system cannot be used. A modified method based on the finite difference model by Maclaine-cross [1] is presented. This method predicts the outlet conditions of the air streams and determines temperature and moisture content profiles of the matrix. The physical behavior of rotary dehumidifiers using LiCl is described.

By replacing enthalpy and moisture content by characteristic potentials F_i, the governing equations may be transformed to two uncoupled sets of equations that are

analogous to the common model of a heat regenerator. A psychrometric chart with lines of constant F_i-potential that also includes the phase regions of anhydrous LiCl and monohydrate is presented. It is shown that the lines where the phase changes of LiCl occur are also lines of constant F_2. The intersection points of the lines of constant F_i through the inlet states of the process and regenerating air stream may be used to predict the outlet states of the rotary heat and mass exchanger. However, these intersection points cannot be identified, if the inlet states are in regions that correspond to different phases of LiCl.

Acknowledgements

Even if you think two months before the deadline you're pretty good in time, it is always going to be a hassle with several "all-nighters" in the last week.

When I went into one of my last advisor meetings before I handed in my thesis, the results of my simulations seemed to make no sense and I was totally frustrated. However, my advisors convinced me once more that they did make sense. Actually, they had such great enthusiasm that I left this advisor meeting with a 180 ° turn of my state of mind and went back to work freshly motivated. Thank you, Sandy Klein and John Mitchell, for this endless confidence into my research.

I enjoyed working in the Solar Lab very much. It is certainly one of the best organized research groups on campus thanks to Jack Duffie, the founder of the Lab and also my advisor in the first semester, and Bill Beckman, the director of the Solar Lab. I admit that I needed the "pressure" of the weekly advisor meetings and without them I would not have reached the point where I am right now. Also the obligatory seminars I had to give certainly developed my rhetorical as well as my baking skills. I really enjoyed my time in the Solar Lab also thanks to all the grad students in the Lab.

My stay in Madison was made possible by the scholarship of the German Academic Exchange Service (DAAD) and by Professor Zeitz who, with much personal effort, organizes this exchange program every year. I dreamed about studying abroad already for a long time before I received this scholarship and I am very grateful to Professor Zeitz for giving me the opportunity to come here. Living and studying in Madison was a great and

unforgettable experience for me.

The funding for this project in the last semester was provided by the US department of energy.

In memory of great lunch parties, I want to mention Achim Gerstlauer and Richard Biener. Without the moral and physical support of the inevitable "Geräte", we probably would not have survived the first semester.

Last not least, I want to thank my parents for their financial and moral support. I am glad that they were able to visit me here in Madison. I missed you and Cornelia and Hella very much.

Table of Contents

List of Figures

Nomenclature

Text symbol	Dimension	Meaning

1. Dependent Variables

I	[J/kg DS]	enthalpy of matrix
i	[J/kg DA]	enthalpy of fluid
t_f, t_m	[°C]	temperature of fluid and matrix
W	[kg W/kg DS]	water content of matrix
w	[kg W/kg DA]	absolut humidity of fluid
w_m	[kg W/kg DA]	abs. humidity of fluid in equilibrium with matrix
F_{if}, F_{im}		characteristic F-potential for fluid and matrix

2. Coordinates

z	[m]	coordinate in axial direction
Θ	[s]	time or circumferential coordinate
x		dimensionless: $x = z/L$
τ		dimensionless: $\tau = \Theta/\Theta_j$
ξ		$\xi = NTU_{w,j}\ x$
ζ		$\zeta = NTU_{w,j}\ \tau\ \ 1/\Gamma_j$

Text symbol	Dimension	Meaning

3. Alphabetic order

Latin letters

A	[m^2/kgDS]	exchange area per dry salt mass
a		dimensionless function of temperature defined by (3.26 a)
b		dimensionless function of temperature defined by (3.26 b)
b		right hand side vector in matrix equation (4.5)
c	[kg DS/kg W]	concentration c = 1/W
c_{da}	[J/kg DA K]	specific heat of dry air
c_f	[J/kg DA K]	specific heat of wet fluid
c_{lim}		concentration at solubility limit
c_m	[J/kg DS K]	specific heat of the wet matrix
c_{dil}	[J/kg DS K]	specific heat of the dilute solution
c_{sup}	[J/kg Sup K]	specific heat of the supporter
F_i		characteristic F-potentials
G_0		dimensionless function of c defined by (3.10)
G_1		dimensionless function of c defined by (3.11)
h	[J/kg]	enthalpy

Text symbol	Dimension	Meaning
h_{lat}	[J/kg W]	latent heat of condensation
h_s	[J/kg W]	heat of sorption
$h_{s,dil}$	[J/kg W]	heat of sorption of the dilute solution
$h_{s,sat}$	[J/kg W]	heat of sorption of the saturated solution
$h_{t,j}$	[J/m^2 s K]	overall heat transfer coefficient
$h_{w,j}$	[kg W/m^{2}s]	overall mass transfer coefficient
h_{wv}	[J/kg W]	enthalpy of water vapor
I	[J/kg DS]	enthalpy of matrix
i	[J/kg DA]	enthalpy of fluid
$i_{j\ in}$	[J/kg DA]	inlet fluid enthalpy of period j
k		parameter for continuous approximation of isotherms
L	[m]	depth of wheel
Le_j		Lewis number of period j, $Le_j = h_{t,j} / c_f h_{w,j}$
m(t)		slope for linear approximated isotherms
M		matrix in (4.5)
$M_{m\,j}$	[kg DS]	dry sorbent mass of period j
$M_{f\,j}$	[kg DA]	dry air mass contained in matrix in period j
$\dot{m}_j$	[kg DA/s]	dry air mass flow rate of period j
$NTU_{w,j}$		number of transfer units for mass transfer

Text symbol	Dimension	Meaning
p	[mbar]	vapor pressure
p_0	[mbar]	vapor pressure of dilute solution at 50 °C
		reference temperature
p_{tot}	[mbar]	total system pressure p_{tot} = 1013.25 mbar
R	[J/kg W K]	ideal gas constant for water vapor
		R = 461.51532 J/kg K
r	[m]	radius of wheel
T	[K]	absolute temperature
T_0	[K]	reference temperature T_0 = 323.15 K
t_f	[°C]	temperature of fluid
t_m	[°C]	temperature of matrix
v_j	[m/s]	air velocity
W	[kg W/kg DS]	water content of matrix
W_{mono}	[kg W/kg DS]	water content of pure monohydrate
W_{lim}	[kg W/kg DS]	water content at solubility limit
w	[kg W/kg DA]	absolut humidity of fluid
$w_{j\ in}$	[kg W/kg DA]	inlet fluid humidity of period j
w_m	[kg W/kg DA]	humidity in equilibrium with matrix
x		dimensionless axial coordinate x = z/L
x_{new}		vector of grid element outlet conditions
x_{old}		vector of grid element inlet conditions

Text symbol	Dimension	Meaning
X_{sup}	[kg sup/kg DS]	mass ratio of supporter and dry LiCl
z	[m]	axial coordinate

Greek letters

Δ		difference
Γ_j		ratio of dry matrix mass flow rate to fluid flow rate
μ_j		ratio of dry matrix and fluid mass $\mu_j = M_{fj}/M_{mj}$
τ		dimensionless time $\tau = \Theta/\Theta_j$
Θ	[s]	circumferential or time coordinate
Θ_j	[s]	duration of period j
ξ		transformed dimensionless axial variable
ζ		transformed dimensionless time variable

Text symbol	Meaning

Subscripts

am	system of anhydrous LiCl and monohydrate
as	saturated solution with anhydrous LiCl
f	fluid
i	axial index of finite difference grid
j	period
k	time index in finite difference grid
m	matrix
ms	saturated solution with monohydrate

4. Abbreviations

DA	dry air
DS	dry sorbent
RHMX	rotary heat and mass exchanger
RHX	rotary heat exchanger
W	water

Chapter 1

Introduction

1.1 Introduction to Sorption Processes on Lithium Chloride

Sorption of vapors on solid or liquid sorbents is an important separation process in chemical engineering. The physical process can either be adsorption or absorption. In the case of adsorption, the adsorbed gas is attracted to the surface of the sorbent by either Van der Waals forces (physical adsorption) or by chemical bonds (chemisorption). In the case of absorption the absorbed gas will diffuse into the sorbent and will physically or chemically change the sorbent itself. Again Van der Waals forces or chemical bonds can be responsible for the process.

This thesis investigates the thermodynamic characteristics of lithium chloride as sorptive agent for water vapor. In a system of LiCl and water, both are involved: Van der Waals forces (solution) and chemical bonds (hydrates). LiCl can collect water vapor as solid (anhydrous salt or monohydrate crystals) or liquid after the sorbed water has dissolved the solid into an aqueous solution. It is called a deliquescent desiccant. The water will always diffuse into the LiCl crystal or the LiCl solution and will change it physically (phase change) and chemically (different hydrates) during the process. Therefore, according to ASHRAE [2], "absorption" is the correct term in this case. Since many

parts of this thesis also apply to adsorption on microporous desiccants the more general term "sorption" is used throughout this thesis.

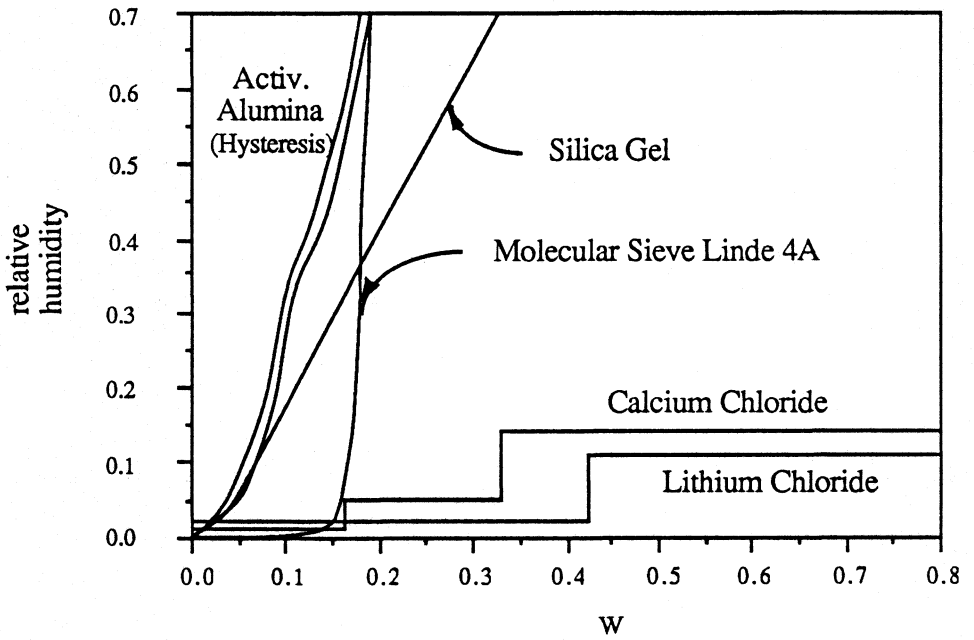

Fig. 1.1: Equilibrium isotherms for different microporous and chemical desiccants

LiCl is a hygroscopic salt with high moisture capacity, easy regenerability and high chemical stability. It is the most widely used desiccant in commercial rotary dehumidifiers. Figure 1.1 shows a comparison of the equilibrium sorption isotherms for microporous adsorbents and halogenated salts. The graph shows the outstanding ability of the chemical sorptive agents to reach very low humidities even at higher moisture content. The much higher capacity of the salts is only limited if the solution starts to drip off the supporter when the dilution gets too high.

The LiCl salt is impregnated on a supporter. This supporter provides a greatly extended surface through which the LiCl crystals are finely dispersed. The supporter must also be able to hold the LiCl when it is in solution up to a certain degree of dilution. The LiCl impregnated supporter is referred to as the "matrix", while the air carrying the water vapor is referred to as the "fluid". In rotary dehumidifiers the sorbent matrix is mounted in a frame. This frame has the form of a wheel and rotates in a housing. The air streams are separated by seals and flow in the axial direction.

The driving force for the mass transfer is the difference between the fluid vapor pressure and the equilibrium vapor pressure of the matrix for a given matrix water content. The driving force for the heat transfer is the temperature difference of matrix and fluid.

All sorption processes are exothermic with the heat of sorption being usually larger than the heat of condensation. According to Le Chatelier's principle, the equilibrium extent of an exothermic process is smaller for higher temperatures. Therefore, the equilibrium vapor pressure increases with higher temperature. Hence the mass transfer rate depends on temperature. Because of the involved heat of sorption, the heat transfer depends on the latent load of the mass transfer. Heat and mass transfer are therefore coupled.

The sorption process can be realized in fixed bed reactors or rotary regenerators. Since the sorbed water needs to be removed from the matrix to reactivate the sorbent, the fixed bed must be regenerated before the entire bed is exhausted and the unprocessed air breaks through. Hence the fixed bed has to be operated in two modes: Process and regeneration. To meet a continuous load two fixed beds are required. This is the fundamental advantage of rotary regenerators since they sorb and desorb the process and regenerating gas stream simultaneously. The size of the rotary regenerator is considerably smaller than an equivalent pair of fixed beds.

The major applications for rotary regenerators are air or gas drying and solvent recovery. Solvent recovery in the exhaust of spray paint booths, e. g. in the automobile industry, becomes increasingly important because of the impact of the solvent load in the exhaust air on the environment. Dry air is necessary for many manufacturing processes in industry such as powdered food products. Commercial solid desiccant air conditioning systems are becoming more competitive to conventional space conditioning systems.

1.2 Application in Air Conditioning Systems

Air conditioning is responsible for a large portion of today's energy usage. Air quality depends on temperature and humidity. Therefore, both, heat and mass transfer operations are necessary. Figure 1.2 shows a schematic diagram and the psychrometric chart for a typical ventilation cycle of a conventional system on a hot and humid summer day. Outdoor air is passed through a cooling coil and cooled by the refrigerant until it reaches the dew point temperature. The air is dehumidified by cooling down to the dew point temperature of the desired humidity which causes water to condense on the cooling coil. The process moves along the saturation line. To obtain a comfortable room temperature, the air has to be reheated, but this heat can usually be provided inexpensively from the condenser of the refrigerant. However, it seems obvious that desiccants are more suitable to remove the moisture and meet the corresponding latent loads. In buildings with high latent loads compared to the sensible load or in commercial applications where low humidities are desired, desiccant air conditioning systems are expected to be more cost-effective.

As an alternative to the cooling coil and the refrigerant vapor compression cycle, the

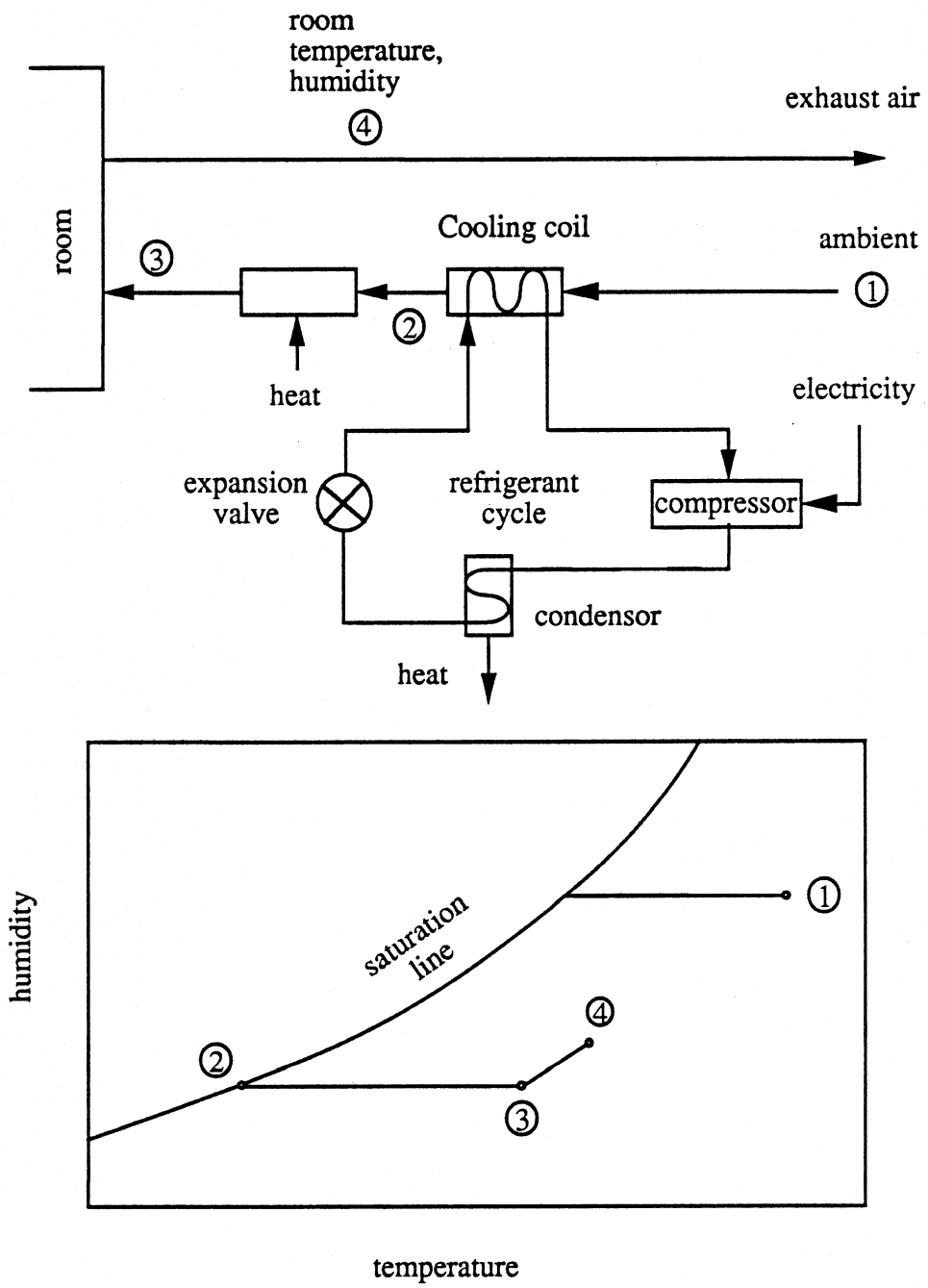

Fig. 1.2: Schematic and psychrometric diagram
for conventional air conditioning system

sensible heat load could be removed by evaporative coolers. However, these evaporative coolers increase the air humidity again and will not function acceptably in cases of high humidity. Hence a combination of evaporative coolers and rotary dehumidifiers is an attractive solution.

Many desiccant cooling cycles have been proposed and investigated. Figure 1.3 shows a ventilation cycle desiccant cooling system and the corresponding psychrometric diagram. Ambient air is dried by a rotary dehumidifier. The price for this dehumidification is the additional sensible load since the air is also heated by the dehumidifier. Thus the air has to be cooled by a rotary heat exchanger and finally cooled and humidified by an evaporative cooler to the desired conditions. The exhaust room air is used to take up the heat from the heat exchanger and to regenerate the rotary dehumidifier. In order to have a sufficient temperature difference as driving force for the heat exchanger the exhaust air needs first to be evaporatively cooled. Then it needs to be heated to reactivate the sorbent in the dehumidifier. This is the only energy input into the system besides the fans and the drive motors for the rotary components.

Solar energy could be used to provide this energy. This potential application of solar heat sources initiated the interest of the Solar Energy Laboratory of the University of Wisconsin in desiccant cooling. The peak times when air conditioning is needed most often fall together with high energy output of solar collectors. Also electricity costs are high at these peak times. Therefore, a major advantage of heat driven air conditioners is the low cost thermal energy usage by either solar collectors or gas burners compared to the high peak costs of electricity that is needed for the compressor of the Rankine cycle.

Another advantage of desiccant air conditioning systems is their mechanical simplicity.

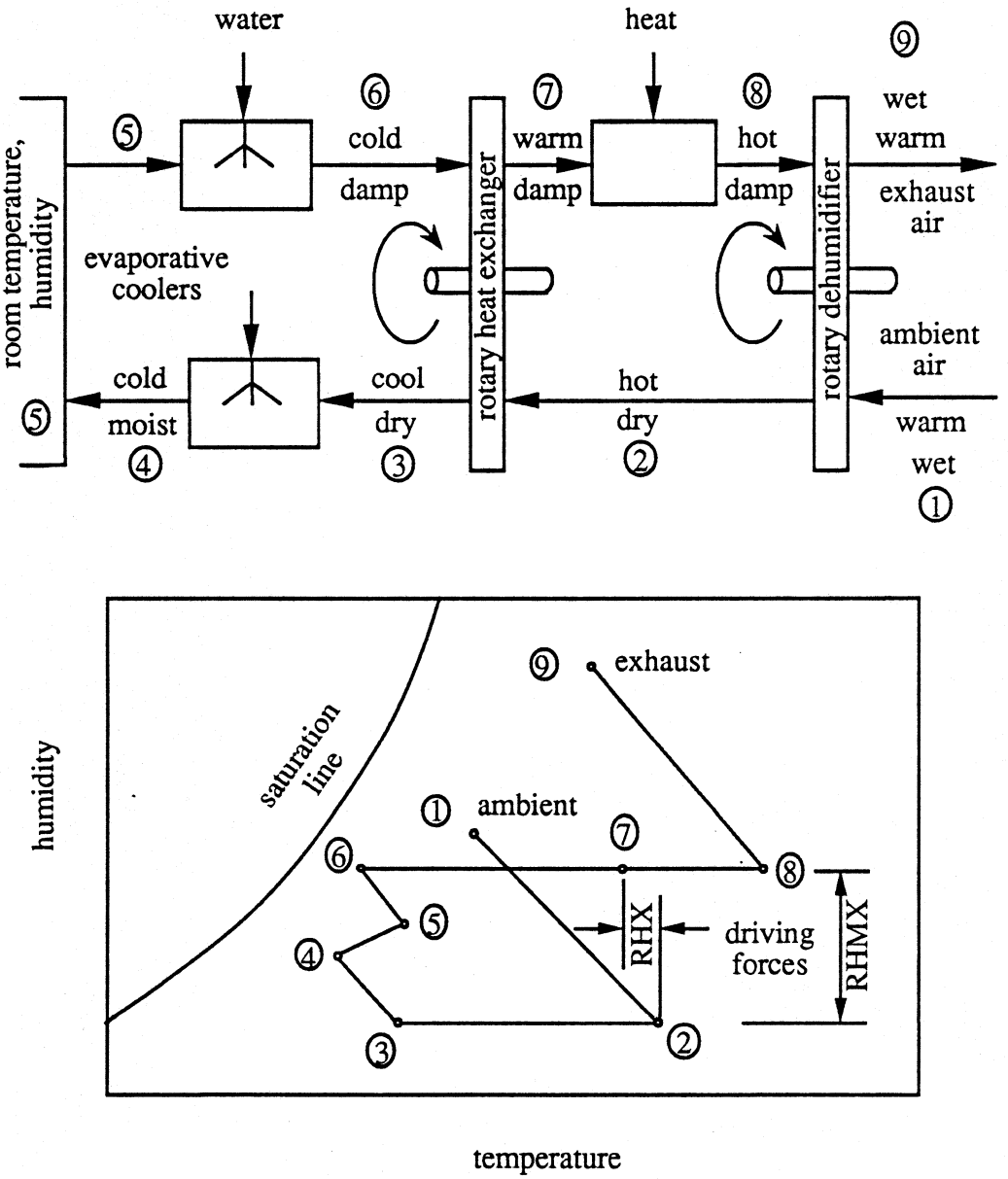

Fig. 1.3: Schematic and psychrometric diagram
for ventilation desiccant cooling system

No mechanically sophisticated devices like turbines and compressors of conventional refrigerant systems are needed. All operations are at ambient pressure.

Current users of desiccant air conditioning systems include supermarkets. Dry air in supermarkets is crucial to maintain the quality of the products and to reduce the build up of ice in the refrigerated display cases. Because of the additional cooling by the refrigerated cases the sensible heat load is small compared to the latent load. In hospitals, restaurants and hotels, the latent loads are also large compared to sensible loads because of high ventilation or high people traffic.

Humidity and temperature can be controlled independently with a combination of desiccant and conventional systems. The capacity of the conventional system can be much smaller if it only has to meet the sensible heat load. If high latent loads occur only at peak times, a conventional system without desiccants that is designed for these peak times runs the rest of the time inefficiently.

1.3 Thesis Objectives

Most published studies of rotary heat and mass exchangers (RHMX) evaluated silica gel [3,4,5,9,10] or microporous adsorbents as the desiccant. The governing equations were solved by either numerical finite difference models [1,4,7,8] or approximate analytical methods [1,9,10,11]. However, LiCl is commonly used in commercial desiccant air conditioning systems. These methods are not applicable for the simulation of rotary heat and mass exchangers with LiCl as the desiccant since the sorption isotherm and isopiestic of LiCl exhibit discontinuities. The primary goal of this thesis was to develop a model that simulates rotary heat and mass exchangers that use LiCl as desiccant. The LiCl is impregnated on a supporter and may be in solid or liquid state.

Chapter 2 describes the general model of rotary heat and mass exchangers and derives the governing equations, the conservation laws and transfer rate equations. Chapter 3 investigates the thermodynamic behavior of the air-water vapor-LiCl system and presents relationships for the sorption equilibria, heat of sorption and specific heat. In Chapter 4 the finite difference model by Maclaine-cross [1] is described and a modification for the discontinuous properties of LiCl is developed. This method is used to simulate sorption processes on LiCl. The results of these simulations are presented in Chapter 5. The performance of rotary dehumidifiers is described. The analogy method and its applicability for LiCl is discussed in Chapter 6.

Model Formulation for the Rotary Heat and Mass Exchanger

In this chapter, the fundamental conservation laws and transfer equations for mass and enthalpy are derived and the necessary assumptions are made. Similar equations and corresponding assumptions can be found in many other publications [1,3,5,6,10,11].

Figure 2.1 shows a schematic diagram of a rotary heat and mass exchanger (RHMX). The sorbent material, i.e. the LiCl impregnated on the supporter, is arranged in a rotating cylindrical wheel of depth L. The two air streams that pass in counterflow through the wheel are physically separated. They flow in axial direction through parallel passages. The cool and moist process stream corresponds to period $j = 1$ while the hot regenerating stream corresponds to period $j = 2$. The coordinate system is defined as shown in Figure 2.1. For each period, the axial coordinate z is defined as positive in fluid direction. Therefore its direction has to be reversed at the beginning of each period. The circumferential coordinate Θ can be regarded as angle position or time since the rotation speed is constant. Θ is set to zero at the beginning of each period. The RHMX may be asymmetric, i. e. the duration of each period Θ_j may be different; their sum gives the time of one complete rotation. The RHMX may be unbalanced with different air flow rates for the process and regeneration stream.

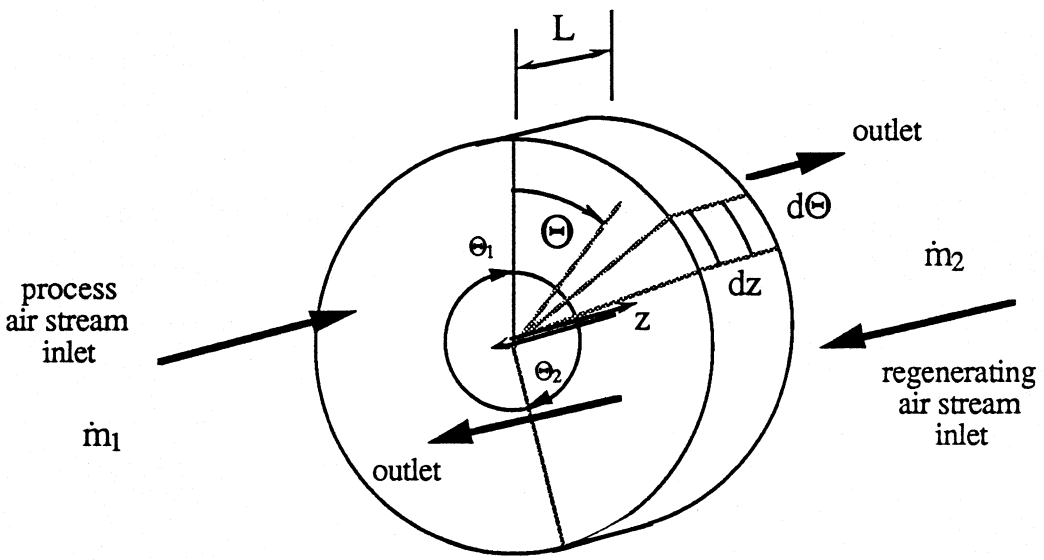

Fig. 2.1: Schematic diagram of a RHMX, definition of coordinates

The mathematical model for the RHMX is based on a set of standard assumptions:

1. The energy and water transport between matrix and fluid can be described by over-all or lumped transfer coefficients. There is no transfer flux coupling through thermal diffusion or Dufor effects.

2. The transfer coefficients and all matrix characteristics remain constant throughout the exchanger; the matrix is considered homogeneous.

3. Heat conduction and water diffusion in matrix and fluid are negligible in the angular or axial direction.

4. Heat and mass storage in the fluid is negligible compared to the storage in the matrix

5. The inlet streams are well mixed; their temperature and humidity are constant and uniform when they enter the RHMX.

6. The RHMX operates adiabatically. Fluid and matrix properties do not vary with the radius of the wheel.

7. The pressure drop along the flow length is negligible; the fluid flows with constant velocity v_j.

8. There is no mixing or carry over between the two fluid streams.

The first assumption allows the use of a simple transfer rate equation with a linear driving force between the matrix and fluid bulk properties for a simple transfer equation, without considering the resistances in fluid, matrix and interphase separately. The transfer coefficients have to be found by experiment. Convective transfer coefficients only can be used if the solid phase resistance can be neglected. To assume that they do not change together with other matrix characteristics is one of the most critical approximations of this model. This assumption was found to be valid for silica gel by Van den Bulck [3] who analyzed the temperature and humidity response of adiabatic single blow experiments.

The third assumption keeps the conservation laws of first order since heat conduction or diffusion terms would contain second order derivatives. Holmberg [4] has developed a finite difference model that includes axial heat conduction. The energy conservation law

then becomes a parabolic partial differential equation. The finite difference scheme was solved with a Gauss Seidel iterative method.

Assumption 4 reduces the complexity of the conservation laws. The fluid storage terms in heat and mass conservation relations are negligible for conventional dehumidifier operations.

The finite difference model developed in this thesis also allows dynamic simulations. However, to reach a unique steady state of the dehumidifier, constant inlet conditions are required. Also non-uniform inlet conditions can be simulated, as they might occur when the outlet stream of one wheel is the direct inlet of another one or when a purge stream is used. Brandemuehl [5] has investigated such situations. For the simulations in this thesis, the incoming air streams are considered to be well mixed and therefore uniform.

Heat losses, fluid carry over and pressure drop cannot be avoided when carrying out an experiment. Their influence has to be estimated when experimental results are compared with simulations.

Since the matrix and fluid properties do not change with the radius, the conservation laws and transfer equations can be derived by mass and energy balances for a pie-shaped differential element such as shown in Figure 2.2. It is assumed that the fluid that is carried over by the rotating matrix in the circumferential direction does not change it's heat and mass storage which corresponds to the 4th assumption above. Hence, the differential element is treated as if no fluid enters or leaves in circumferential direction.

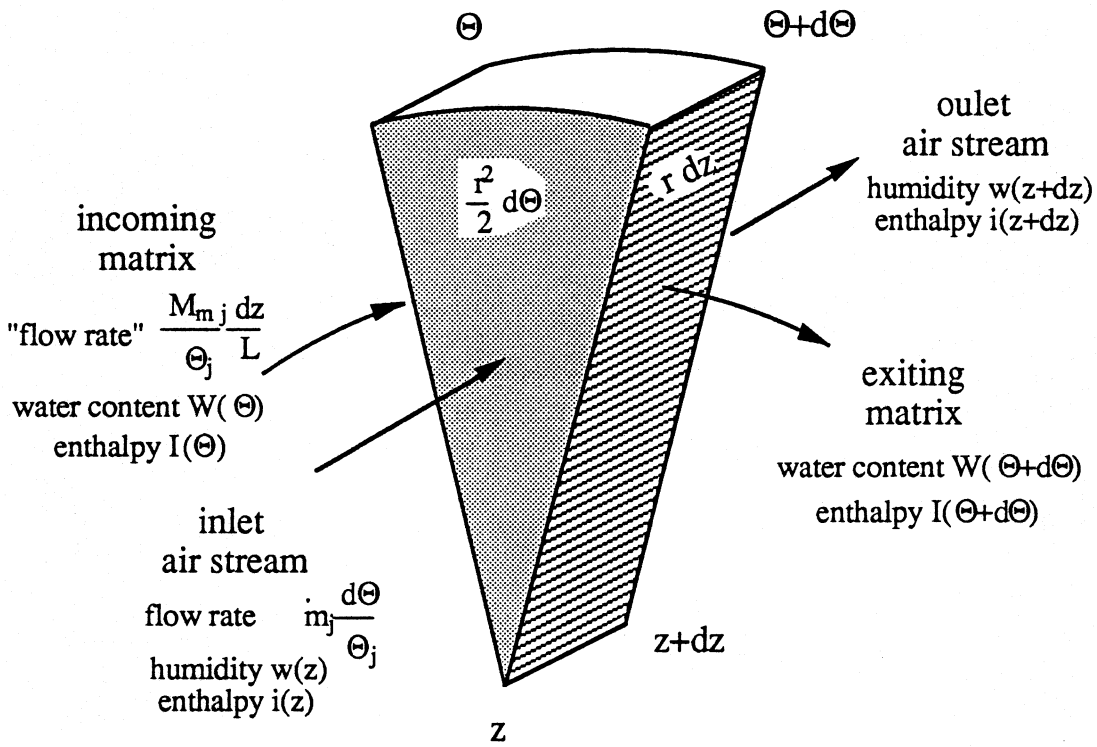

Fig. 2.2: Pie-shaped differential element

For the fluid properties at z+dz and the matrix properties at Θ+dΘ first order Taylor expansion are employed [1]:

$$w(z+dz) = w(z) + \frac{\partial w}{\partial z} dz$$

$$W(\Theta+d\Theta) = W(\Theta) + \frac{\partial W}{\partial \Theta} d\Theta$$

[1] partial derivatives with respect to z are at constant Θ and vice versa

Then the conservation equation for water is:

$$\dot{m}_j \frac{d\Theta}{\Theta_j}\left(-\frac{\partial w}{\partial z}dz\right)+\frac{M_{m\,j}}{\Theta_j}\frac{dz}{L}\left(-\frac{\partial W}{\partial \Theta}d\Theta\right)=0$$

where $\dot{m}_j$ is the dry fluid mass flow rate and $M_{m\,j}$ is the dry sorbent mass of period j. Thus $\dot{m}_j \frac{d\Theta}{\Theta_j}$ is the fraction of the dry fluid mass flow rate through the element and $\frac{M_{m\,j}}{\Theta_j}\frac{dz}{L}$ is the fraction of the dry matrix "flow rate" that enters the element. The dry fluid mass flow rate $\dot{m}_j$ may be replaced by the fluid mass $M_{f\,j}$ in the system, the air velocity v_j and the flow length L:

$$\dot{m}_j = \frac{M_{f\,j}\,v_j}{L} \tag{2.1}$$

Introducing the ratio of dry matrix and fluid mass

$$\mu_j = \frac{M_{m\,j}}{M_{f\,j}} \tag{2.2}$$

the conservation equation yields:

$$v_j \frac{\partial w}{\partial z}+\mu_j \frac{\partial W}{\partial \Theta}=0 \tag{2.3 a}$$

Analogous to the mass conservation law the energy conservation law is

$$v_j \frac{\partial i}{\partial z} + \mu_j \frac{\partial I}{\partial \Theta} = 0 \qquad (2.3\ b)$$

For the transfer equation of water vapor, the water balance just for the fluid is used. The difference in water content of the fluid flow into the element and out of the element must equal the amount that is sorbed or desorbed over the interphase. This amount depends on the overall transfer coefficient, the driving force and the exchange area:

$$\dot{m}_j \frac{d\Theta}{\Theta_j} \left(- \frac{\partial w}{\partial z} dz \right) = h_{w,j}\, A\, M_{m\,j} \frac{d\Theta}{\Theta_j} \frac{dz}{L} (w - w_m)$$

where $h_{w,j}$ is the overall mass transfer coefficient and A is the exchange area per dry matrix mass. Therefore, $A\, M_{m\,j} \frac{d\Theta}{\Theta_j} \frac{dz}{L}$ is the exchange area in the differential element. Replacing $\dot{m}_j$ with equation (2.1) yields:

$$-v_j \frac{\partial w}{\partial z} = h_{w,j}\, A\, \mu_j\, (w - w_m) \qquad (2.3\ c)$$

The transfer equation for the heat exchange is obtained in the same manner. The enthalpy content of the sorbed or desorbed water vapor adds another term to the equation:

$$\dot{m}_j \frac{d\Theta}{\Theta_j} \left(- \frac{\partial i}{\partial z} dz \right) = h_{t,j}\, A\, M_{m\,j} \frac{d\Theta}{\Theta_j} \frac{dz}{L} (t_f - t_m) + h_{wv}\, h_{w,j}\, A\, M_{m\,j} \frac{d\Theta}{\Theta_j} \frac{dz}{L} (w - w_m)$$

where h_{wv} is the enthalpy of water vapor.

Introducing the Lewis number $Le_j = h_{t,j} / c_f h_{w,j}$ the heat transfer equation can be expressed as:

$$- v_j \frac{\partial i}{\partial z} = h_{w,j} A \mu_j [Le_j c_f (t_f - t_m) + h_{wv} (w - w_m)] \qquad (2.3\ d)$$

With dimensionless variables and NTU numbers

$$x = \frac{z}{L} \qquad \tau = \frac{\Theta}{\Theta_j} \qquad (2.4)$$

$$NTU_{w,j} = \frac{h_{w,j} A \mu_j L}{v_j} \qquad (2.5)$$

and by combining all the parameters into one dimensionless group

$$\Gamma_j = \frac{\mu_j L}{v_j \Theta_j} \qquad (2.6)$$

the governing equations for each period are

$$\Gamma_j \frac{\partial W}{\partial \tau} + \frac{\partial w}{\partial x} = 0$$

$$\Gamma_j \frac{\partial I}{\partial \tau} + \frac{\partial i}{\partial x} = 0 \qquad (2.7\ a)$$

$$\frac{\partial w}{\partial x} = NTU_{w,j} (w_m - w)$$

$$\frac{\partial i}{\partial x} = NTU_{w,j} [Le_j c_f (t_m - t_f) + h_{wv}(t_f) (w_m - w)] \qquad (2.7\ b)$$

These equations represent two hyperbolic wave equations and two ordinary differential equations and contain seven unknown fluid and matrix properties. These properties are the water content, enthalpy and temperature of fluid and matrix and the air humidity in equilibrium with the matrix. Additional thermodynamic relationships are needed. These are the equilibrium air humidity as function of matrix temperature and water content

$$w_m = f(W,t_m) \qquad (2.8\ a)$$

the enthalpy of the matrix as function of temperature and water content

$$I = f(W,t_m) \qquad (2.8\ b)$$

and the enthalpy of the fluid

$$i = f(w,t_f) \qquad (2.8\ c)$$

Most of these relationships are non-linear. The equilibrium relationship may be discontinuous as it is the case for chemical sorptive agents like LiCl.

The seven equations (2.7) and (2.8) can be reduced to five if the enthalpies in the

energy conservation law and transfer equation are replaced by temperatures using equations (2.8 b,c). This will be done in Chapter 4 where the finite difference model is developed.

The boundary conditions for the system are

$$w\ (x=0) = w_{j\ in}$$
$$i\ (x=0) = i_{j\ in} \qquad (2.9)$$

The initial conditions for the matrix properties are periodic and therefore unknown. The reversal condition at the boundary where the matrix leaves the regenerating period 2 and enters the process period 1 is

$$W\ (\tau_1=0) = W\ (\tau_2=1)$$
$$I\ (\tau_1=0) = I\ (\tau_2=1) \qquad (2.10\ a)$$

and at the transition from period 1 to period 2

$$W\ (\tau_2=0) = W\ (\tau_1=1)$$
$$I\ (\tau_2=0) = I\ (\tau_1=1) \qquad (2.10\ b)$$

where the subscript of τ refers to the current period.

The conservation laws and transfer equations (2.7) together with the thermodynamic relationships (2.8) and the boundary and periodic initial conditions (2.9) and (2.10) form a complete set of algebraic and differential equations that determines the behavior of the

RHMX. This model can also be applied to dynamic fixed beds that are periodically processed and regenerated.

Since the differential equations are coupled through the non-linear thermodynamic relationships, there is no exact analytical solution to the system. Many numerical schemes have been proposed [1,4,7,8]. The finite difference model that is modified in this thesis was developed by Maclaine-cross [1] in 1974. VanLeersum [6] used this model to study the effect of condensation on the matrix. Other numerical methods were developed by Pla-Barby 1978 [7] and Mathriprakasam 1980 [8] who studied cross cooling of RHMX. In principle, every dynamic model for fixed beds is applicable by cycling the method to reach steady state. However, all of the methods are more or less computational expensive. This has motivated the search for approximate analytical methods.

The most promising method seems to be the analogy method that was developed by Close, Banks and Maclaine-cross [9] and is applied since by many others [10]. This method is based on the transformation of the governing equations by replacing enthalpy and water content with new combined characteristic potentials. With certain assumptions the transformed equations are uncoupled and completely analogous to the governing equations of the sensible heat exchanger. Thus the RHMX is characterized by the super-position of two wave fronts that propagate through the matrix. Jurinak [10] examined the numerical accuracy of the analogy method and used it for simulations of desiccant air conditioning systems. This method and its applicability for LiCl will be discussed in Chapter 6.

If infinite heat and mass transfer coefficients are assumed, the transfer equations become unnecessary and the system is described by the conservation laws only. There is

complete thermodynamic equilibrium. For this case Van den Bulck [11] developed analytical solutions by applying the method of characteristics and the shock wave method. He used an effectiveness to account for finite transfer coefficients. This effectiveness was determined by numerical solutions.

Thermodynamic Properties of the Air-Water Vapor-LiCl System

The thermodynamic behavior of the air-water vapor-LiCl system is of central interest in this work. The interaction of the moist air with the sorbent determines the performance of the rotary dehumidifier and of the entire desiccant cooling system.

Maclaine-cross [1] studied the thermodynamic properties of three halogenated salts, $CaCl_2$, LiBr and LiCl, but all three only in dilute solution. Chi [12] used LiCl on a Torvex supporter for his study of fixed bed absorbers. In this thesis a method to simulate rotary heat and mass exchangers will be presented using LiCl in solid phase as well as in solution as desiccant over a temperature range of 19.1 °C to 93.5 °C. The total system pressure was taken to be constant at atmospheric pressure (1,013 bar).

3.1 Properties of Moist Air

In order to use the methods of Chapters 4 and 5 to solve the governing equations, derivatives of the moist air enthalpy with respect to temperature t and absolute humidity w are required. The moist air is assumed to be an ideal mixture of dry air and water vapor.

In this case, the enthalpy of the mixture equals the sum of the individual partial enthalpies:

$$i = c_{da}\, t + w\ h_{wv}(t) \tag{3.1}$$

The specific heat of dry air c_{da} is taken to be constant with respect to temperature:

$$c_{da} = 1.0048\ \ [\text{kJ/kg dry air K}]$$

The enthalpy of water vapor is approximated by [2]:

$$h_{wv} = 2502.68 + 1.8003\ t\ \ [\text{kJ/kg}] \tag{3.2}$$

Therefore, the derivatives of enthalpy are:

$$\frac{\partial i}{\partial t} = c_f = 1.0048 + 1.8003\ w\ \ [\text{kJ/kg dry air K}] \tag{3.3}$$

$$\frac{\partial i}{\partial w} = h_{wv} = 2502.68 + 1.8003\ t\ \ [\text{kJ/kg}] \tag{3.4}$$

The water content or absolute humidity of the air may be calculated from the vapor pressure p by:

$$w = 0.62198\ \frac{p}{p_{tot} - p} \tag{3.5}$$

3.2 Equilibrium Sorption Isotherm of LiCl

While microporous adsorbents retain the adsorbed gas on their surface by Van der Waals forces (physical adsorption), LiCl combines with the water vapor and forms hydrates. Also the water vapor does not stay at the surface, but diffuses into the salt crystal (or solution). With increasing water content, LiCl dissolves into an aqueous solution.

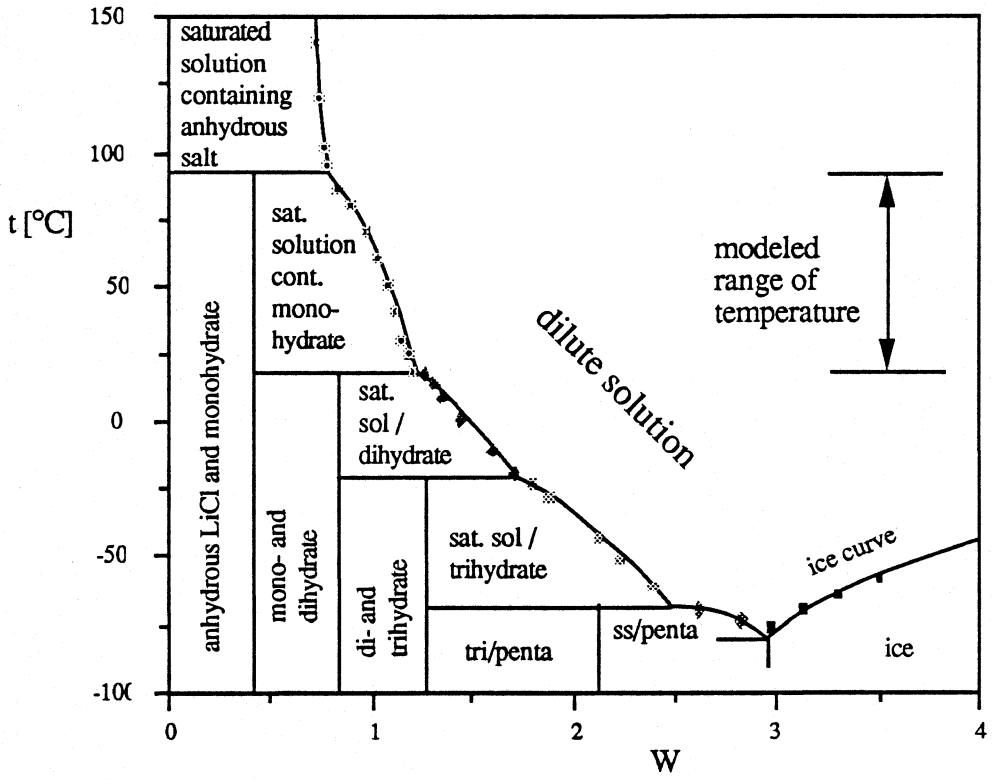

Fig. 3.1 Phase diagram of Lithium Chloride

Figure 3.1 shows a phase diagram for the LiCl-water system. Over the temperature range of 19.1 to 93.5 °C, there is either a system of anhydrous LiCl and monohydrate, i. e. solid LiCl, saturated solution containing monohydrate or dilute solution. Above 93.5 °C the saturated solution contains anhydrous salt. Monohydrate crystals are not stable at these high temperatures. Hence, if the matrix is cooled or heated across this temperature of 93.5 °C it will suffer a phase change. This phase change involves the release or the consumption of heat since the reaction of water and anhydrous salt to monohydrate is an exothermic process. Therefore, the cooling or heating process will stagnate at 93.5 °C until sufficient cooling or heating is supplied to complete this phase change.

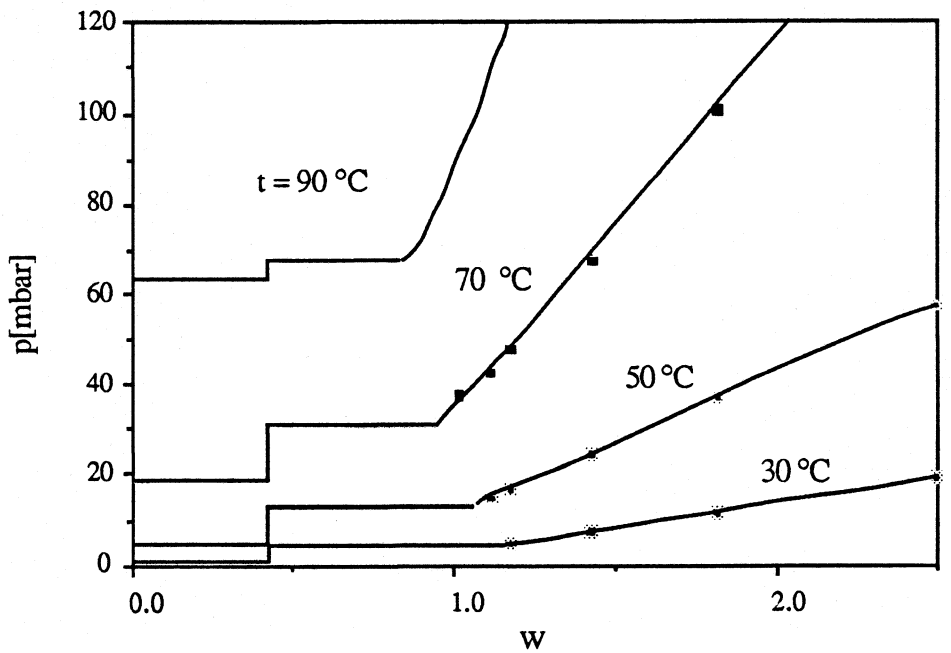

Fig. 3.2 Lithium Chloride isotherms, data by Johnson & Molstad

Figure 3.2 shows the step-like shape of the LiCl isotherms. According to Gibb's phase rule, the mixture of two phases of LiCl, e. g. anhydrous LiCl and monohydrate, has a constant equilibrium vapor pressure, here p_{am}, regardless of the water content. Such a system of two phases can react to changes of the vapor pressure by forming more or less monohydrate. The proportion of anhydrous salt and monohydrate represents a degree of freedom. Hence the equilibrium vapor pressure remains constant. Thus an arbitrarily small amount of water contained in the matrix will create the equilibrium vapor pressure p_{am}. The isotherm starts out with a discontinuity at zero water content. This means that moisture in air with a vapor pressure below p_{am} cannot be sorbed.

Also a saturated solution represents a system of two phases and therefore has a constant vapor pressure. If the saturated solution contains monohydrate this vapor pressure is denoted by p_{ms} ; if it contains anhydrous salt as it is the case above 93.5 °C, the vapor pressure is denoted by p_{as}.

Thus the isotherm will jump from p_{am} to p_{ms} at the weight ratio of pure monohydrate W_{mono}= 0.4245. This discontinuity only exists below 93.5 °C since above 93.5 °C monohydrate is unstable. Hence, if the air vapor pressure lies within this interval [p_{am}, p_{ms}], the sorption or desorption process will stop at W_{mono}.

At the solubility limit the LiCl will turn into a dilute solution. Now the vapor pressure will depend on the water content and the temperature. For very high dilution the vapor pressure approaches the saturation pressure of water vapor (relative humidity of 1, see Figure 3.3).

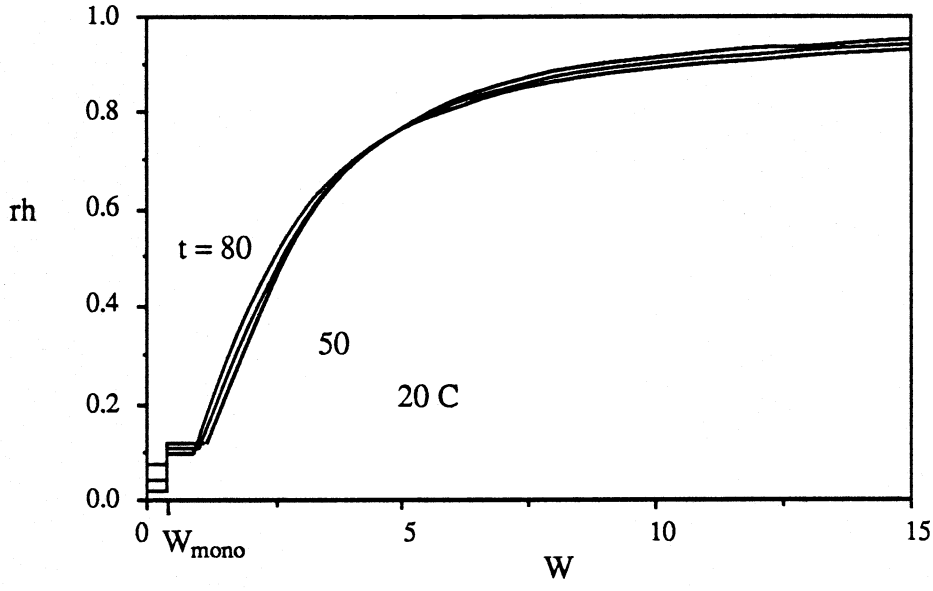

Fig 3.3 Relative humidity at high dilution

To model the isotherms, expressions are needed for

1. The vapor pressure p_{am} (T) for a system of anhydrous LiCl and monohydrate
2. The vapor pressure p_{ms} (T) for the saturated solution containing monohydrate LiCl
3. The vapor pressure p_{as} (T) for the saturated solution containing anhydrous LiCl for temperatures above 93.5 °C
4. The vapor pressure of the dilute solution as a function of t and W

It is also necessary to know at what water content the saturated solution will turn into a dilute solution. This solubility limit is a function of temperature. The solubility data by Appleby, Crawford, and Gordon [13] show transition points at 94.1 °C and 19.0 °C (see

Figure 3.4). Below 19.0 °C the solid phase consists of dihydrate. Above 94.1 °C it consists of anhydrous LiCl.

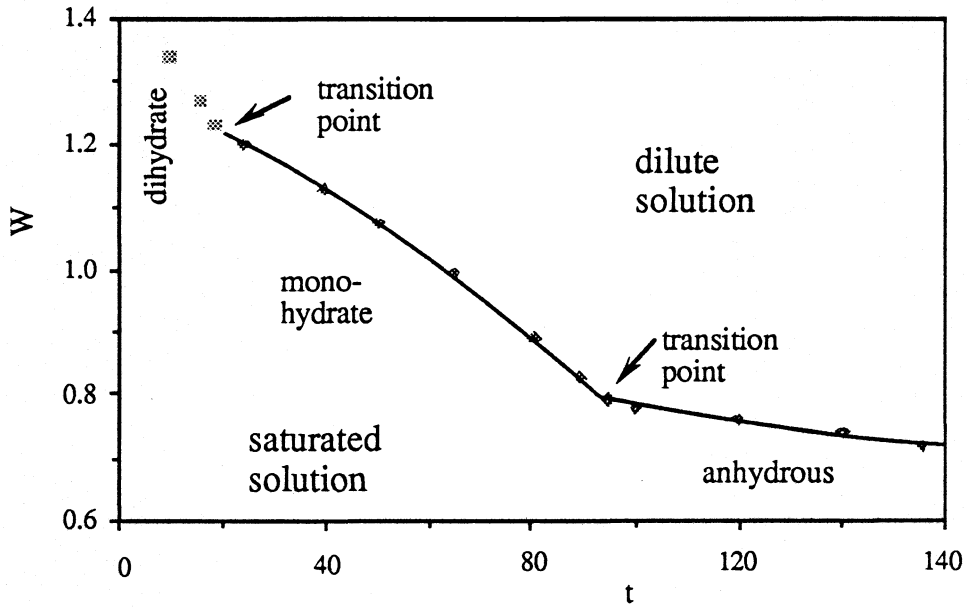

Fig. 3.4: Solubility limit, data by Applebey *et al.* [13]

In the temperature range between these transition points the data are fit by a second order polynomial (see Fig. 3.4):

$$W_{lim} = -2.1\ 10^{-5}\ t^2 - 3.47\ 10^{-3}\ t + 1.3 \qquad (3.6\ a)$$

Above 94.1 °C the solubility data are fit by

$$W_{lim} = 3.54\ 10^{-7}\ t^2 - 1.26\ 10^{-3}\ t + 0.90 \qquad (3.6\ b)$$

The upper transition temperature differs slightly from 93.5 °C which is obtained by density measurements and which is considered by Applebey to be the most probable value.

3.2.1 Vapor Pressure of Solid LiCl and Saturated Solution

Figure 3.5 shows log p versus 1/T plots for the saturated solution and the system of anhydrous salt and monohydrate. For the latter one the data by Slonim and Hüttig describe a fairly straight line (see Figure 3.5, lower curve), so the Clausius Clapeyron equation appears to be valid. Chi [12] fitted data by Slonim and Hüttig [14] and by Thakker [15] to the ln p versus 1/T relation to obtain:

$$\ln p_{am} = 24.976 - 7663/T \quad [\text{torr}] \tag{3.7}$$

Plotting data by Appleby, Crawford, and Gordon [13] for the saturated solution the graph shows a transition point at 93.4 °C (see Figure 3.5, upper curves). Below this temperature, the saturated solution contains monohydrate. Although some data sets (e.g. Gokcen [16]) show a curvature in this region, Chi uses a best line approximation:

$$\ln p_{ms} = 17.378 - 4881.5/T \quad [\text{torr}] \tag{3.8 a}$$

Above 93.4 °C the data by Applebey *et al.* [13] are fit by the author:

$$\ln p_{as} = 19\ 067 - 5484.5/T \quad [\text{torr}] \tag{3.8 b}$$

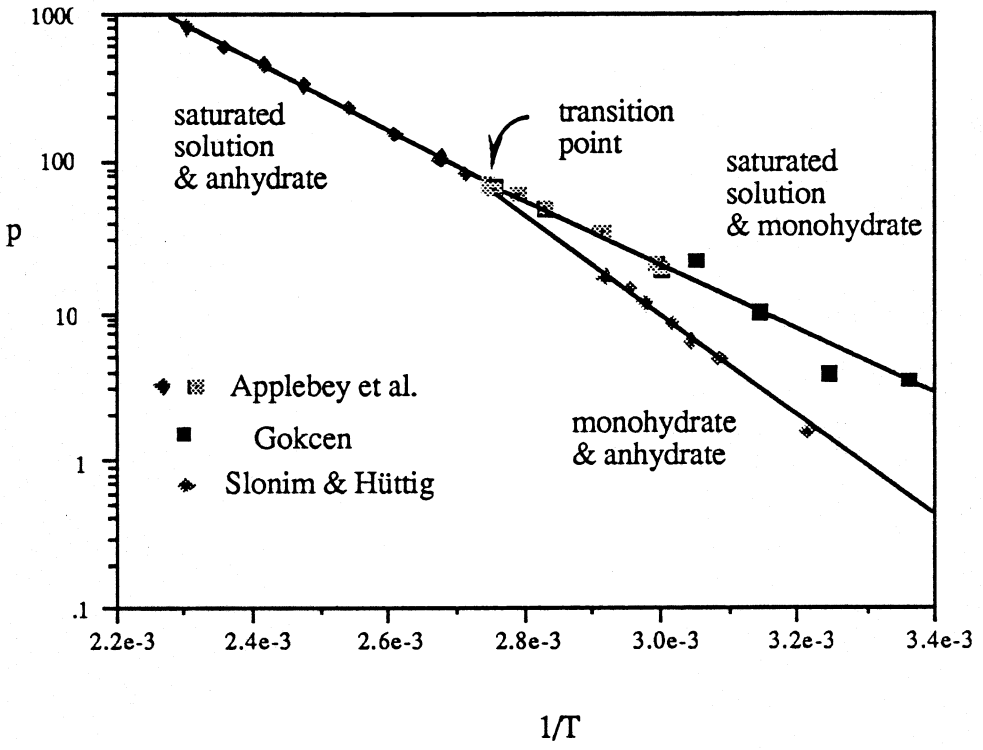

Fig.3.5: Isosteres for the saturated solution and solid LiCl, i. e. a system of anhydrate & monohydrate

3.2.2 Vapor Pressure of the Dilute Solution of LiCl

The large data set of Schlünder [17] shows approximately linear curves in a log p - 1/T diagram for concentrations from 0.1 to 0.8. This leads again to the Clausius Clapeyron equation. Maclaine-cross [1] has integrated this equation assuming the heat of sorption to be a linear function of T:

$$\ln \frac{p}{p_0} = G_0\left[1-\frac{T_0}{T}\right] - G_1 \ln \frac{T_0}{T} \tag{3.9}$$

where

$$G_0 = \frac{h_{lat\,0}}{RT_0}\left[\frac{h_s}{h_{lat}}\right]_{T_0} - G_1\,; \quad \frac{h_{lat\,0}}{RT_0} = 15.94777 \tag{3.10}$$

$$\begin{aligned} G_1 &= \frac{1}{R}\frac{\partial h_{wv}}{\partial T} + c^2 \frac{\partial c_{dil}}{\partial c} \\ &= -\,5.013918 + 3.726854\,c^2 \\ &\quad + 14.101374\,c^3 - 23.440175\,c^4 \end{aligned} \tag{3.11}$$

He chose the 50 °C isotherm for the evaluation of p_0 and restricted the concentrations to be below c = 0.9455, the solubility limit at 50 °C. But his fifth order polynomial fit of the data of Johnson and Molstad [18] yields incorrect values outside the approximated region. Since p_0 is also needed near saturation for higher temperatures, i.e. at higher concentrations, the data are fit by the author to an exponential expression:

$$\begin{aligned} p_0 = {} & 90.5107 \exp\{-4.9869\,(c+0.06655)^2\} \\ & + 33.1074 \exp\{-0.91363\,(c+0.06655)^2\} \end{aligned} \tag{3.12}$$

This approximation has a smaller error and approaches zero as c becomes large (see Figure 3.6) ; thermodynamically this is more reasonable.

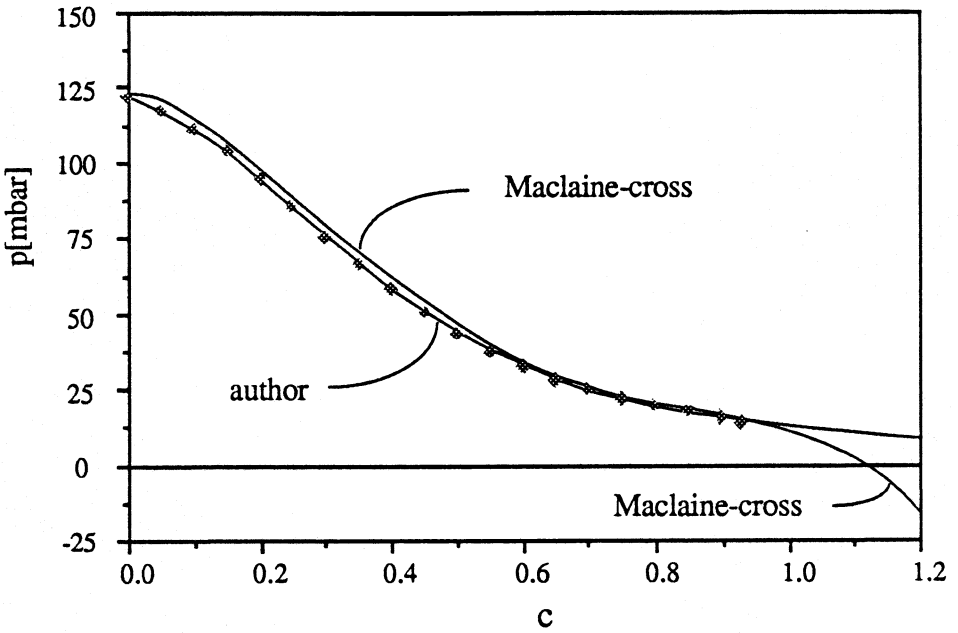

Fig. 3.6: 50 °C isotherm, Johnson & Molstad data

exponential fit versus polynomial fit

Fitting the heat of sorption data by Johnson and Molstad [18], the polynomial by Maclaine-cross is:

$$\left[\frac{h_s}{h_{lat}}\right]_{T_0} = 1 - 0.3755\, c^2 + 3.1321\, c^3 - 4.5742\, c^4 + 1.9829\, c^5 \qquad (3.13)$$

With the new 50 °C isotherm expression, the results near saturation are improved considerably, so the isotherms match well at the solubility limit. Figure 3.7 shows how close the values of the dilute solution at the solubility limit get to those of the saturated

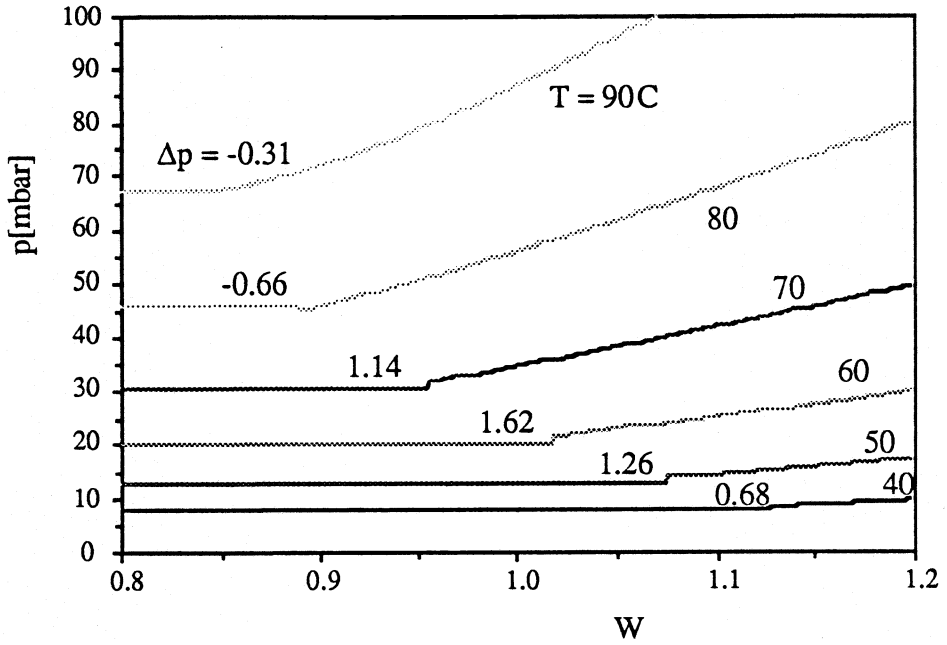

Fig. 3.7: Matching of isotherms at saturation using exponential fit for p_0

solution; the largest remaining difference occurs with the 60 °C isotherm (1.62 mbar) and it is smaller than the errors for the p_{ms} expression. Figure 3.8 shows that the isotherms do not match at all if the polynomial fit by Maclaine-cross is used.

Figure 3.2 shows the resulting isotherms for several temperatures and compares it with data by Johnson and Molstad [18]. The question arises, how are these isotherms affected by a supporter. Chi [12] has measured vapor pressure for a Torvex supporter (alumina and mullite compositions) and shows that Torvex does not decrease the vapor pressure as it has been reported for other types. Also the discontinuity stays as sharp as it is for LiCl alone.

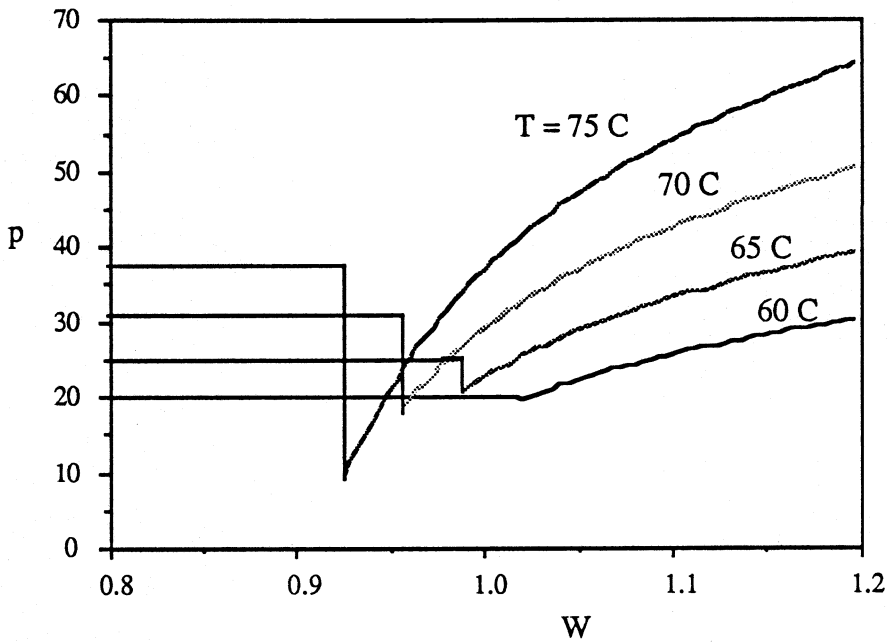

Fig. 3.8: Matching of isotherms at saturation using the polynomial fit for p_0

3.3 Heat of Sorption and Specific Heat

According to the Clausius Clapeyron equation, the slope in the ln p versus 1/T plot corresponds to the heat of sorption:

$$\frac{d \ln p}{d (1/T)} = \frac{h_s}{R} \tag{3.14}$$

From Figure 3.5 it can be seen that the slope for the system of anhydrous LiCl and monohydrate is constant. This line is used to evaluate:

$$h_{s,am} = 3536.\ kJ/kg$$

This value is in good agreement with the value by Thakker [15] at 25 °C of 3466 kJ/kg. Also it can be seen that the slope for the saturated solution is significantly different from the slope for the system of anhydrous LiCl and monohydrate. Therefore a step change for h_s is expected at the transition to the saturated solution at $W_{mono} = 0.4245$. This is shown in Figure 3.9.

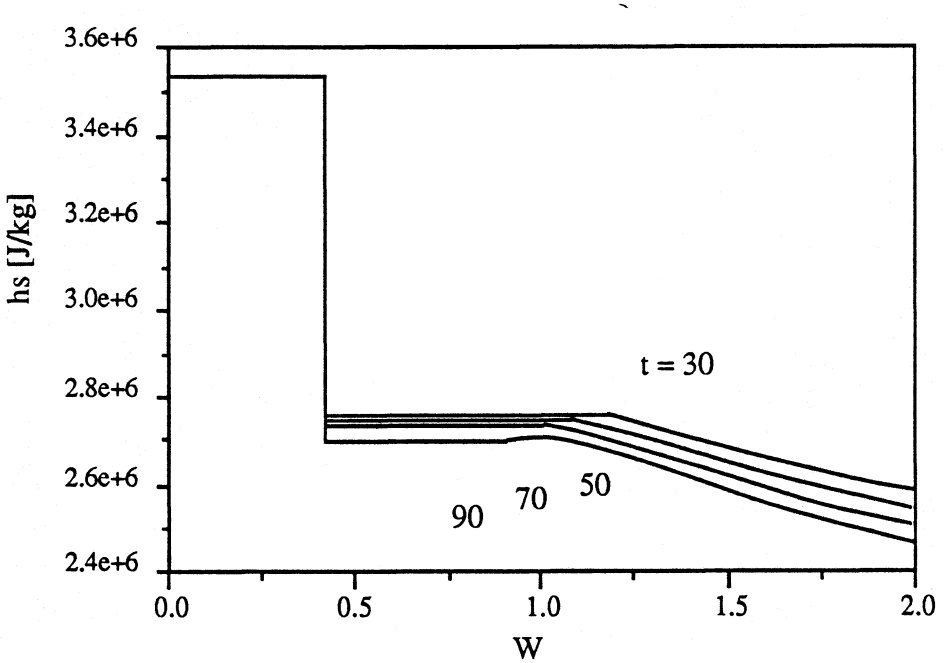

Fig. 3.9: Heat of Sorption

For the heat of sorption of the saturated solution, the expression by Maclaine-cross for h_s is evaluated at the solubility limit. Maclaine-cross assumes the heat of sorption to be a linear function of t and corrects the h_s / h_{lat} curve fit using data at 50 °C for other tempera-

tures. For the dilute and saturated solution h_s can be written as

$$h_{s,dil} = R\,(G_0\,t_0 + G_1\,t)\,,\;\; G_1 = G_1(c) \qquad (3.15\ a)$$

$$h_{s,sat} = R\,(G_0\,t_0 + G_1\,t)\,,\;\; G_1 = G_1(c_{lim}) \qquad (3.15\ b)$$

Maclaine-cross' polynomial for G_1 is derived from the curve fit for the specific heat using data by Lange and Dürr [19]. Again this approximation is unreasonable for concentrations near saturation (see Figure 3.10). Therefore, a new curve fit is used:

$$c_{dil} = 4.125 - 4.054\,c + 3.663\,c^2 - 1.194\,c^3 \qquad (3.16)$$

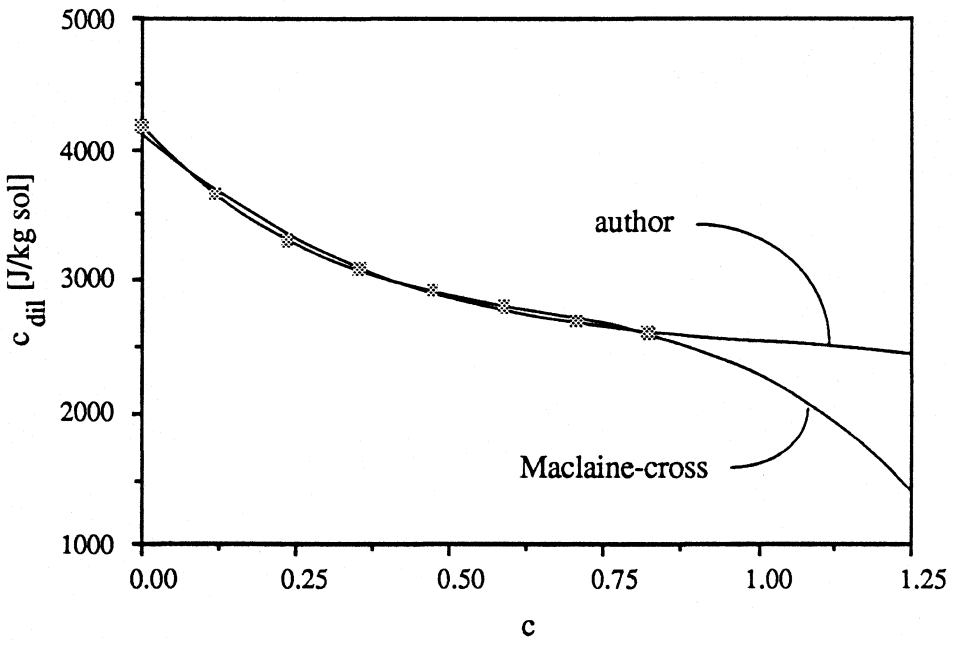

Fig. 3.10: Specific heat, new polynomial fit vs. Maclaine-cross fit, data by Lange & Dürr

This curve fit gives a better extrapolation into the region near saturation (c>0.8). This yields for G_1:

$$G_1 = - 4.889 - 0.847\, c^2 + 10.700\, c^3 - 7.761\, c^4 \qquad (3.17)$$

The heat of sorption h_s for the saturated and dilute solution is calculated using this polynomial. However, it is not used for the equilibrium vapor pressure since it is less accurate in the region of $c < 0.8$ and it does not improve the matching of the isotherms at saturation. Figure 3.9 shows the resulting values of h_s over the entire range of moisture content.

The above curve fit (3.16) is used for the specific heat of the dilute solution. To relate it to the mass of dry desiccant it is transformed:

$$c_{dil}\ [\text{kJ/kg DS K}] = c_{dil}\ [\text{kJ/kg solution K}] * (1+W)\ [\text{kg sol./kg DS}] \qquad (3.18)$$

The specific heat of the anhydrous salt is

$$c_{anhydrate} = 1.140\ \text{kJ/kg salt K}$$

The enthalpy of the matrix can be written as

$$I(W,t) = c_{dry\ matrix}\, t + \int_0^W h_{sorbed\ water}(W,t)\, dW \qquad (3.19)$$

where $h_{sorbed\ water} = h_{wv}(t) - h_S(W,t)$

For the system of anhydrous LiCl and monohydrate the heat of sorption is not a function of W. Therefore

$$I(W,t) = c_{anhydrate}\, t + (h_{wv}(t) - h_{s,am})\, W$$

Differentiation gives the specific heat of the system of anhydrous LiCl and monohydrate:

$$c_{am} = \frac{\partial I}{\partial t} = c_{anhyd} + W \frac{\partial h_{wv}}{\partial t} = 1.140 + 1.8\ W\ [kJ/kg\ salt\ K] \qquad (3.20)$$

Applying this equation for W_{mono} yields the specific heat of pure monohydrate:

$$c_{mono} = 1.904\ kJ/kg\ salt\ K]$$

For the saturated solution this value and the one calculated by the equation (3.18) at the solubility limit is interpolated.

To take into account the influence of a supporter, the specific heat is corrected:

$$c_m = c + c_{sup}\, X_{sup} \qquad (3.21)$$

3.4 Continuous Representation of LiCl Properties

Below the solubility limit, the LiCl isotherms consist of two horizontal and vertical lines. These jump discontinuities cause instabilities in current numerical models. To avoid such problems in computer programs simulating heat and mass exchangers, it is useful to have a continuous model of the isotherm. The discontinuities may be approximated by a sine function with the parameter k that allows an approach as close to the actual isotherm shape as desired:

$$
\begin{array}{ll}
p = p_{am} \sin\left(k\frac{w}{0.2}\frac{\pi}{2}\right) & W < \frac{0.2}{k} \\
p = p_{am} & W \le \frac{0.2}{k} W \le W_{mono} - \frac{0.2}{k} \\
p = p_{am} + \frac{1}{2}(p_{ms} - p_{am})\left[1+\sin\left(k\frac{W-W_{mono}}{0.2}\frac{p}{2}\right)\right] & W_{mono} - \frac{0.2}{k} < W < W_{mono} + \frac{0.2}{k} \\
p = p_{ms} & W_{mono} + \frac{0.2}{k} < W \le W_{lim} \\
p = p(W,t) & W > W_{lim}
\end{array}
\qquad (3.22)
$$

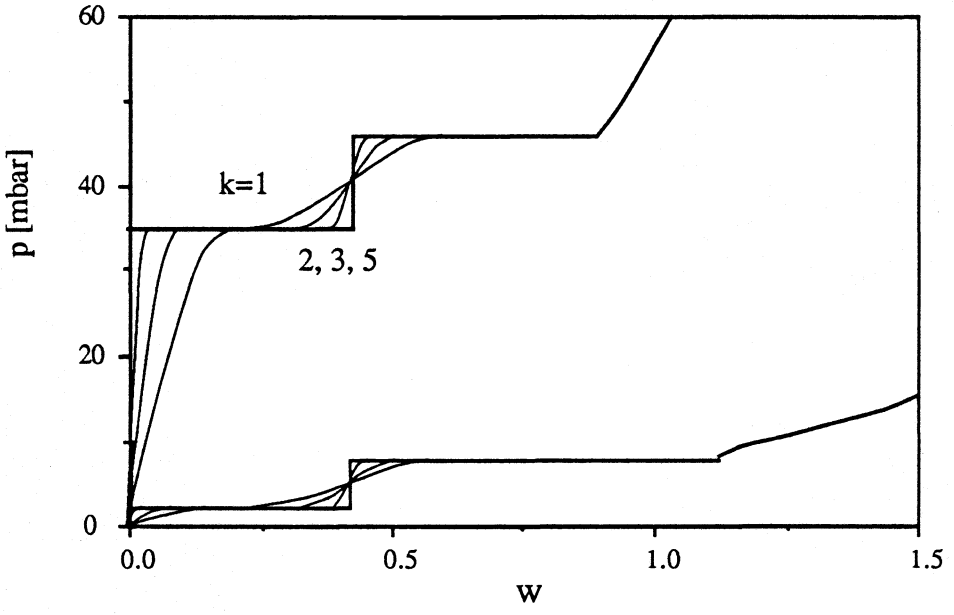

Fig 3.11: Continuous approximated 40 °C and 80 °C isotherms

The isotherm is cut into five pieces; the first piece approximates the discontinuity at zero water content, the third piece approximates the discontinuity at W_{mono}. With increasing parameter k the isotherms become steeper in these transition regions. This is shown in Figure 3.11 where k=5 represents already a very steep curve. Also the boundaries of these transition regions move together with increasing k.

Since the heat of sorption has a strong influence on the temperature profiles, h_s may also be approximated by:

$$
\begin{aligned}
h_s &= h_{s,am} && W \le W_{mono} - \frac{0.2}{k} \\
h_s &= h_{s,am} + \frac{1}{2}(h_{s,ms} - h_{s,am})\left[1+\sin\left(k\frac{W-W_{mono}}{0.2}\frac{p}{2}\right)\right] && W_{mono} - \frac{0.2}{k} < W < W_{mono} + \frac{0.2}{k} \\
h_s &= h_{s,ms} && W_{mono} + \frac{0.2}{k} < W \le W_{lim} \\
h_s &= h_{s,dil} && W > W_{lim}
\end{aligned}
\tag{3.23}
$$

3.5 Properties Required for Analogy and Finite Difference Methods

For the finite difference method, the equilibrium humidity of the air has to be determined for a given temperature and moisture content of the matrix. Chapter 3.2 gives the necessary formulas that are implemented in a subroutine together with the required derivatives (see below).

However, for the analogy method the situation is reverse: The equilibrium moisture content for the matrix has to be computed with an input of temperature and humidity of the air. To solve the equations for W (or c) a Newton iteration loop is used. To reach convergence with few iterations, it is crucial to have a close initial guess to the real value. For that the p(W,t) function is approximated by lines for constant temperatures

$$p(W,t) = p_{ms}(t) + m(t)\,(W-W_{lim}) \tag{3.24}$$

where the slopes m(t) are evaluated by a quadratic expression.

3.5.1 Derivatives of the Moisture Content

The finite difference model (Chapter 4) requires partial derivatives of the equilibrium humidity of the air with respect to temperature and moisture content of the matrix. These derivatives become infinite at the jump discontinuities of isotherm and isopiestic, so we have to exclude these points.

Both derivatives can be reduced to the derivatives of the vapor pressure by differentiating equation (3.5) and using the chain rule:

$$\left[\frac{\partial w_m}{\partial t}\right]_W = \frac{\partial p}{\partial t}\,\frac{0.62198 + w_m}{p_{tot} - p} \tag{3.25 a}$$

$$\left[\frac{\partial w_m}{\partial W}\right]_t = \frac{\partial p}{\partial W}\,\frac{0.62198 + w_m}{p_{tot} - p} \tag{3.25 b}$$

For the system of anhydrous LiCl and monohydrate, and also for the saturated solution, the vapor pressure is constant with respect to the moisture content but varies with respect to temperature; therefore:

$$\frac{\partial p}{\partial W} = 0 \qquad W < W_{lim} \tag{3.26}$$

$$\frac{\partial p}{\partial t} = \frac{\partial p_{am}}{\partial t} = p_{am} \frac{7663.}{T^2} \qquad W < W_{mono} \qquad (3.27\ a)$$

$$\frac{\partial p}{\partial t} = \frac{\partial p_{ms}}{\partial t} = p_{ms} \frac{4881.}{T^2} \qquad W_{mono} < W < W_{lim} \qquad (3.27\ b)$$

To calculate the derivative with respect to W for the dilute solution, all the expressions for p_0, h_s/h_{lat}, G_1 need to be differentiated with respect to c. The formula for p can be re-written:

$$p = p_0 \exp \{ 15.977 \left(1 - \frac{T_0}{T}\right) \frac{h_s}{h_{lat}} - G_1 \left(1 - \frac{T_0}{T} + \ln \frac{T_0}{T}\right)\}$$

Using the abbreviations

$$a = 15.977 \left(1 - \frac{T_0}{T}\right) \qquad (3.28\ a)$$

$$b = \left(1 - \frac{T_0}{T} + \ln \frac{T_0}{T}\right) \qquad (3.28\ b)$$

yields

$$p(c,t) = p_0(c) \exp \{ a(t) \frac{h_s}{h_{lat}}(c) - b(t)\, G_1(c) \} \qquad (3.29)$$

Differentiation gives:

$$\frac{\partial p}{\partial c} = \frac{\partial p_0}{\partial c} \exp\left\{ a \frac{h_s}{h_{lat}} - b\, G_1 \right\} + p \left(a \frac{\partial h_s / h_{lat}}{\partial c} - b \frac{\partial G_1}{\partial c} \right) \tag{3.30}$$

From the chain rule it follows:

$$\frac{\partial p}{\partial W} = - \frac{1}{W^2} \frac{\partial p}{\partial c} \tag{3.31}$$

For the partial derivative with respect to t, the matrix water content W and therefore p_0, h_s/h_{lat} and G_1 are constant, but a and b are not:

$$\frac{da}{dt} = 15.977 \frac{T_0}{T^2} \tag{3.32 a}$$

$$\frac{db}{dt} = - \frac{1}{T} + \frac{T_0}{T^2} \tag{3.32 b}$$

Using these expressions the desired derivative is:

$$\frac{\partial p}{\partial t} = p \left(\frac{h_s}{h_{wv}} \frac{da}{dt} - G_1 \frac{db}{dt} \right) \tag{3.33}$$

For computing lines of constant F potential (Chapter 6) we need the partial derivative of W with respect to t and w_m:

$$\left[\frac{\partial W}{\partial t}\right]_{w_m} = -\left[\frac{\partial w_m}{\partial t}\right]_W \Big/ \left[\frac{\partial w_m}{\partial W}\right]_t \tag{3.34}$$

$$\left[\frac{\partial W}{\partial w_m}\right]_t = 1 \Big/ \left[\frac{\partial w_m}{\partial W}\right]_t \tag{3.35}$$

3.4.2 Derivatives of Enthalpy

Equation (3.19) can be easily differentiated:

$$\left[\frac{\partial I}{\partial W}\right]_t = h_{wv}\,(t) - h_s\,(W,t) \tag{3.36}$$

For the derivative with respect to temperature the specific heat of the wet matrix from Chapter 3.3 is used:

$$\left[\frac{\partial I}{\partial t}\right]_W = c_m\,(W) \tag{3.37}$$

For the by analogy required derivatives we need to do a change of variables from (W,t) to (w_m,t) using the chain rule:

$$\left[\frac{\partial I}{\partial w_m}\right]_t = \left[\frac{\partial I}{\partial W}\right]_t \left[\frac{\partial W}{\partial w_m}\right]_t = c_m \left[\frac{\partial W}{\partial w_m}\right]_t \tag{3.38}$$

$$\left[\frac{\partial I}{\partial t}\right]_{w_m} = \left[\frac{\partial I}{\partial t}\right]_W + \left[\frac{\partial I}{\partial W}\right]_t \left[\frac{\partial W}{\partial t}\right]_{w_m} = c_m + (h_{wv} - h_s)\left[\frac{\partial W}{\partial t}\right]_{w_m} \tag{3.39}$$

Finite Difference Method

4.1. The Numerical Model for Rotary Heat and Mass Exchangers

The numerical model to solve the governing differential equations of the rotary heat and mass exchanger was developed by Maclaine-cross [1] and was modified by the author for desiccants with discontinuous isotherms. This model does not employ restrictive assumptions such as analogy between heat and mass transfer or equilibrium between matrix and fluid. The latter assumption is especially invalid for desiccants such as LiCl with discontinuities in the isotherm. Therefore, the numerical model that is developed in this Chapter is suitable for these sorbents.

As a first step, new non-dimensional variables are introduced:

$$\xi = NTU_{w,j}\, x$$

$$\zeta = NTU_{w,j}\, \tau / \Gamma_j \qquad (4.1)$$

Substituting these dimensionless variables into the governing heat and mass conservation and mechanism equations (2.7) results in:

$$\frac{\partial W}{\partial \zeta} + \frac{\partial w}{\partial \xi} = 0$$

$$\frac{\partial w}{\partial \xi} = w_m - w$$

$$\frac{\partial I}{\partial \zeta} + \frac{\partial i}{\partial \xi} = 0 \qquad (4.2)$$

$$\frac{\partial i}{\partial \xi} = Le\, c_f (t_m - t_f) + h_{wv} (w_m - w)$$

Since the enthalpy relations of air and matrix are known as functions of temperature and moisture content, the enthalpies are replaced with temperatures as dependent variables. From the chain rule it follows:

$$\frac{\partial i}{\partial \xi} = \left[\frac{\partial i}{\partial t_f}\right]_w \frac{\partial t_f}{\partial \xi} + \left[\frac{\partial i}{\partial w}\right]_{t_f} \frac{\partial w}{\partial \xi}$$
$$= c_f \frac{\partial t_f}{\partial \xi} + h_{wv} \frac{\partial w}{\partial \xi}$$

$$\frac{\partial I}{\partial \zeta} = \left[\frac{\partial I}{\partial t_m}\right]_w \frac{\partial t_m}{\partial \zeta} + \left[\frac{\partial I}{\partial W}\right]_{t_m} \frac{\partial W}{\partial \zeta}$$

Expressed in terms of temperature and water content, equations (4.2) can be rewritten as:

$$\frac{\partial W}{\partial \zeta} + \frac{\partial w}{\partial \xi} = 0$$

$$\frac{\partial I}{\partial t_m}\frac{\partial t_m}{\partial \zeta} + \frac{\partial I}{\partial W}\frac{\partial W}{\partial \zeta} + c_f \frac{\partial t_f}{\partial \xi} + h_{wv}\frac{\partial w_f}{\partial \xi} = 0 \qquad (4.3)$$

$$\frac{\partial w}{\partial \xi} = w_m - w$$

$$\frac{\partial t_f}{\partial \xi} = Le\,(t_m - t_f)$$

This transformation of the dependent variables, however, causes the major shortcoming of this model. Now the model is no longer applicable for temperature changes in the matrix across phase change temperatures such as 93.5 °C for LiCl. As it is shown in Chapter 3, there is a latent heat due to the phase change from anhydrous LiCl and water to mono-hydrate at this temperature. This latent heat is independent of any sorption or desorption process. Hence the matrix enthalpy changes discontinuously with temperature and the derivative $\left[\frac{\partial I}{\partial t_m}\right]_W$ becomes infinite. For this reason, this model can only simulate RHMX with LiCl in the temperature range of 19.1 °C and 93.5 °C. Only if the LiCl remains in dilute solution the RHMX can be simulated for all temperatures.

In the numerical solution to equations (4.3), the matrix is discretized in time and space using a staggered mesh, where the matrix and fluid dependent variables are evaluated at different nodes in the mesh (see Figure 4.1). Each grid element is regarded as a cross flow exchanger (fig.4.2). The equations are applied for the center of the grid element.

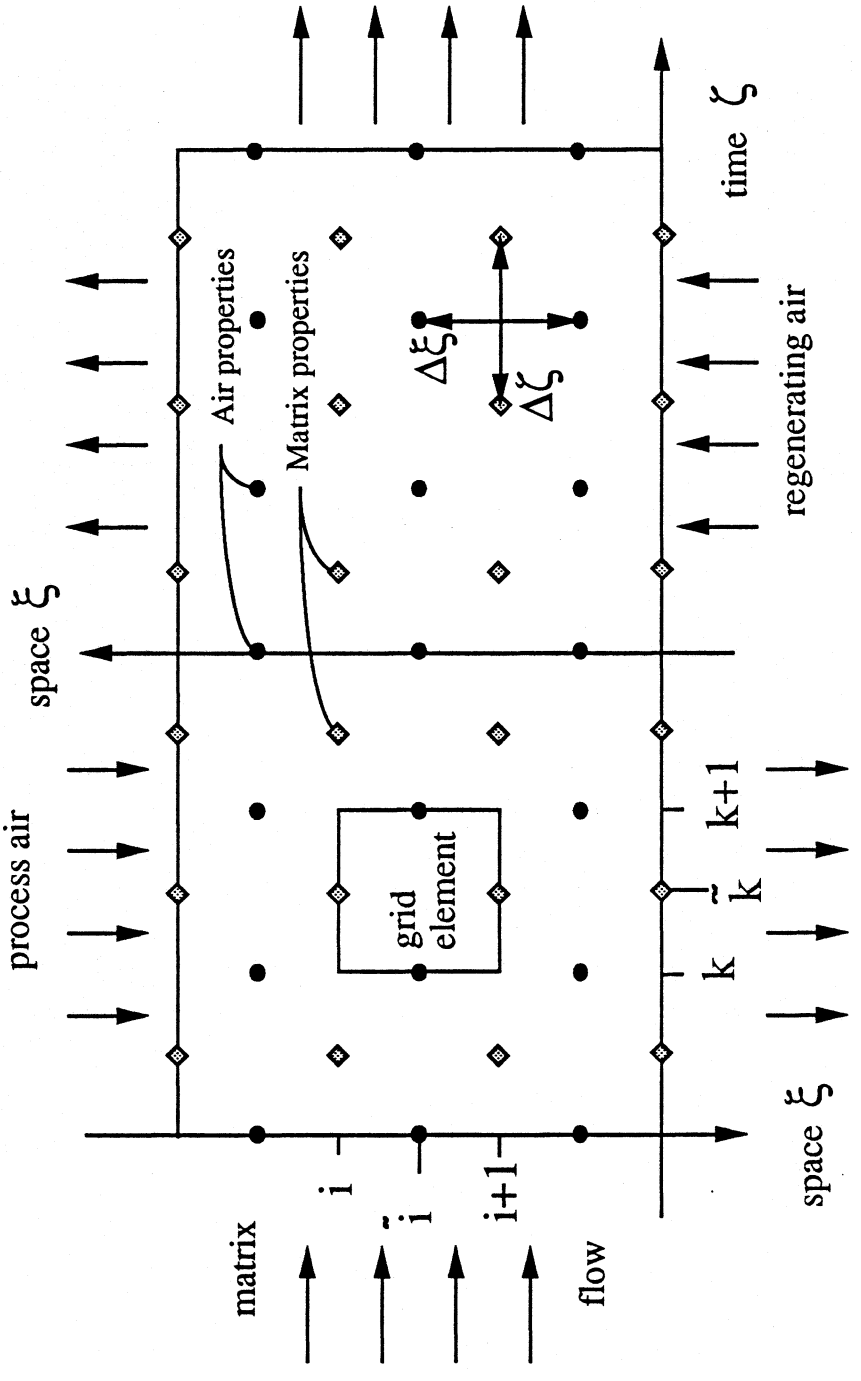

Fig 4.1: Staggered mesh

Therefore the Taylor expansions

$$\frac{\partial w}{\partial \xi} = \frac{w_{i+1,\tilde{k}} - w_{i,\tilde{k}}}{\Delta \xi} + O(\Delta \xi^2)$$

$$\frac{\partial t_f}{\partial \xi} = \frac{t_{f\, i+1,\tilde{k}} - t_{f\, i,\tilde{k}}}{\Delta \xi} + O(\Delta \xi^2)$$

$$\frac{\partial W}{\partial \zeta} = \frac{W_{\tilde{i},k+1} - W_{\tilde{i},k}}{\Delta \zeta} + O(\Delta \zeta^2) \qquad (4.4)$$

$$\frac{\partial t_m}{\partial \zeta} = \frac{t_{m\, \tilde{i},k+1} - t_{m\, \tilde{i},k}}{\Delta \zeta} + O(\Delta \zeta^2)$$

are actually central differences and second order accurate. The resulting finite difference equations are written in matrix form as

$$\begin{bmatrix} \frac{1}{\Delta \xi} & 0 & 0 & 0 \\ 0 & \frac{1}{\Delta \xi} & 0 & \frac{1}{\Delta \zeta} \\ 0 & \frac{1}{\Delta \xi} & 0 & 0 \\ \frac{c_f}{\Delta \xi} & \frac{h_{wv}}{\Delta \xi} & \frac{\partial I}{\partial t_m}\frac{1}{\Delta \zeta} & \frac{\partial I}{\partial W}\frac{1}{\Delta \zeta} \end{bmatrix} \begin{bmatrix} t_{f\, i+1,\tilde{k}} - t_{f\, i,\tilde{k}} \\ w_{i+1,\tilde{k}} - w_{i,\tilde{k}} \\ t_{m\, \tilde{i},k+1} - t_{m\, \tilde{i},k} \\ W_{\tilde{i},k+1} - W_{\tilde{i},k} \end{bmatrix} = \begin{bmatrix} Le\left[t_m - t_f\right]_{\tilde{i},\tilde{k}} \\ 0 \\ \left[w_m - w_f\right]_{\tilde{i},\tilde{k}} \\ 0 \end{bmatrix}$$

or $$M\,(x_{new} - x_{old}) = b \qquad (4.5)$$

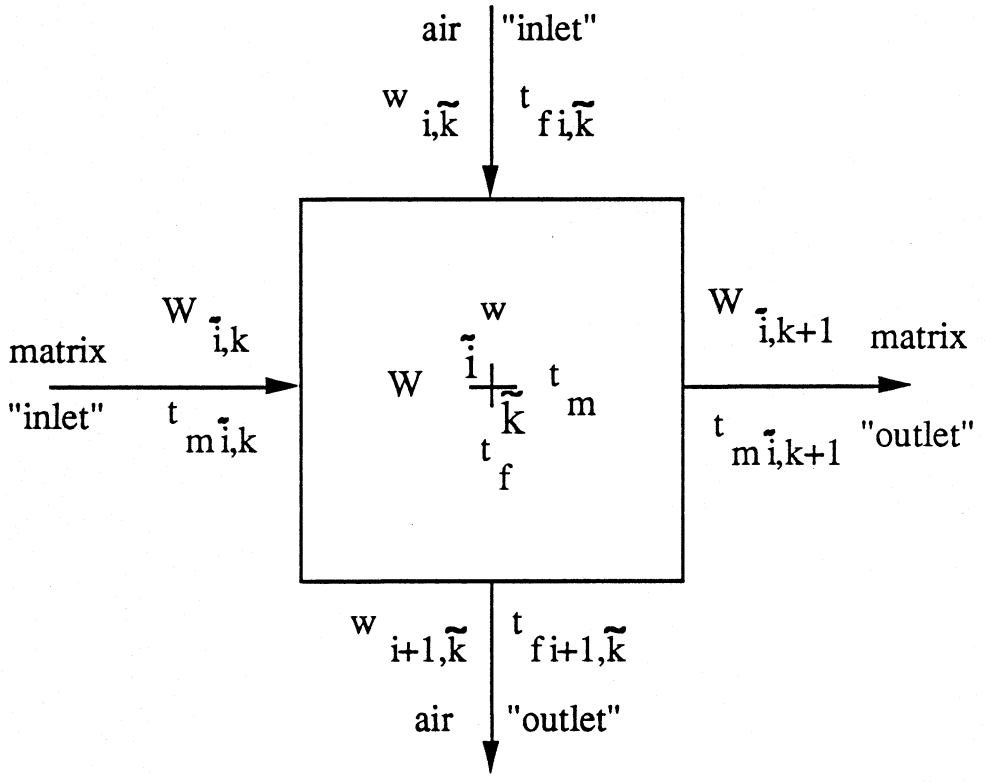

Fig. 4.2: Grid element as cross flow exchanger

Now $[t_m-t_f]^{\sim}_{i,\tilde{k}}$ and $[w_m-w_f]^{\sim}_{i,\tilde{k}}$ must be known at the center of the element. To keep the second order accuracy, the arithmetric mean is used to provide an estimate [1]:

$$[t_m-t_f]^{\sim}_{i,\tilde{k}} = \frac{1}{2}(t_{m\ i,k+1}+t_{m\ i,k}) - \frac{1}{2}(t_{f\ i+1,k}+t_{f\ i,k})$$
$$= t_{m\ i,k}-t_{f\ i,k} + \frac{1}{2}(t_{m\ i,k+1}-t_{m\ i,k}) - \frac{1}{2}(t_{f\ i+1,k}-t_{f\ i,k}) \qquad (4.6\ a)$$

$$[w_m-w_f]^{\sim}_{i,\tilde{k}} = \frac{1}{2}(w_{m\ i,k+1}+w_{m\ i,k}) - \frac{1}{2}(w_{f\ i+1,k}+w_{f\ i,k})$$

[1] The superscript ~ is suppressed on the right hand side

Since $w_{m\,\tilde{i,k+1}}$ is contained in this expression the equations are implicit. To solve them $w_{m\,\tilde{i,k+1}}$ is eliminated by using a Taylor expansion for $W_{\tilde{i,k+1}}$:

$$W_{i,k+1} = W_{i,k} + \left[\frac{\partial W}{\partial t_m}\right]_{w_m} (t_{m\,i,k+1} - t_{m\,i,k}) + \left[\frac{\partial W}{\partial w_m}\right]_{t_m} (w_{m\,i,k+1} - w_{m\,i,k})$$

Elimination of $w_{m\,\tilde{i,k+1}}$ yields:

$$[w_m - w_f]_{\tilde{i,k}} = w_{f\,i,k} - w_{m\,i,k} + \frac{1}{2}(w_{f\,i+1,k} - w_{f\,i,k}) - \frac{1}{2\left[\frac{\partial W}{\partial w_m}\right]_{t_m}} (W_{i,k+1} - W_{i,k}) - \frac{\left[\frac{\partial W}{\partial t_m}\right]_{w_m}}{2\left[\frac{\partial W}{\partial w_m}\right]_{t_m}} (t_{m\,i,k+1} - t_{m\,i,k}) \qquad (4.6\ b)$$

In this equation the ratio of the partial derivatives can be replaced by:

$$\frac{\left[\frac{\partial W}{\partial t_m}\right]_{w_m}}{\left[\frac{\partial W}{\partial w_m}\right]_{t_m}} = -\left[\frac{\partial w_m}{\partial t_m}\right]_W$$

Substituting equations (4.6) in the system (4.5) yields

$$\tilde{M}(x_{new} - x_{old}) = \tilde{b}$$

or

$$x_{new} = x_{old} + \tilde{M}^{-1}\tilde{b}$$

where

$$\tilde{M}^{-1}\tilde{b} = \begin{bmatrix} \frac{1}{\Delta\xi}+\frac{Le}{2} & 0 & -\frac{Le}{2} & 0 \\ 0 & \frac{1}{\Delta\xi} & 0 & \frac{1}{\Delta\zeta} \\ 0 & \frac{1}{\Delta\xi}+\frac{1}{2} & -\frac{1}{2}\left[\frac{\partial w_m}{\partial t_m}\right]_W & -\frac{1}{2}\left[\frac{\partial w_m}{\partial W}\right]_{t_m} \\ \frac{c_f}{\Delta\xi} & \frac{h_{wv}}{\Delta\xi} & \frac{\partial I}{\partial t_m}\frac{1}{\Delta\zeta} & \frac{\partial I}{\partial W}\frac{1}{\Delta\zeta} \end{bmatrix}^{-1} \begin{bmatrix} Le\left[t_{m\tilde{i},k}-t_{f\tilde{i},k}\right] \\ 0 \\ w_{m\tilde{i},k}-w_{f\tilde{i},k} \\ 0 \end{bmatrix} \tag{4.7}$$

Appendix A gives the details of how this system is solved.

To calculate x_{new} with second order accuracy all the state property functions in $\tilde{M}$ must be evaluated as functions of t_m, W, t_f and w at the center of the grid element $(\tilde{i},\tilde{k})$. Since these values are not known, the "inlet" conditions of the element x_{old} are used first. Then the "outlet" conditions x_{new} are computed and the mean of x_{new} and x_{old} is used as a second approximation to evaluate the state property functions. Now x_{new} can be updated with second order accuracy.

4.2 Modified Model for Discontinuous Sorbents

Rotary heat and mass exchangers with discontinuous sorbents can be simulated with Macclaine-cross' finite difference model using continuous approximations of the jump such as developed in Chapter 3.4. The method works even for very high values of the parameter k, i. e. for very steep isotherms. For the real shape of the isotherms with an actual step, however, the method fails. The reason for this is due to the Taylor expansion for $W(t_m,w_m)$ that is used to solve the in $w_{m\,\tilde{i},k+1}$ implicit equations. At the jump the derivatives become infinite and the Taylor expansion is no longer feasible. The Taylor expansion was needed to find an expression for $[w_m\text{-}w_f]_{\tilde{i},\tilde{k}}$. Assuming that the jump occurs in the current grid element, w_m could be approximated at the center of the grid element by the value of the "inlet" condition $w_{m\,\tilde{i},k}$, by adding (process period) or subtracting (regenerating period) the height of the jump $\Delta w_m(t_m)$ only, if the jump occurs before the center (which is not known). However, there will be still a large numerical error due to the discretizing of the matrix. In order to accomodate the jump, a different numerical scheme is employed.

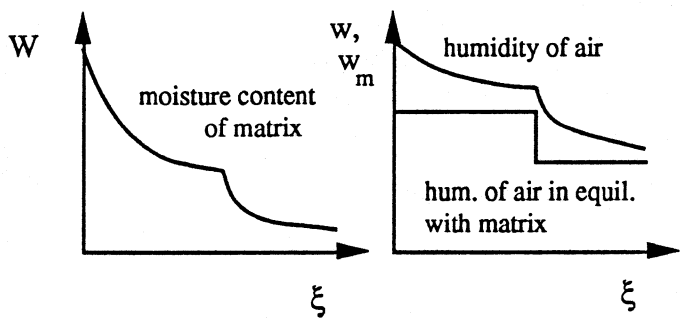

Fig. 4.3 Qualitative shape of water content profiles

The original differential equation (4.2 b) is

$$\frac{\partial w}{\partial \xi} = w_m - w \qquad (\zeta = \text{const})$$

where $w_m = w_m(\xi)$ has a jump discontinuity. Therefore, $w(\xi)$ will exhibit a knee, as it is shown in Figure 4.3. Now the coordinate ξ is discretized and the discontinuity is assumed to be between $\xi-\Delta\xi/2$ and $\xi+\Delta\xi/2$. Predicting $w(\xi+\Delta\xi/2)$ using $w(\xi-\Delta\xi/2)$ and evaluating the slope with w_m-w at ξ which is either before the jump or after, will yield a significant error (see Figure 4.4). However, using the mean of the slopes at $\xi-\Delta\xi/2$ and $\xi+\Delta\xi/2$ will take both sides of the discontinuity into account and therefore results in the best prediction for $w(\xi+\Delta\xi/2)$. This is shown qualitatively in Figure 4.5. The accuracy is the better the closer the jump is to the center of this interval.

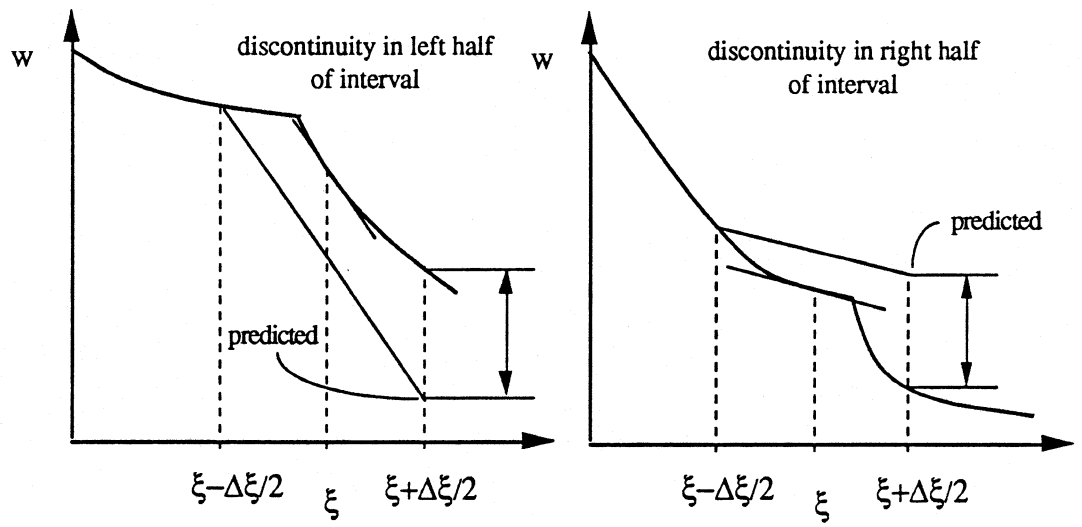

Fig. 4.4: Predicition of $w(\xi+\Delta\xi/2)$ at discontinuity using slopes at ξ

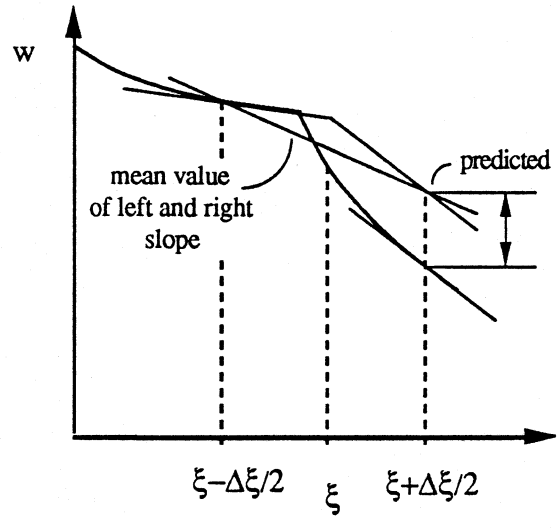

Fig. 4.5: Prediction of w(ξ+Δξ/2) at discontinuity using mean value of slopes on both sides of discontinuity

Hence $w_{m\,\tilde{i},\tilde{k}}$ is evaluated by the mean of $w_{m\,\tilde{i},k}$ and $w_{m\,\tilde{i},k+1}$ where $w_{m\,\tilde{i},k+1}$ is known to be after the jump and can be approximated by

$$w_{m\,\tilde{i},k+1} = w_{m\,\tilde{i},k} +/- \Delta w_m(t_m)$$

the sign depending on the period (process +, regenerating period -). The change of w_m from k to k+1 in addition to the jump due to changes in temperature is neglected. Therefore

$$w_{m\,\tilde{i},\tilde{k}} = w_{m\,\tilde{i},k} +/- \frac{1}{2} \Delta w_m(t_m)$$

and

$$[w_m - w_f]_{i,k} = w_{m\,i,k} \pm \frac{1}{2}\,\Delta w_m - w_{f\,i,k} - \frac{1}{2}(w_{f\,i+1,k} - w_{f\,i,k}) \tag{4.8}$$

The resulting system of equations turns out to be much simpler than the conventional system (4.7):

$$\tilde{M}^{-1}\,\tilde{b} = \begin{bmatrix} \frac{1}{\Delta\xi} + \frac{Le}{2} & 0 & -\frac{Le}{2} & 0 \\ 0 & \frac{1}{\Delta\xi} & 0 & \frac{1}{\Delta\zeta} \\ 0 & \frac{1}{\Delta\xi} + \frac{1}{2} & 0 & 0 \\ \frac{c_f}{\Delta\xi} & \frac{h_{wv}}{\Delta\xi} & \frac{\partial I}{\partial t_m}\frac{1}{\Delta\zeta} & \frac{\partial I}{\partial W}\frac{1}{\Delta\zeta} \end{bmatrix}^{-1} \begin{bmatrix} Le\,[t_{m\,i,k} - t_{f\,i,k}] \\ 0 \\ w_{m\,i,k} - w_{f\,i,k} \pm \frac{1}{2}\Delta w_m \\ 0 \end{bmatrix} \tag{4.9}$$

Because of the additional zeros in the matrix M the system has to be solved in a different (and simpler) way (see Appendix A). As before, the state property functions including $\Delta w_m(t_m)$ have to be evaluated twice using the "inlet" conditions first and the mean values second.

The boundaries of the humidity interval of the jump at W_{mono} are the equilibrium humidity of the system of anhydrous LiCl and monohydrate w_{am} and of the saturated solution w_{ms}. The boundaries of the humidity interval of the jump at zero water content are zero and w_{am}. If the humidity of the air lies within one of these intervals and the matrix has reached the corresponding water content (zero or W_{mono}) water vapor can neither be sorbed nor desorbed. Just a little more sorbed water will cause the equilibrium humidity to

jump over the air humidity and reverse the driving force. If just an arbitrarily small amount of water is desorbed the equilibrium humidity will jump below the air humidity and reverse the driving force again. Sorption or desorption processes come to an halt. Thus there is heat exchange only. In this case, the humidity of the fluid and the water content of the matrix do not change and the numerical mass conservation and transfer rate equations drop out of the system of equations (4.9). The simplified matrix for heat exchange only is

$$\begin{bmatrix} \frac{1}{\Delta\xi} + \frac{Le}{2} & -\frac{Le}{2} \\ \frac{c_f}{\Delta\xi} & \frac{\partial I}{\partial t_m}\frac{1}{\Delta\zeta} \end{bmatrix} \begin{bmatrix} t_{f\,i+1,\tilde{k}} - t_{f\,i,\tilde{k}} \\ t_{m\,\tilde{i},k+1} - t_{m\,\tilde{i},k} \end{bmatrix} = \begin{bmatrix} Le\,(t_{m\,\tilde{i},k} - t_{f\,i,\tilde{k}}) \\ 0 \end{bmatrix} \qquad (4.10)$$

This sytem is also solved in Appendix A.

The algorithm thus has to distinguish four cases:

Case I: The matrix water content is not near a discontinuity. The conventional numerical equations (4.7) are used.

Case II: The sorption (or desorption) process reaches the discontinuity. The air humidity is higher than the upper equilibrium humidity of the discontinuity (or below the lower equilibrium humidity) so the dehumidification process (regeneration) can proceed and crosse the discontinuity. To find out when the algorithm has reached the grid element where the jump occurs, x_{new} is evaluated the conventional way and then checked to determine if the matrix water content has changed into the new state of matter. In that case the algorithm switches over to the new set of

finite difference equations (4.9) and x_{new} is re-evaluated.

Case III: The sorption (or desorption) process reaches the discontinuity and stagnates there since the fluid humidity is within the humidity interval of the jump. The water content of the matrix is set to W_{mono} or zero. For the "outlet" fluid humidity the element mass balance is used. For the temperatures the results of the conventional equations are used. This introduces an error which is acceptable since this case can at most occur once for every space loop.

Case IV: The matrix water content is at the discontinuity. The air humidity lies within the jump interval. There is heat exchange only. Equations (4.10) are employed.

The algorithm moves through the grid with an inner space loop and an outer time loop. Within the space loop the grid element "outlet" states are computed according to the above four cases. Two values for the time increment $\Delta\xi$ may be used corresponding to the two wave fronts that propagate through the matrix with different speeds. To follow the fast front (temperature change), a small time step is needed and subsequently for the slow front (change in moisture content) the step size can be increased considerably. When the summation of squares (L^2 norm) of the matrix temperature change of all grid elements at one time drops below some specified value the fast wave is assumed to have passed through the matrix and the time step may be increased. At the end of the period the matrix state vectors for water content and temperature are reversed since the axial coordinate is defined positive in air flow direction.

The simulation of one complete rotation of the wheel with two periods is implemented

in the subroutine SGITHM. The entire algorithm needs to be cycled to converge upon the solution from some initial guess for the matrix state to the steady state of the dehumidifier; i. e. the matrix state at the beginning of the process period needs to be the same as at the end of the regenerating period after one complete rotation. Hence the main program iterates over SGITHM.

For convergence, two criteria have to be met which are the overall mass and enthalpy balance for the air streams. At steady state of the RHMX the enthalpy and water content of the incoming air streams has to be the same as enthalpy and water content of the outlet air streams.

Simulation of Rotary Heat and Mass Exchangers with LiCl as Desiccant

5.1 Processing a regenerated matrix with uniform initial properties

Chapter 4.2 described a modified finite difference method that can be used to analyze the change of temperature and water content with flow length and time for a specified initial state of the matrix. In this chapter the dehumidifier is simulated in a single blow mode from the initial regenerated state to complete exhaustion in order to gain understanding of the physical behavior of the dehumidifier. The parameters were chosen to be NTU = 5 and Le = 1.

The inlet conditions of the fluid are chosen to be $t_{f\,in}$ = 25 °C and w_{in} = 0.015. The matrix may initially consist of either a dilute solution of LiCl, a saturated solution or solid LiCl, i. e., a mixture of anhydrate and monohydrate. Three cases are simulated to illustrate the behavior for each initial matrix state.

For the first case where the matrix already starts out as a dilute solution, the initial uniform matrix state was chosen to be t_m = 60 °C and W = 1.2. Figures 5.1 to 5.4 show temperature and water content of matrix and fluid as function of axial position with time as

the parameter. In Figure 5.1 and 5.2 it can be seen how the matrix properties change during the very short first time intervals (with 7.5 [1] time steps). The temperature of the matrix is very quickly cooled down to approximately 45 °C by the incoming process air while the moisture content remains nearly constant. Therefore the change in temperature represents a fast wave that propagates through the matrix.

In Figure 5.2 it can be seen how the air properties change during the same time increments. All the air profiles meet at the inlet conditions at x = 0. The air is heated up by the hot matrix, but with time, the matrix temperature drops and the air cannot be heated to the initial high temperatures. In the beginning the hot matrix is not able to dehumidify the air but as soon as the matrix cools down, the air humidity profiles shift to lower values. The first few profiles exhibit a minimum, i.e. the air is dried first and then takes up moisture again while passing through the matrix. This demonstrates how the mass transfer depends on temperature. Where the matrix is still hot the dehumidification process is slow or might be even reversed due to the high equilibrium vapor pressure for high temperatures. As soon as the fast wave has passed through the matrix the profiles of the fluid properties remain relatively constant. The exit conditions do not change significantly and there is a steady dehumidification and heating of the air. The matrix roughly maintains a constant temperature due to the latent heat of the sorption process.

The profiles in Figure 5.3 and 5.4 correspond to much larger time intervals (2000 time steps). The matrix takes up moisture until it is close to exhaustion. With increasing water content of the matrix, the dehumidification process becomes slower and the outlet air humidity increases to higher values. This change in moisture content represents a slow

---

[1] Different time step sizes have been used to follow the different wave speeds. To compare the results, the given number of time steps refer to $\Delta\zeta = 0.5$

wave. Because less water is sorbed, the latent heat is smaller and matrix and fluid temperatures are dropping.

Figures 5.5 and 5.6 show how the air outlet conditions change with time. Again, temperature and humidity drop very fast in the beginning (see Fig 5.5) and then change extremely slowly while approaching the inlet state (see Fig. 5.6).

For the initial matrix consisting of saturated solution (W = 0.5, t_m = 60 °C) the results are similar. First, a very fast wave propagates through the matrix changing the matrix temperature. However, after this wave passed through, there is a constant temperature throughout the matrix (see Fig. 5.7). Because of the constant equilibrium vapor pressure, there is a unique matrix temperature such that the enthalpy transfer meets exactly the latent heat of the mass transfer. This constant matrix temperature is maintained until the matrix reaches the water content of the solubility limit (approximately at W = 1.1 for t_m = 47 °C) and turns into a dilute solution. Now the equilibrium humidity of the matrix increases with increasing water content and the mass transfer slows down. Hence, there is less latent heat and the matrix temperature drops suddenly as shown in Figure 5.8. The front where the solubility limit is reached moves with a medium speed through the matrix. After the entire matrix has turned into a dilute solution, the same slow change of the matrix properties takes place as described above for the first case.

The corresponding results for the air outlet conditions are shown in Figure 5.9 and 5.10. After the fast change in the beginning the fluid properties stay constant for a long time until the above described wave front approaches the end of the bed and affects the outlet conditions. The point of inflexion represents the time when this wave front breaks through and the matrix contains dilute solution only. Finally the outlet conditions approach the inlet conditions.

For the last case, the initial water content of the matrix was taken to be W = 0.3. Therefore, the matrix contains of monohydrate and some anhydrate. The initial temperature was chosen to be t_m = 75 °C. After the first 20 time steps where the fast wave propagates through the matrix, the matrix temperature stagnates at 58 °C. At this high temperature the latent heat of the mass transfer equals the exchanged enthalpy as it also occurred for the saturated solution above.

During the next 420 time steps, the LiCl changes from solid state to saturated solution and crosses the discontinuity at W_{mono}. The profiles for the matrix properties are shown in Figure 5.11. As expected, the moisture content profiles are not differentiable at W_{mono}. Their slopes exhibit a sudden change. On the left side of this point the matrix has already changed its state of matter and now contains the saturated solution of LiCl. Hence the dehumidification process is slowed due to the suddenly smaller driving force. This results in a much smaller latent heat because less water is sorbed and the heat of sorption is smaller also (see Figure 3.10). Hence when the matrix undergoes the phase change, the temperature suddenly drops again, now, to the 47 °C where the latent heat of the mass transfer and the heat transfer are equal for the sorption process on the saturated solution as shown before. The locus where this phase change occurs represents another wave front that propagates through the matrix. This wave front is followed by the next one where the LiCl turns into the dilute solution as it also occurred in the second case as shown above. The effect of these wave fronts on the fluid properties is shown in Figure 5.12. Finally the matrix slowly approaches complete exhaustion.

The resulting air outlet conditions are shown in Figure 5.13. As before there is the fast wave in the beginning. Then temperature and humidity stay constant until the tem-perature drops because of the first wave front. This results first in better dehumidification until the

smaller driving force of the saturated solution reverses this effect and the humidity increases considerably. After this wave front passed through, humidity and temperature stay constant for a long time. Finally the temperature drops and the humidity increases as the second wave front approaches the end of the dehumidifier.

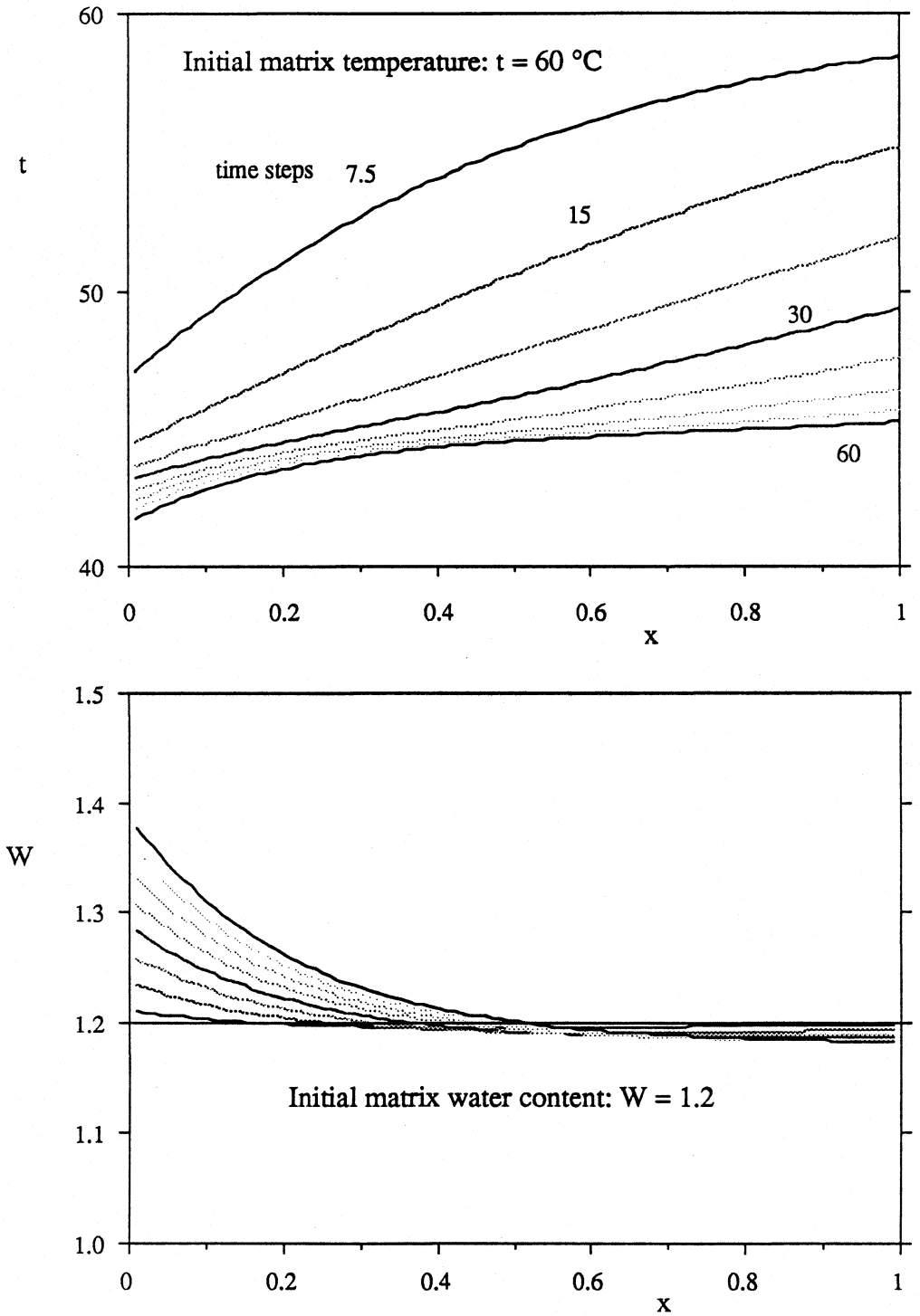

Fig. 5.1: Matrix water content and temperature,
Fast wave during first 60 time steps

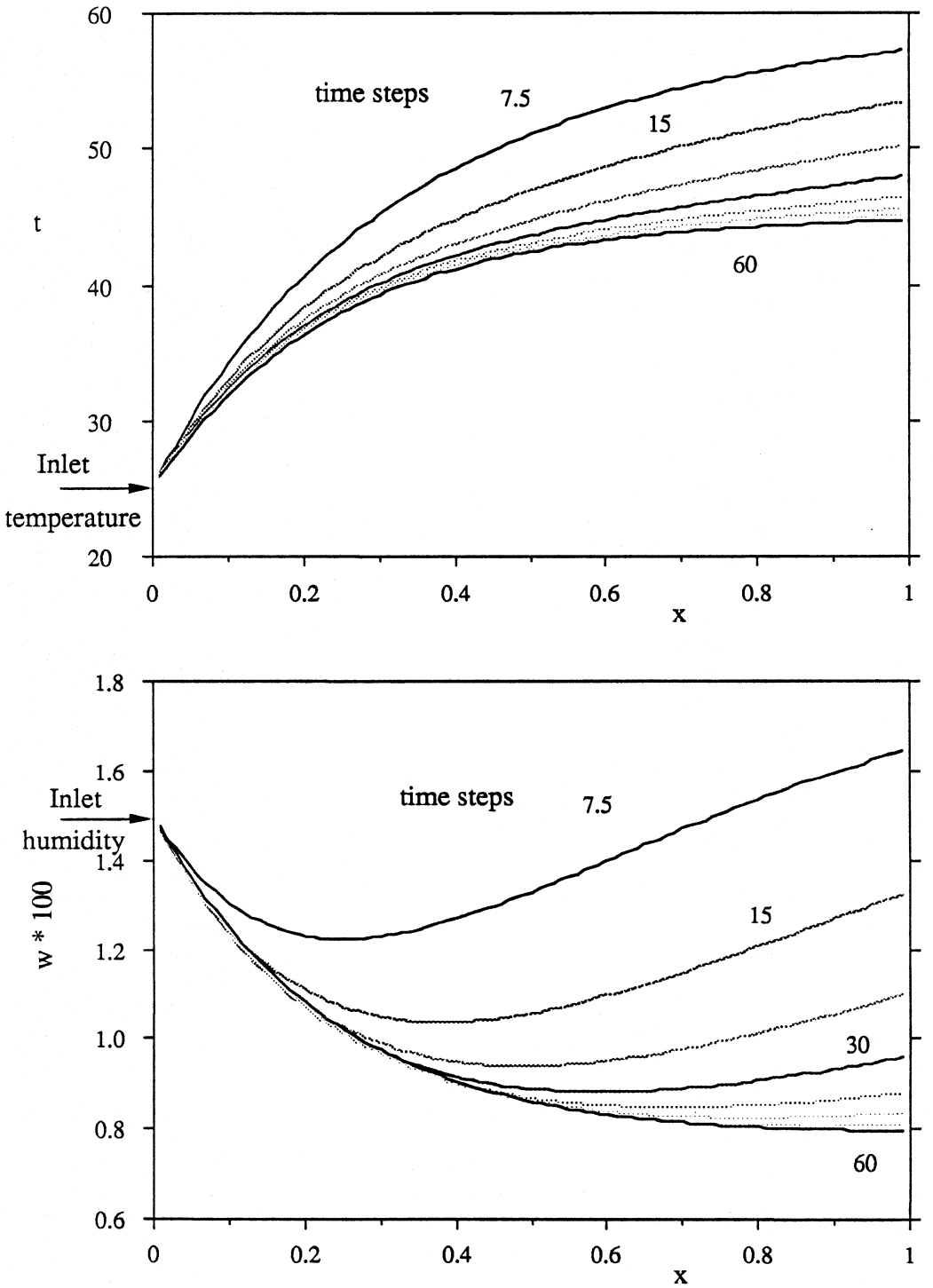

Fig. 5.2: Profiles of air states
during fast wave

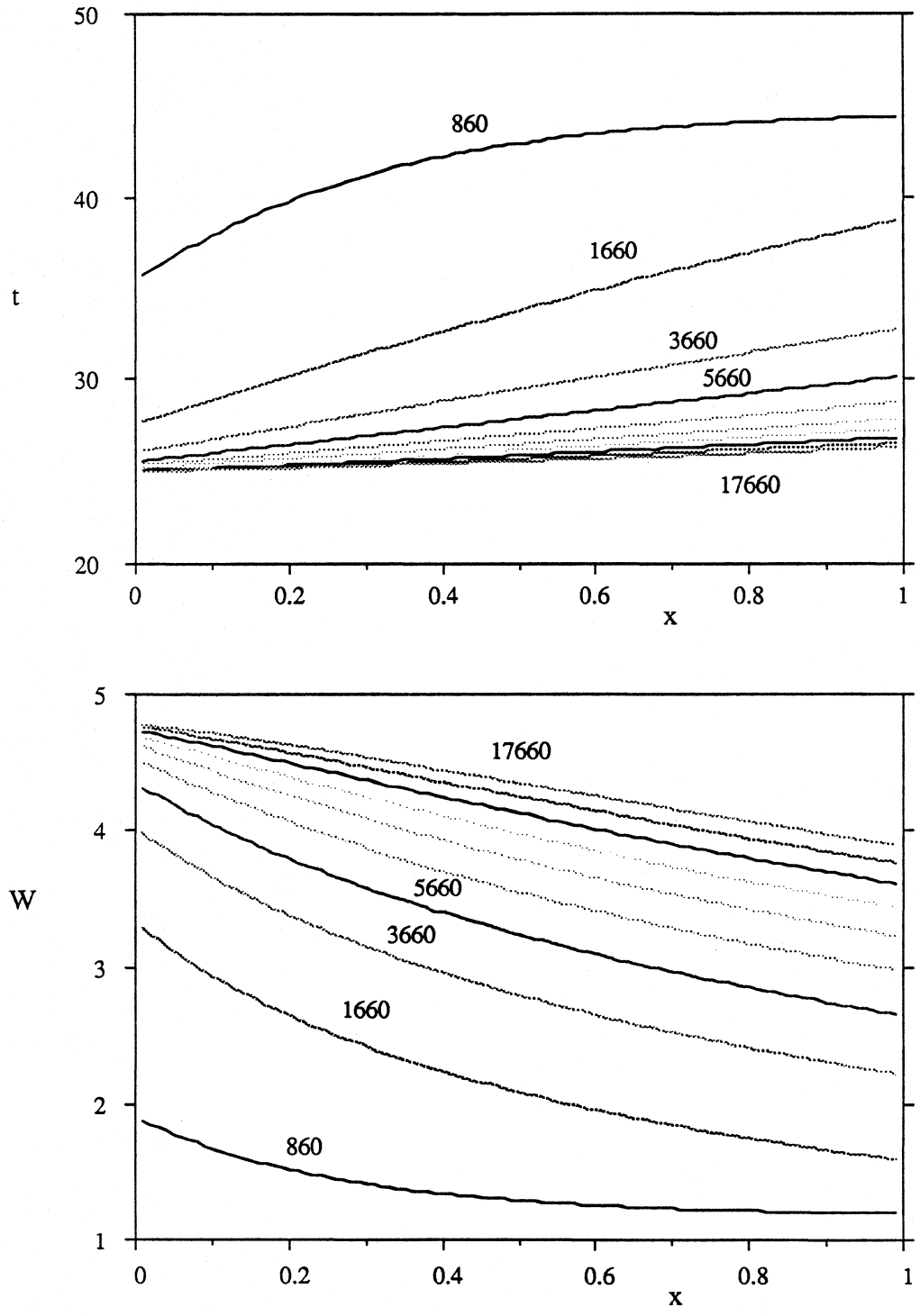

Fig. 5.3: Slow wave, matrix properties approaching exhaustion

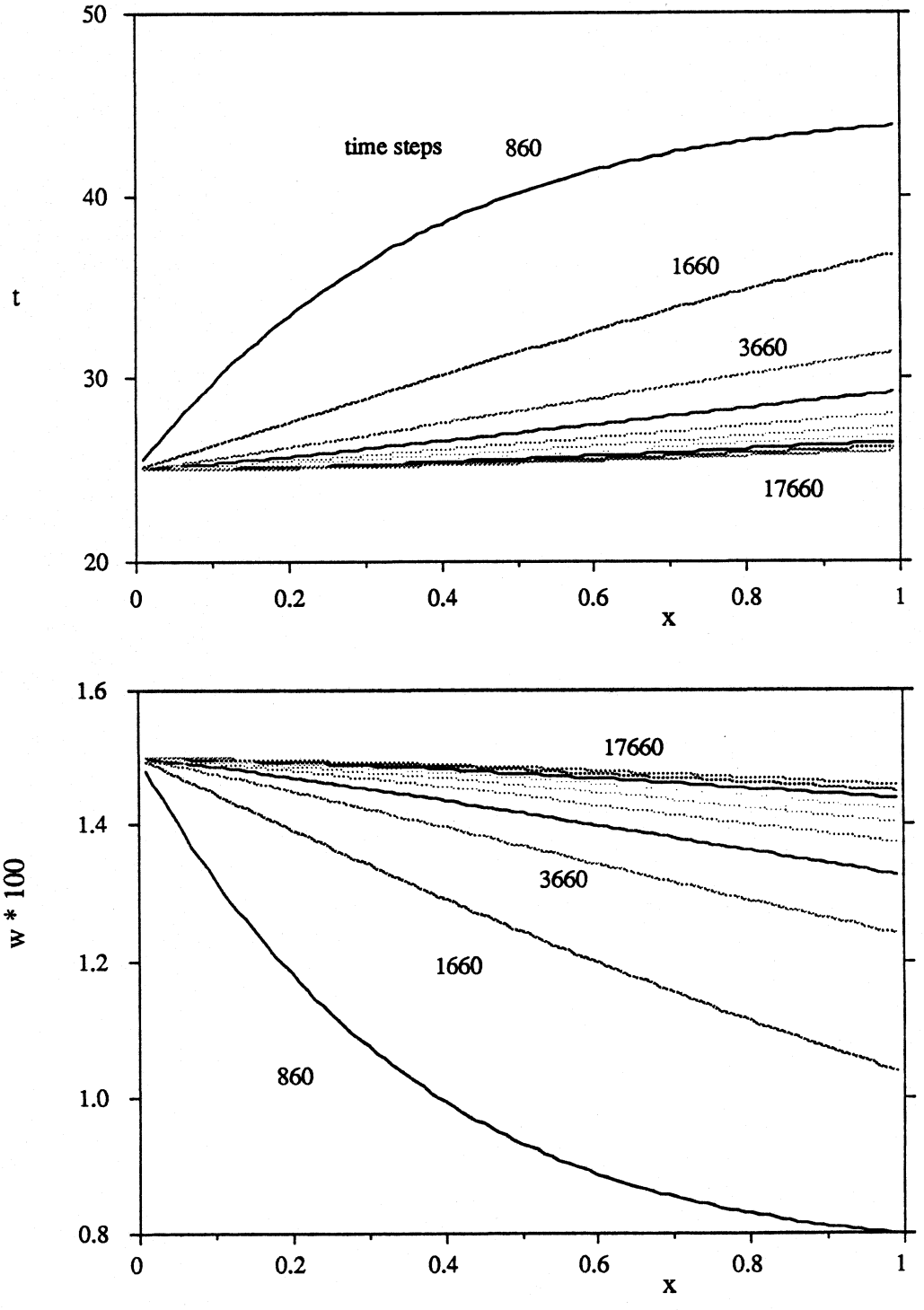

Fig. 5.4: Profiles of air properties, break through of dehumidifier

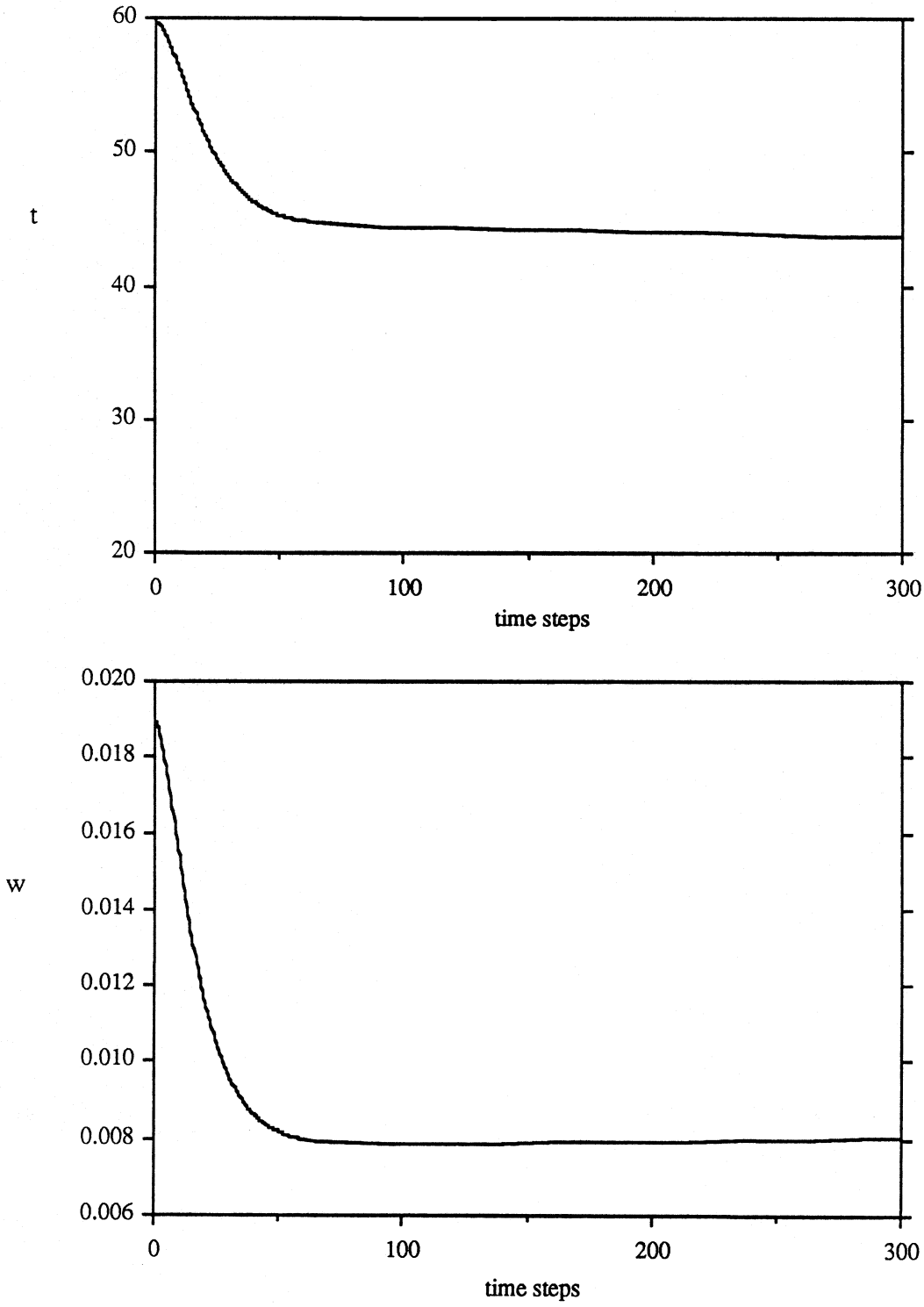

Fig. 5.5: Air outlet conditions, fast wave

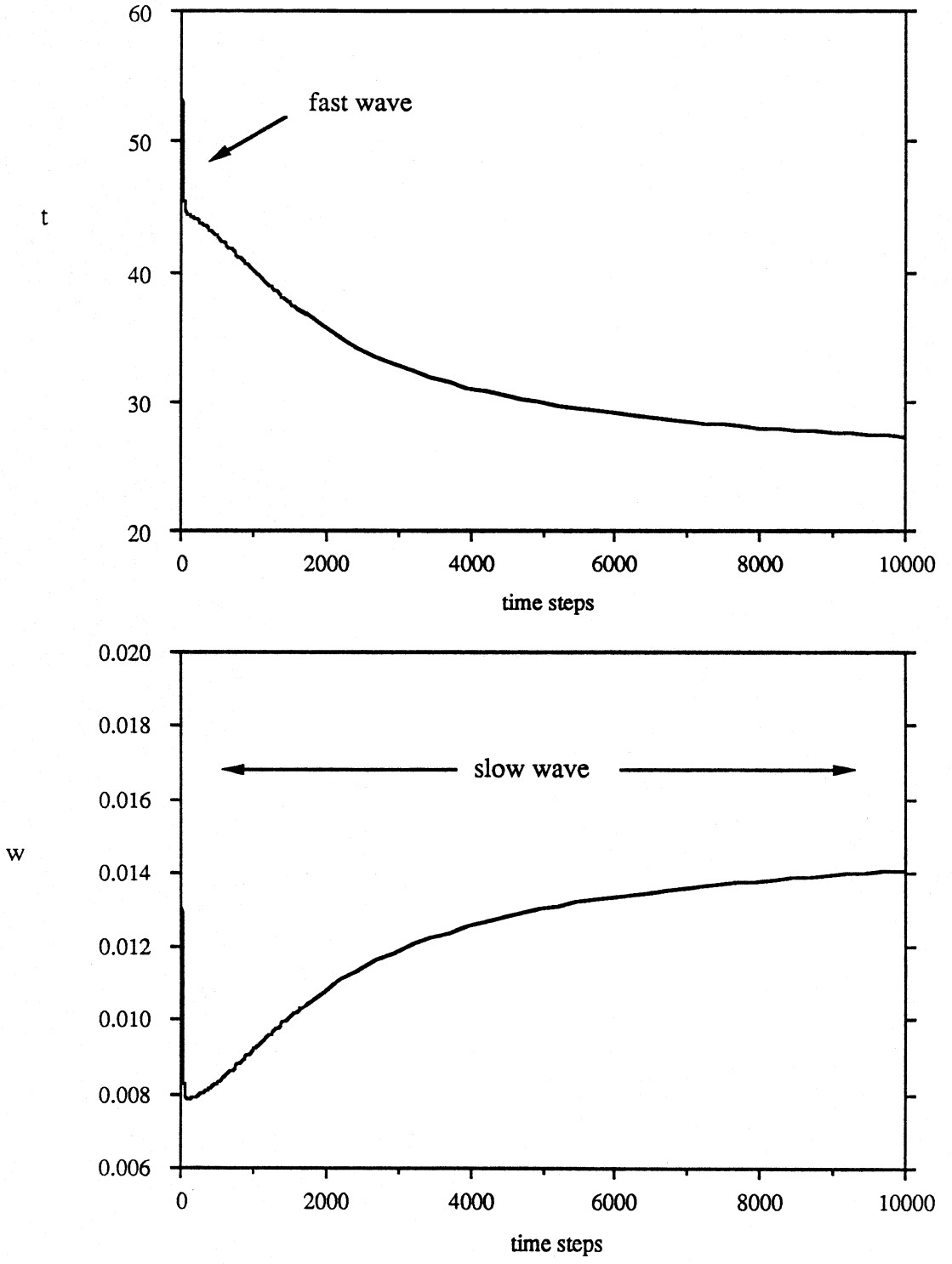

Fig. 5.6: Air outlet conditions, fast wave and break through

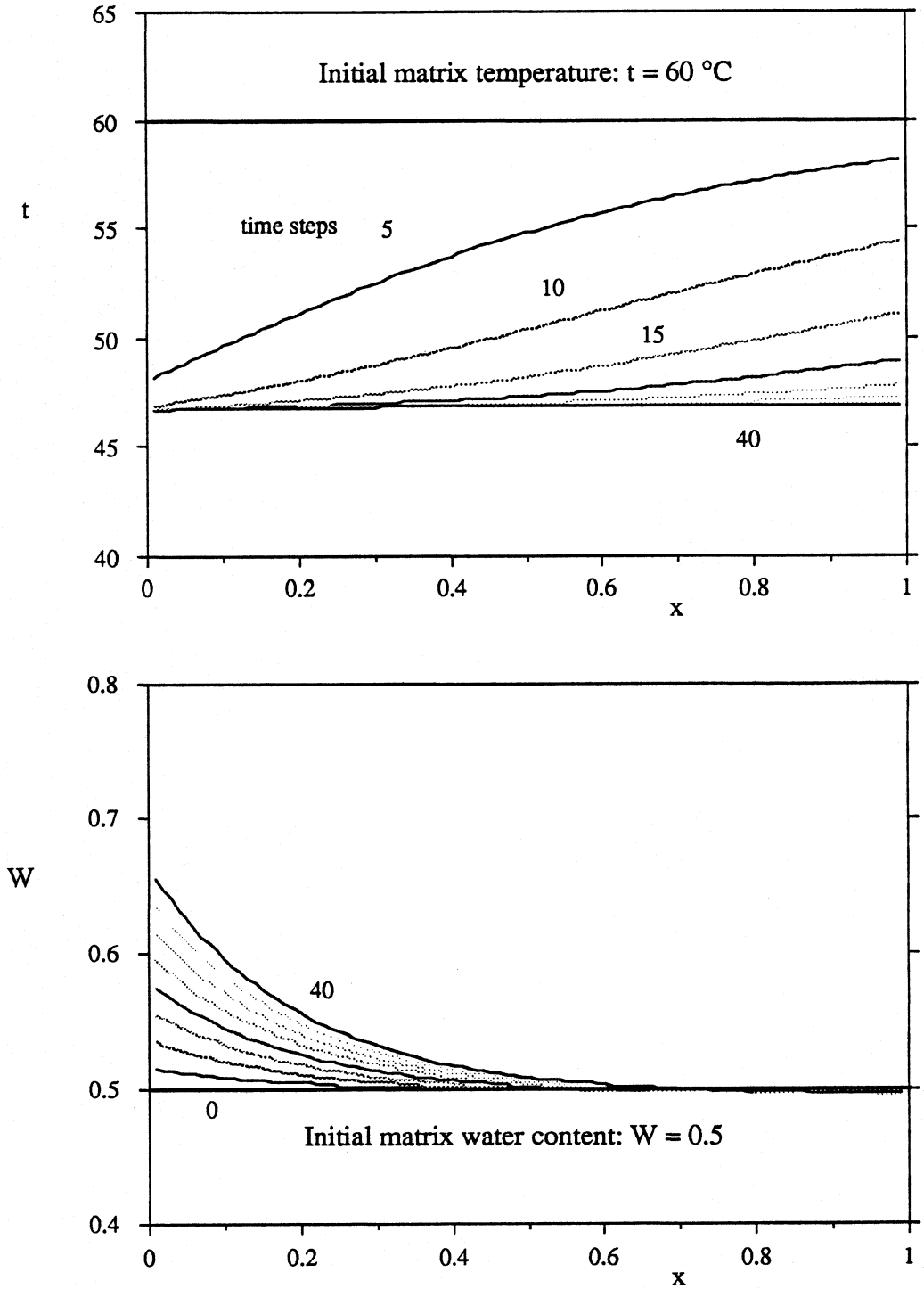

Fig. 5.7: Matrix properties during fast wave

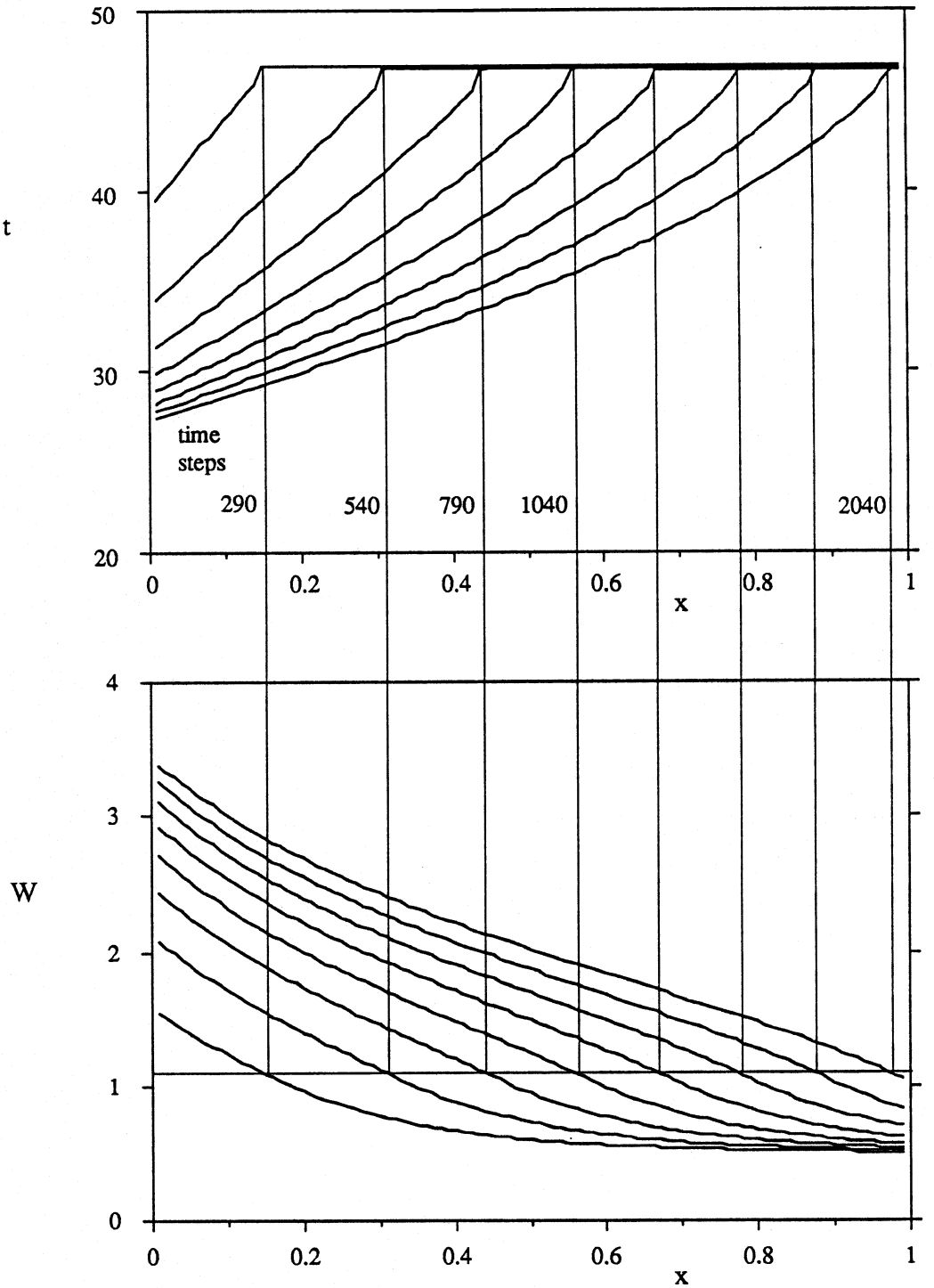

Fig. 5.8: Matrix water content and temperature
wave front corresponding to change to dilute solution

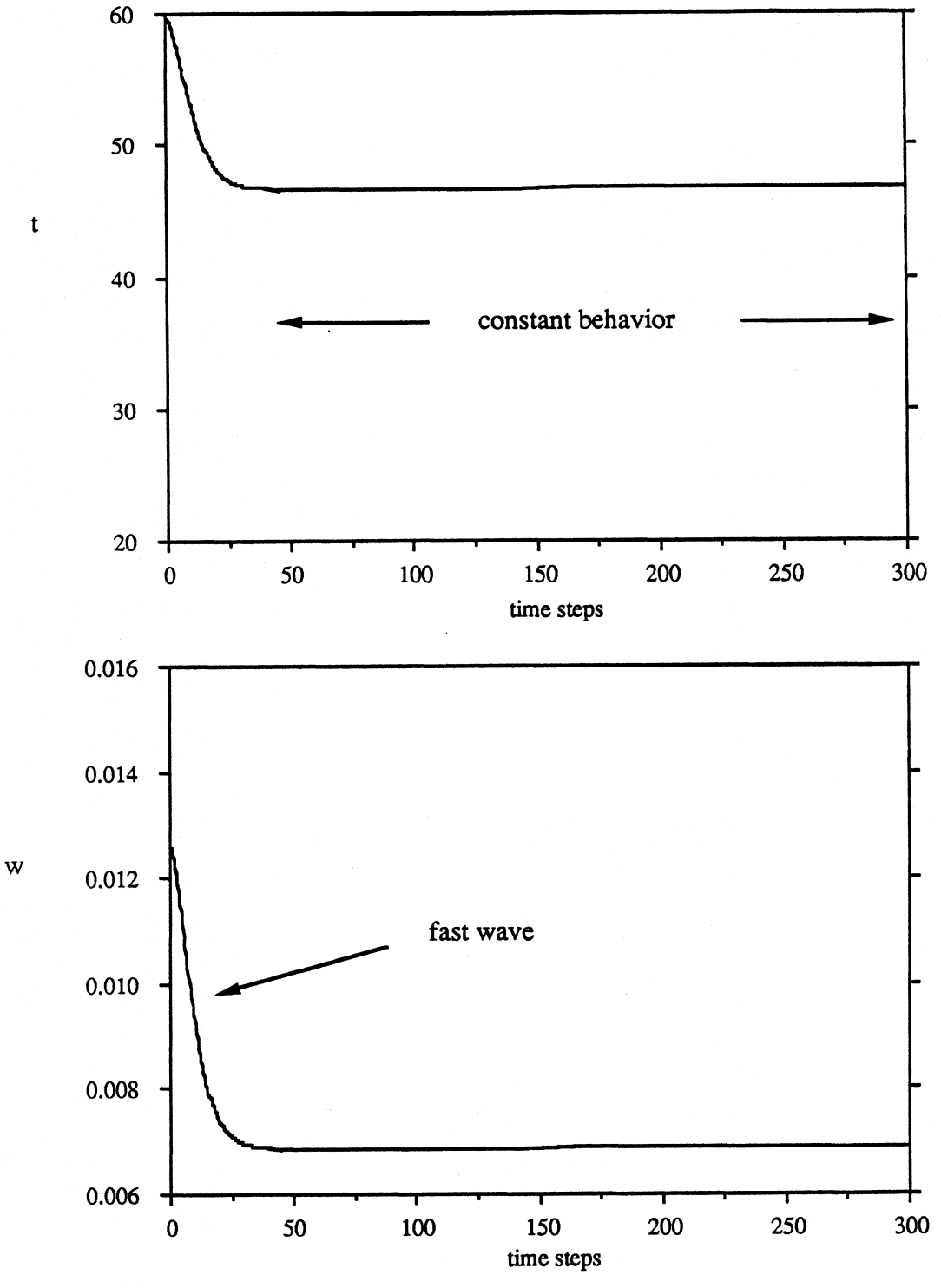

Fig. 5.9: Air outlet conditions, fast wave and constant behavior

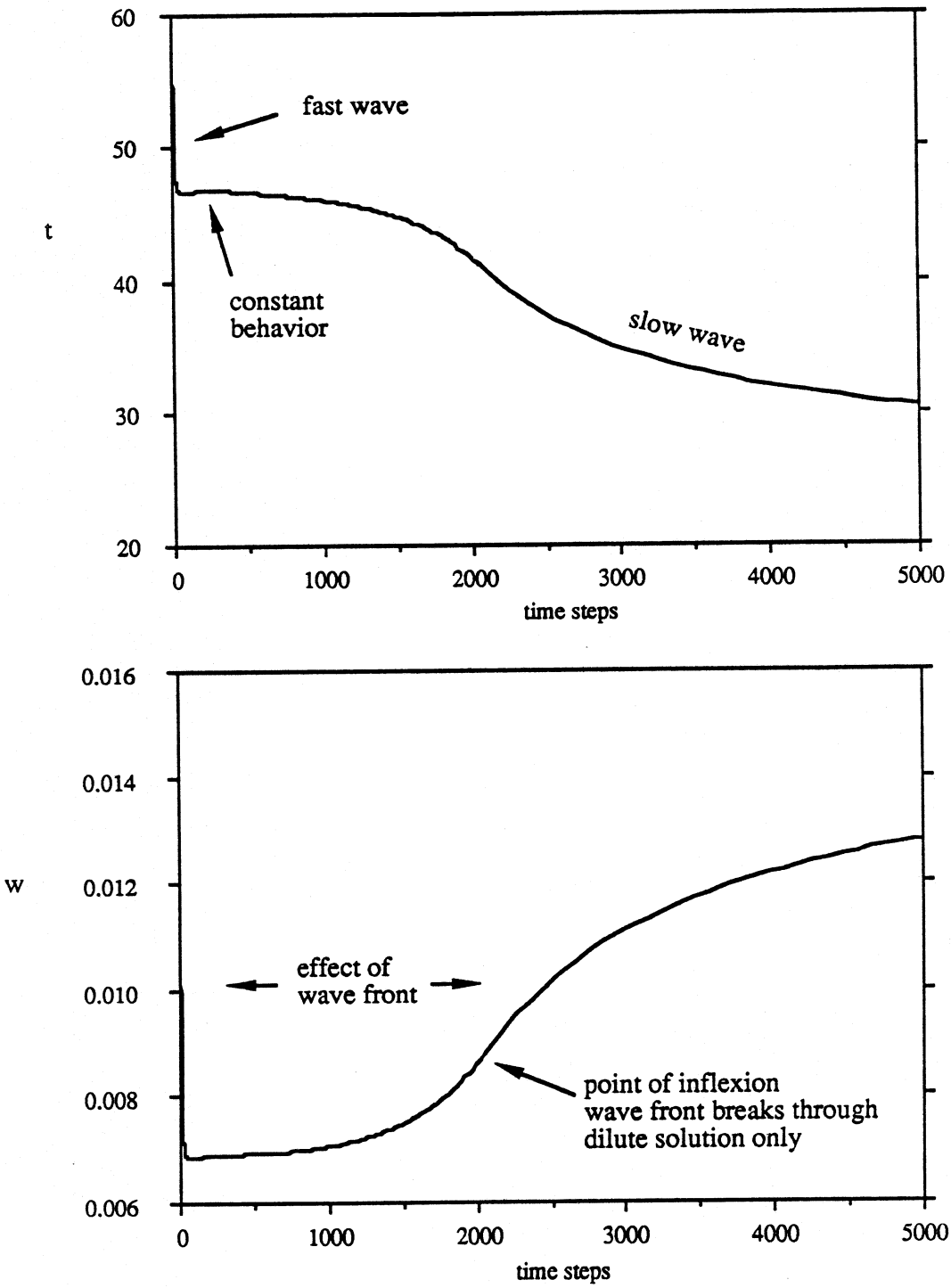

Fig. 5.10: Air outlet conditions, fast wave, constant behavior and break through

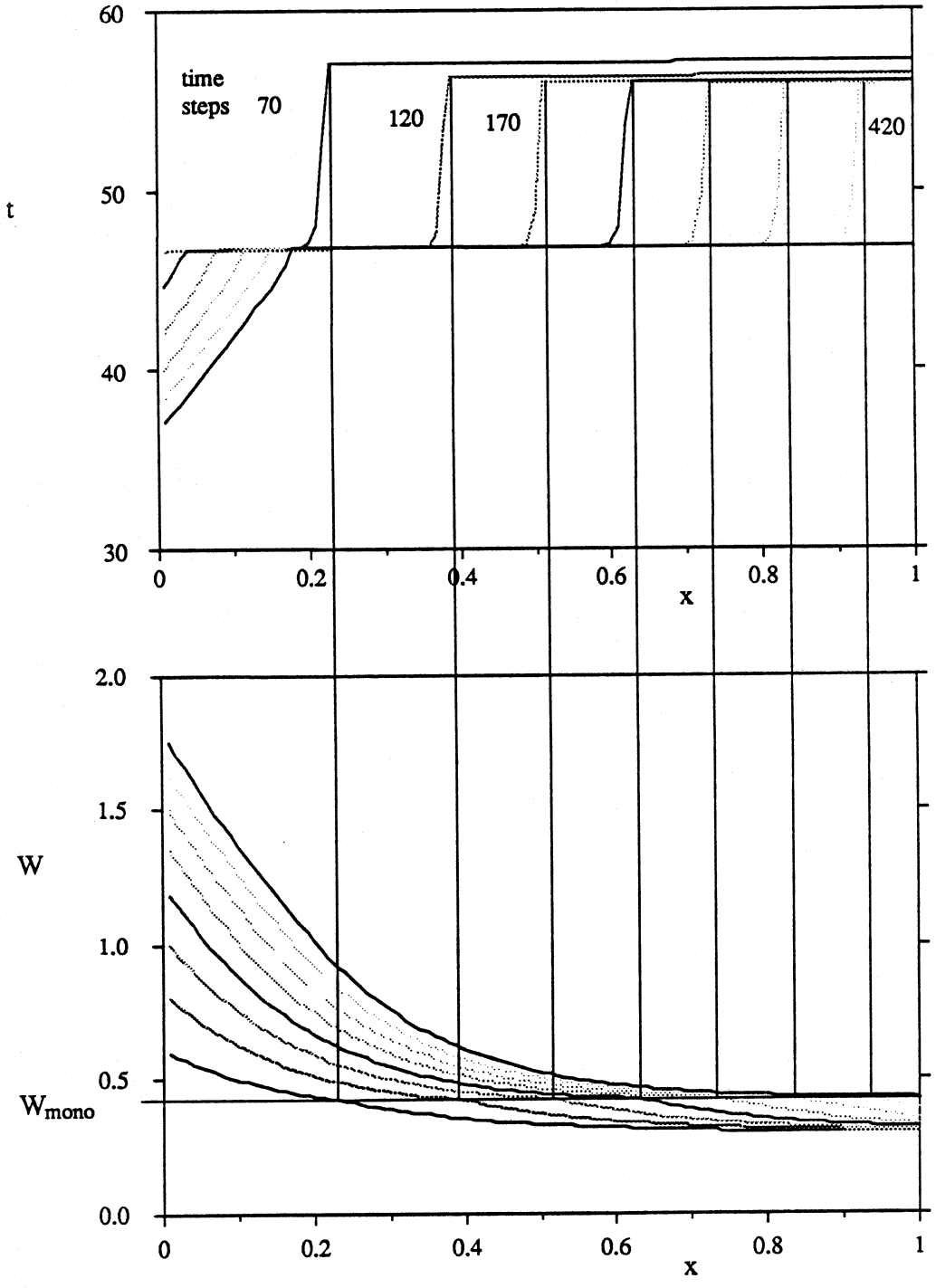

Fig. 5.11: Matrix water content and temperature profile
wave front corresponding to
change from solid to saturated solution

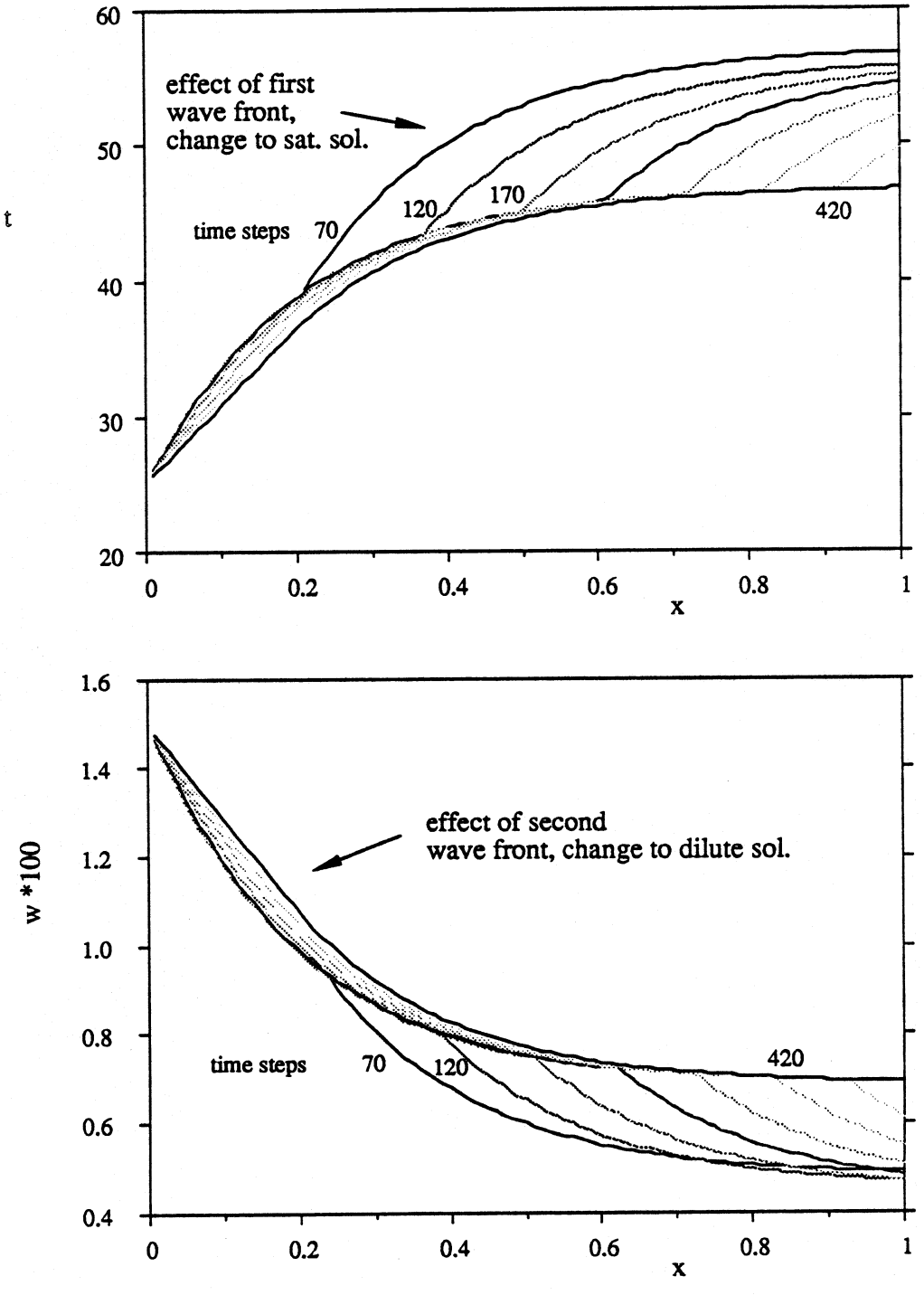

Fig. 5.12: Fluid properties during change
from solid to saturated solution

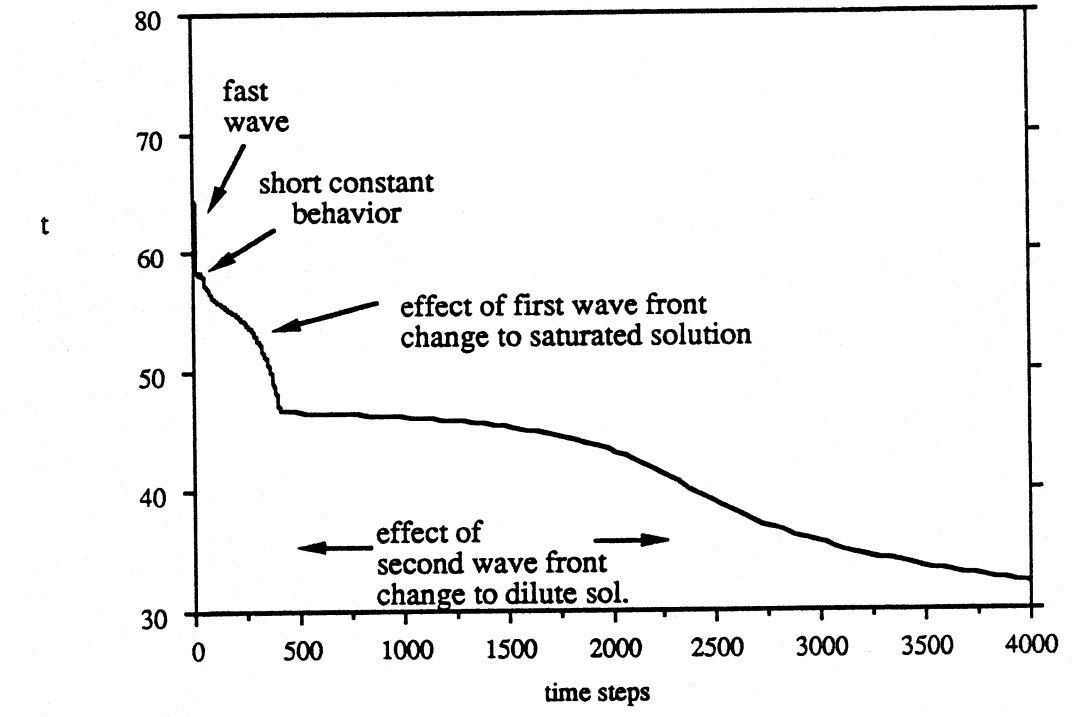

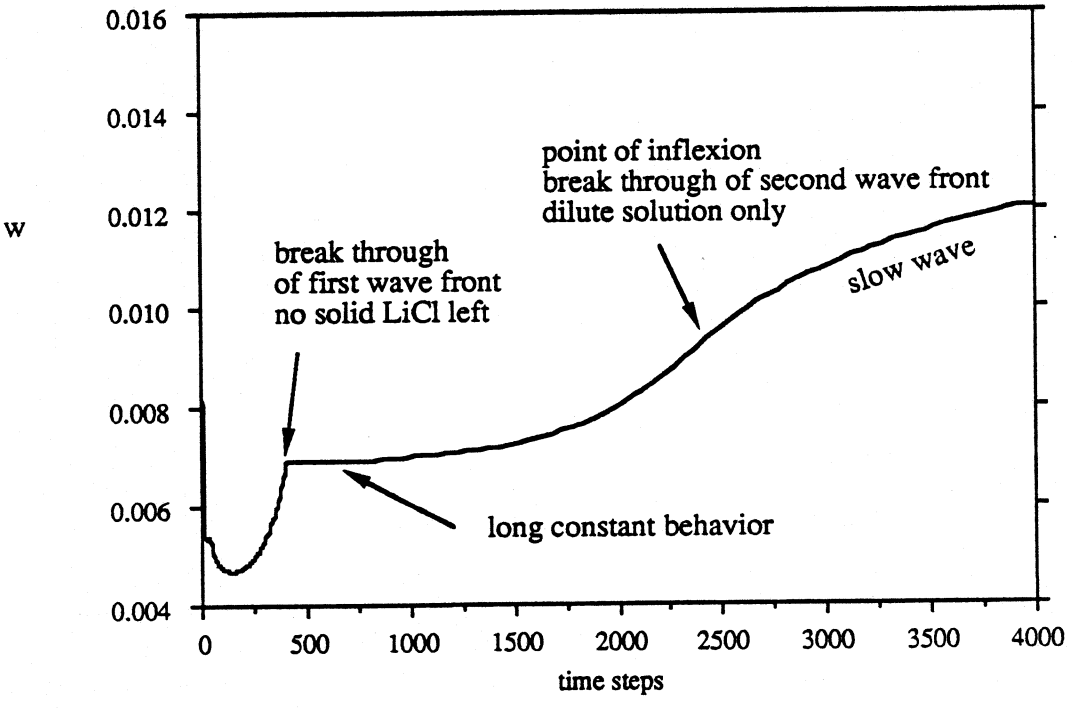

Fig. 5.13: Air outlet states, wave fronts

5.2 Regeneration of a processed matrix with uniform initial properties

For the regeneration period, things are similar to the process period. Again, there are three different cases depending on the inlet conditions of the regenerating air stream. The air inlet humidity may be either higher than the equilibrium humidity of the saturated solution w_{ms}, between w_{ms} and w_{am}, the equilibrium humidity of a mixture of anhydrate and monohydrate, or below w_{am} at inlet temperature. In the first case, the matrix can only be regenerated to a lower water content, but still contains a dilute solution of LiCl. In the second case the matrix may be regenerated to pure monohydrate, and in the third case completely water free anhydrate may be obtained. Since the matrix undergoes all the phase changes with the corresponding wave fronts, this latter case will be closely examined. For the higher inlet humidities in the other cases, one or both of these wave fronts do not take place.

The initial matrix state was chosen to be W = 2 and t_m = 25 °C. The inlet conditions were taken to be $t_{f\,in}$ = 75 °C and w_{in} = 0.008, which is smaller than w_{am} (75 °C) = 0.016. Again, a very fast wave propagates through the matrix first and increases the matrix temperature while the matrix water content hardly changes. This is shown in Figure 5.14 . Then the matrix slowly desorbs water. When it reaches the solubility limit and the LiCl turns into a saturated solution, the matrix temperature does not increase anymore, but stays constant as it also occurred in the process period. The locus where the solubility limit is reached can be identified by the edge in the temperature profiles and moves slowly through the matrix (see Fig. 5.15). It is followed by the wave front where the matrix has desorbed

so much water that it just contains pure monohydrate. Here the discontinuity in the isotherm occurs and the driving force for the mass transfer jumps to a lower value. Hence the water content profiles exhibit a knee and the temperature increases very suddenly due to the slower desorption process. Finally, the wave front follows where the matrix has desorbed all the water and contains anhydrous LiCl only. Now there is no mass transfer anymore and therefore no latent heat either. The temperature of the matrix approaches very fast the inlet air temperature due to the sensible heat exchange.

The effect of the described behavior of the matrix properties on the fluid conditions can be seen in Figure 5.16. The initial fast wave occurs in the first few time steps. Then the air outlet humidity decreases slowly while the temperature increases. Both curves exhibit three inflexion points. When the curves become steeper, one of the wave fronts approaches the end of the dehumidifier. The inflexion point represents the time when the front breaks through the end of the dehumidifier. After it passed through, the curves suddenly become flatter again. When the last wave front reaches the end the outlet conditions are the same as the inlet conditions and the matrix is completely regenerated.

Figure 5.17 show profiles for an inlet temperature of $t_{f\,in}$ = 60 °C and the same inlet humidity of w_{in} = 0.008. However, now the equilibrium humidity of a system of anhydrate and monohydrate w_{am} (60 °C) is 0.0059. Therefore, no anhydrous LiCl can be obtained and the desorption process will stop at W_{mono} = 0.4245. Hence, the last wave front from the previous case is missing and the matrix temperature already jumps to the inlet air temperature when W_{mono} is reached. Also, the air outlet conditions exhibit one less point of inflexion.

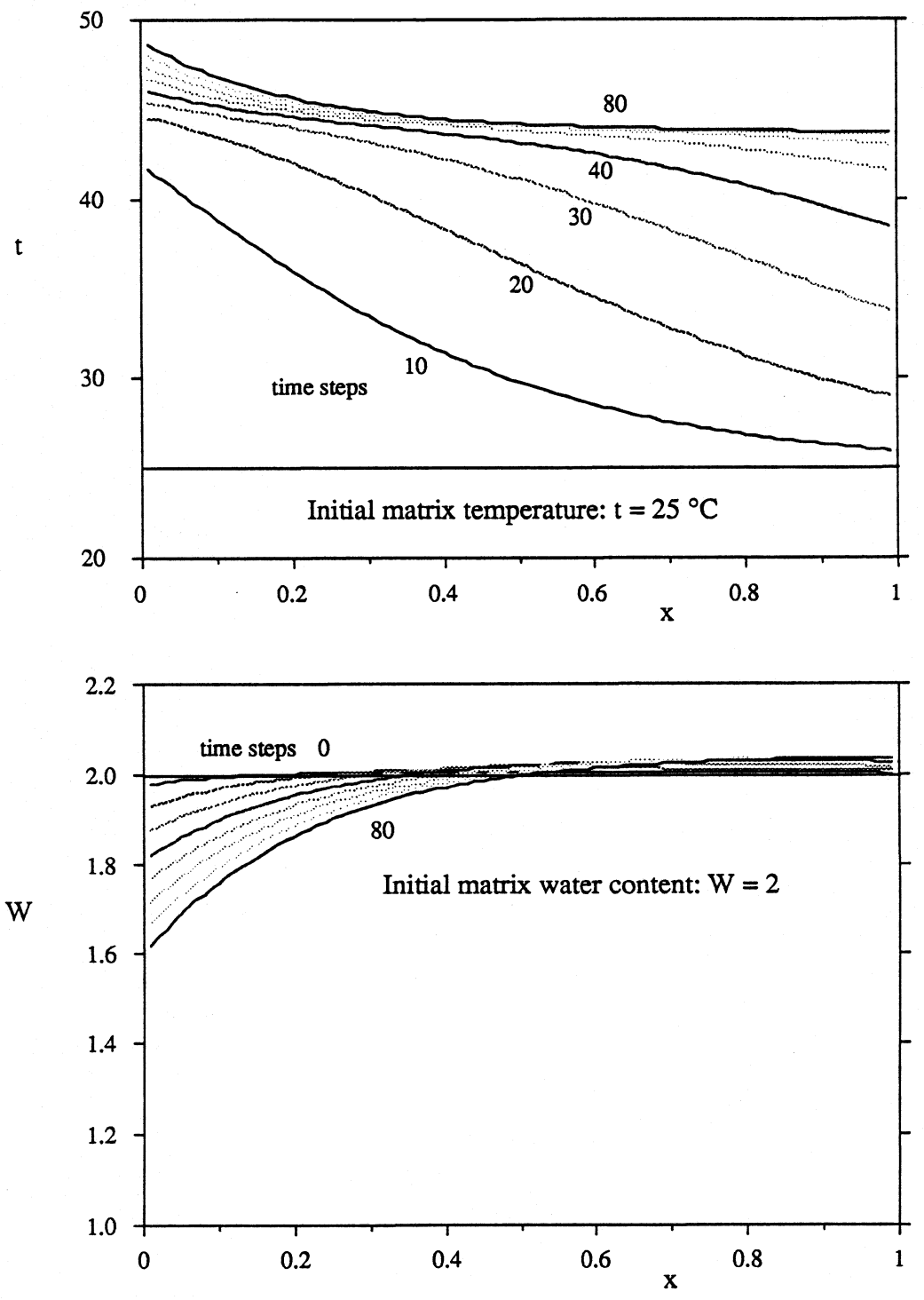

Fig. 5.14: Matrix water content and temperature
fast wave

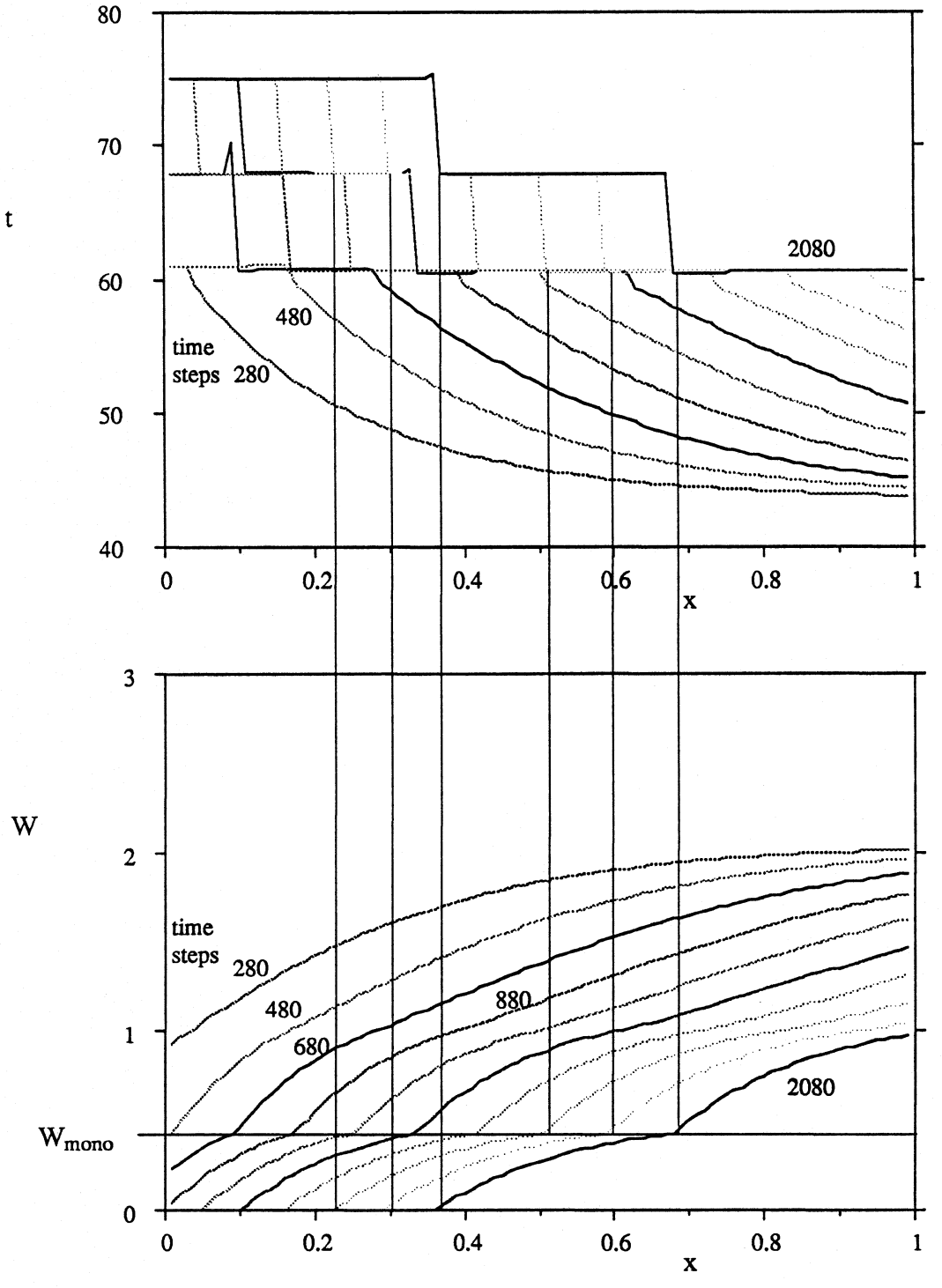

Fig. 5.15: Matrix temperature and water content wave fronts during regeneration

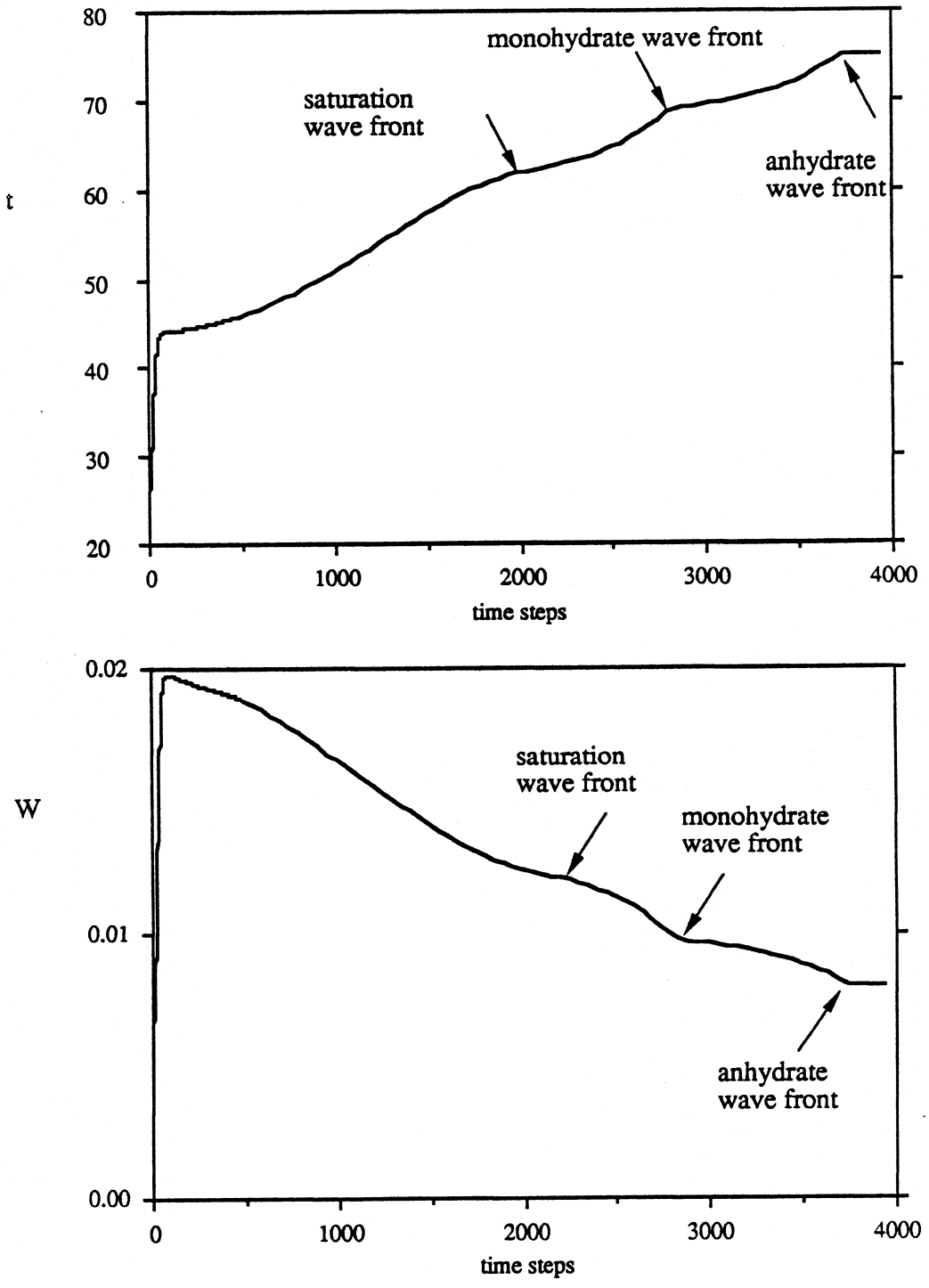

Fig. 5.16: Air outlet states, points of inflexion

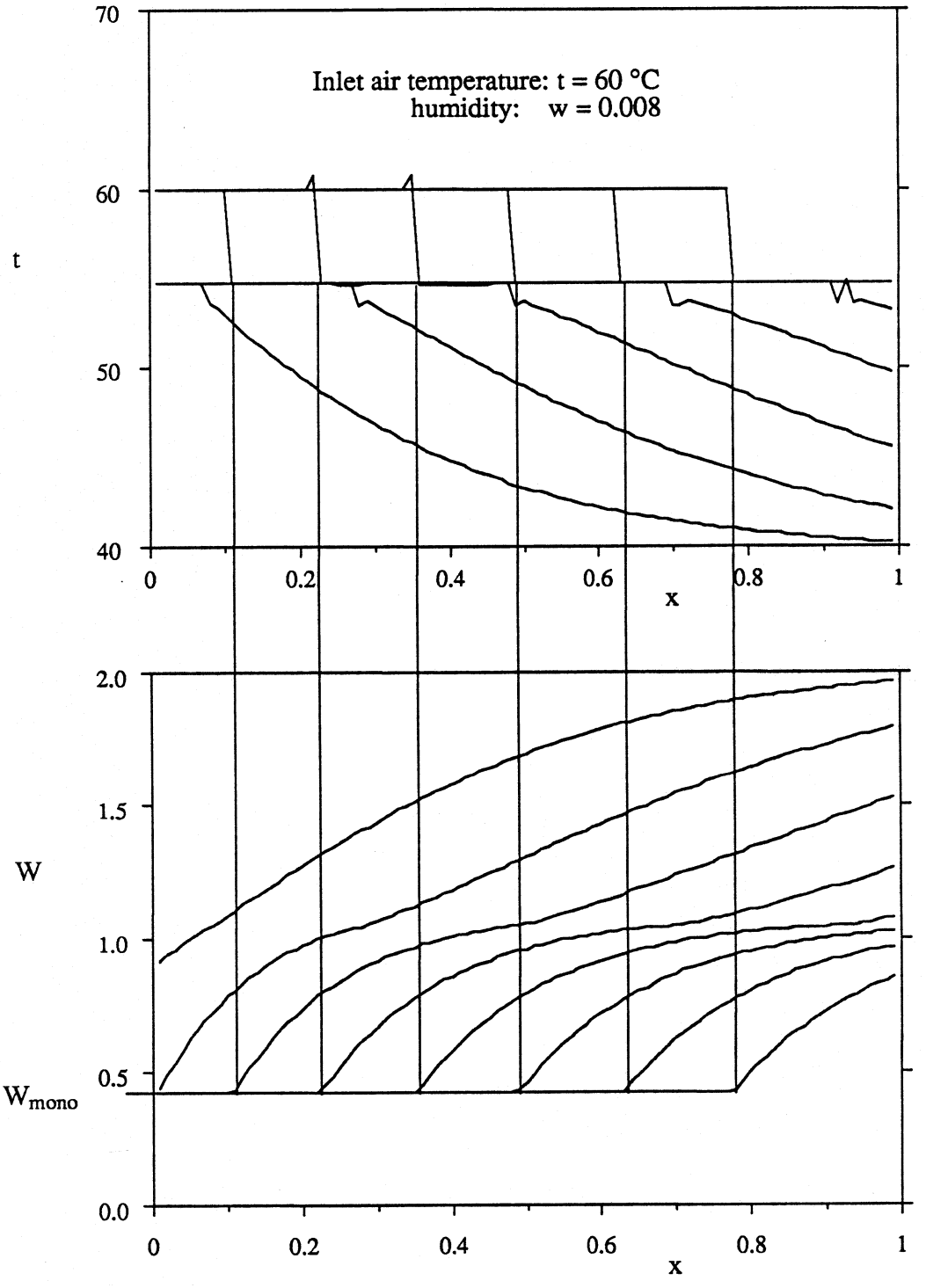

Fig. 5.17: Regeneration period
Matrix temperature and water content

5.3 Steady state of the Lithium Chloride Regenerator

The heat and mass regenerator has reached the steady state if the reversal condition (2.10 a) is met, i. e. the matrix exiting the regeneration period must have the same properties as the matrix entering the process period. Then the water content and the enthalpy of the entire regenerator is constant. Hence the mass and enthalpy balance of the two air streams must equal zero. This criterion for convergence is used in the numerical method of this work.

Figure 5.18 and 5.19 show the profiles of the matrix properties as a function of axial position with circumferential position as a parameter for the regenerator in steady state. For this simulation the process air inlet conditions were taken to be $t_{f\,in}$ = 25 °C and w_{in} = 0.015 while the regenerating air was taken to be at $t_{f\,in}$ = 75 °C with a humidity of w_{in} = 0.008. Hence the regenerating air is dry and hot enough to obtain anhydrous LiCl as shown in the previous chapter.

The bold line in both figures with the lowest water content and the corresponding line with the highest temperature represent the properties of the matrix leaving the regeneration period and entering the process period ($\Theta = \Theta_2$). The two corresponding bold lines with the highest water content and the lowest temperature stand for the state of the matrix leaving the process period and entering the regeneration period ($\Theta = \Theta_1$). At all other circumferential positions the matrix states will be between these limiting lines.

In Figure 5.18 and 5.19 additional profiles for circumferential positions in the process period and regeneration period, respectively, are shown. The limiting lines in both figures are the same due to the periodic initial conditions in steady state.

In the process period the temperature profiles quickly shift down to lower temperatures

due to the fast wave during the first few time steps (thin lines). The water content only changes slightly (no corresponding thin lines). The completely anhydrous matrix near the end of the dehumidifier (x = 0.95...1) immediately starts to sorb water. Hence the wave front in the temperature profile that separates the water free matrix with heat exchange only from the mixture of anhydrate and monohydrate moves immediately out of the matrix.

After the fast wave is over, the temperature profile shifts to the right without changing its shape significantly. The wave front that represents the phase change to saturated solution almost reaches the end of the dehumidifier before it is reflected back by the regeneration period. Its speed is decreasing. The speed of the following wave front that represents the change to dilute solution is slightly smaller and also decreasing.

In the regeneration period, the fast wave first shifts the temperature profile up, before the wave fronts move slowly back to the left.

The different phase regions and the locus of the wave fronts in a x-τ wave diagram can be seen in Figure 5.20. It shows how the wave fronts are reflected back and forth by the two periods. Since the wave speeds are changing the lines that separate the phase regions are not linear. The line that separates saturated and dilute solution is influenced by the fast wave since the solubility limit is temperature dependent.

If the regenerating temperature is lower or the humidity is higher such that w_{in} is larger than w_{am} ($t_{f\,in}$)then the phase region of water free anhydrate is missing in the wave diagram. The temperature profiles will jump up to the regenerating inlet temperature with the wave front where W_{mono} is reached. No anhydrous LiCl can be obtained. The water content profiles will stagnate at W_{mono}. Hence the dehumidification process will stop and very dry process air cannot be obtained. Therefore, it is crucial to heat the regenerating air to a temperature such that the temperature dependent w_{am} becomes smaller than the

regenerating air inlet humidity.

If the regenerating air inlet conditions are in the region of dilute solution none of the wave fronts will take place.

The effect of Γ on the outlet states is shown in Figure 5.21. The optimum value where the best dehumidification is obtained is near 0.02. For larger values of Γ (lower mass flow rate or faster rotating wheel), the water content profiles after processing and regenerating will be closer together than in Figure 5.18 or 5.19 while the temperature profiles will be roughly the same. The transition from dilute to saturated solution and from saturated solution to solid will be much steeper and almost sudden. The entire regenerator will be similar to three single regenerators in series, one containing dilute solution, one saturated solution and one solid LiCl. The process outlet humidity is higher because the fast wave takes relatively more time out of the entire period and the initial high temperatures are less favorable to the dehumidification process.

For smaller values of Γ (slower rotating wheel or increased air flow rate), the wave fronts will move faster and may move out of the regenerator before they are reflected back by the regenerating period. If the wave front where the matrix changes to saturated solution moves out of the regenerator before the end of the period, the dehumidification process near the end of the regenerator where the final outlet humidity is obtained will be slowed down or will even stop. The profiles in Figure 5.18 represent an operation near the optimum because this wave front comes close but does not move out of the dehumidifier.

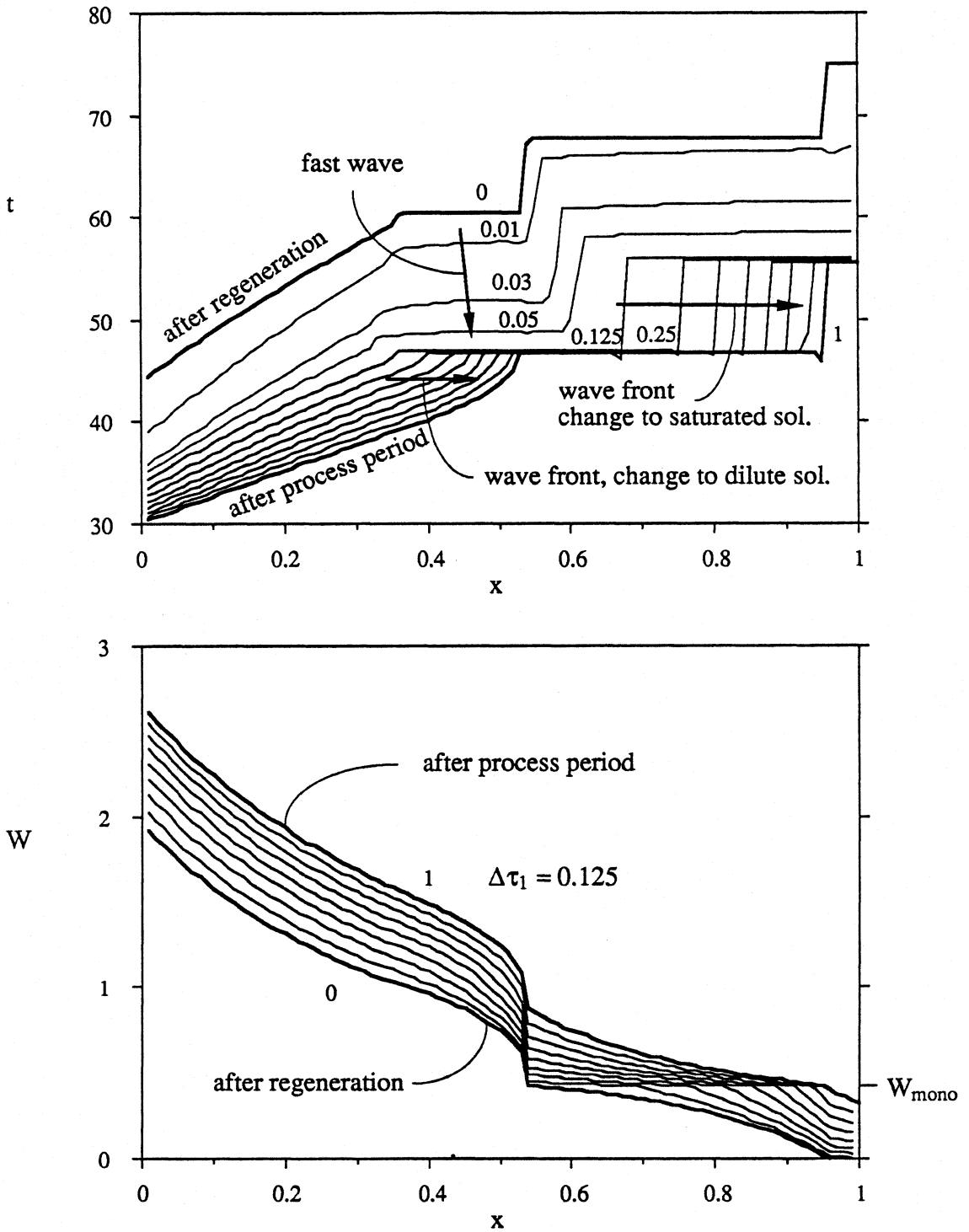

Fig. 5.18: Steady state of regenerator profiles during process period
$\Gamma_1 = \Gamma_2 = 0.02$

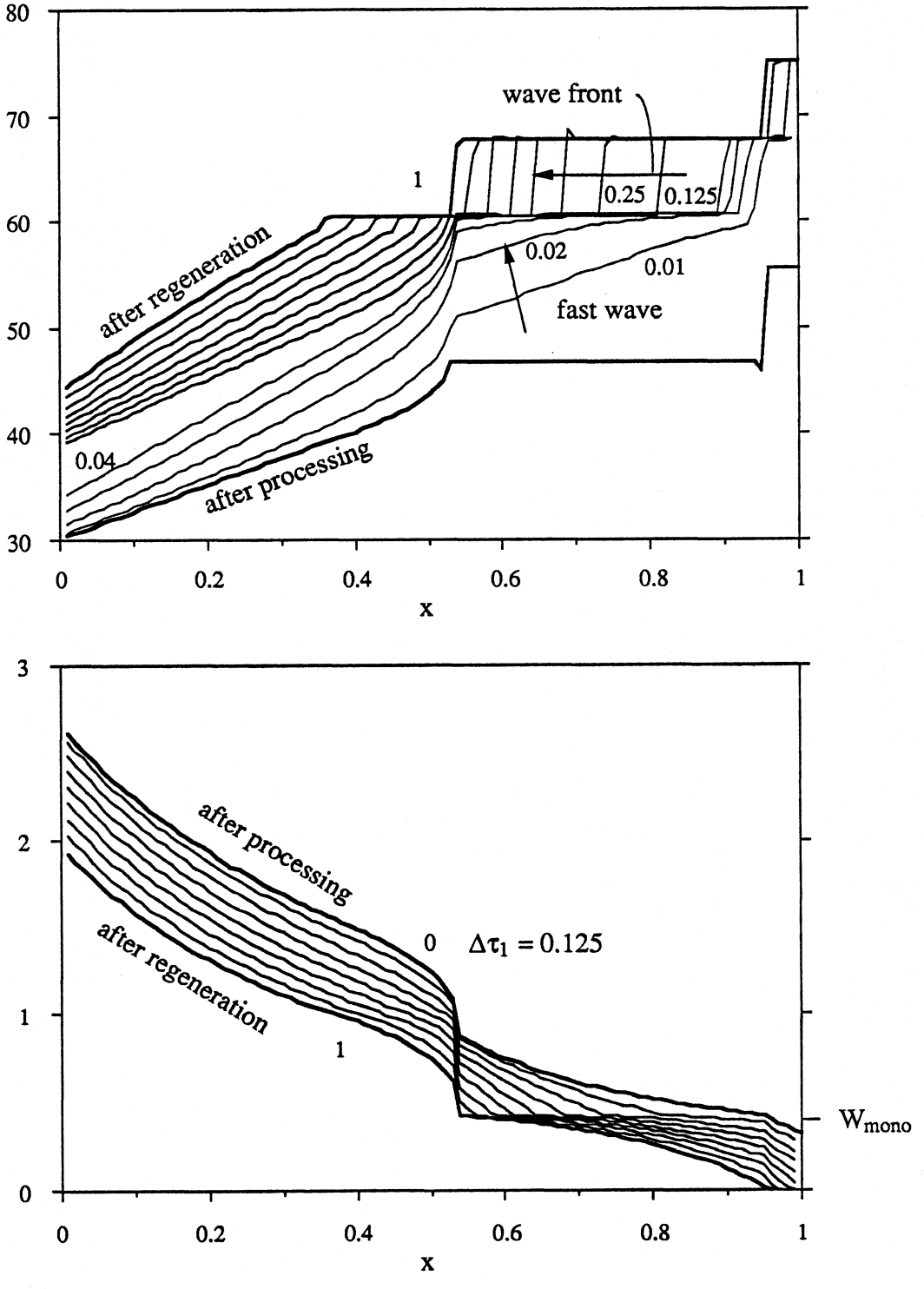

Fig. 5.19: Steady state of regenerator profiles during regeneration

$\Gamma_1 = \Gamma_2 = 0.02$

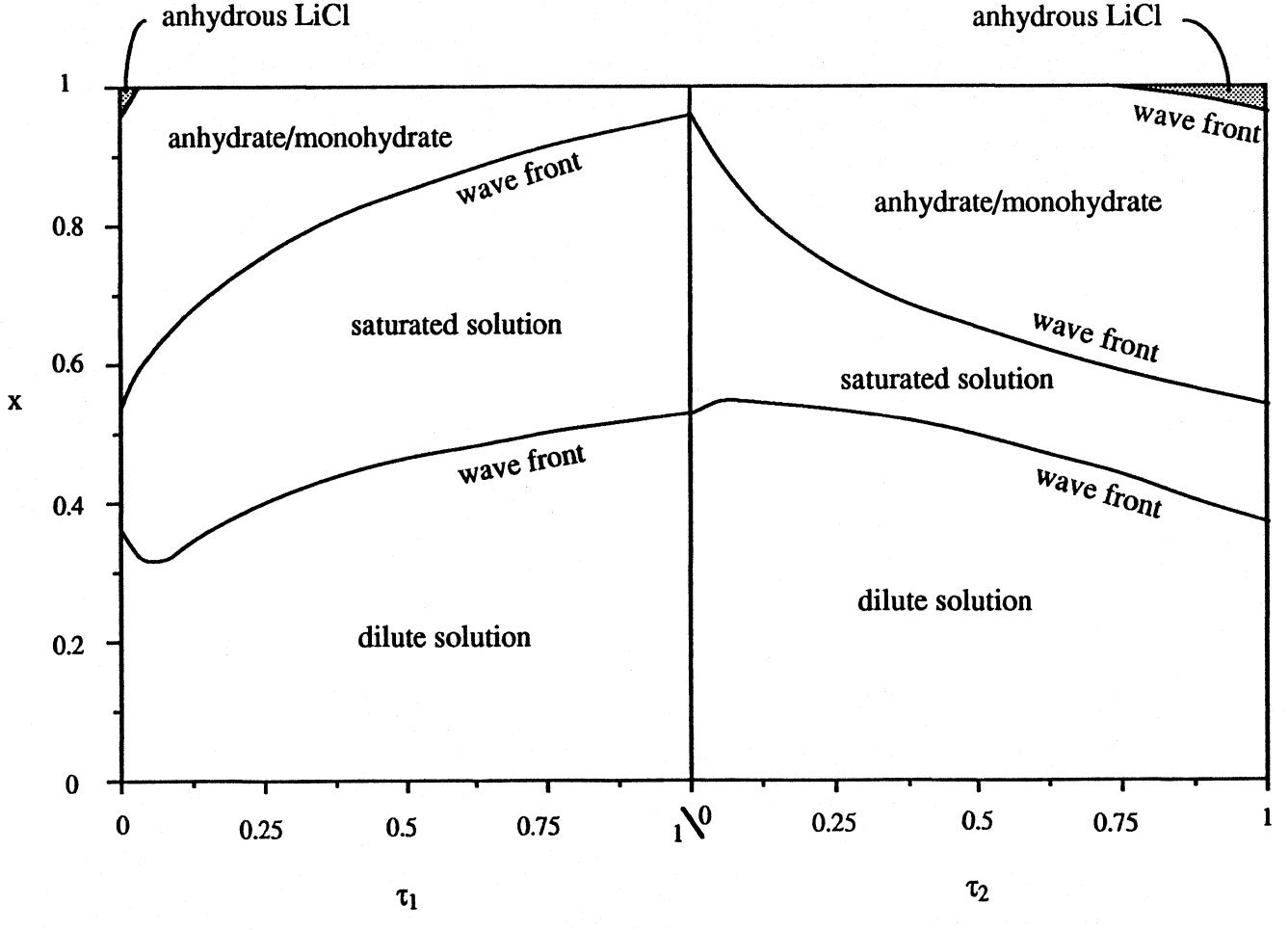

Fig. 5.20: Wave diagram with phase regions

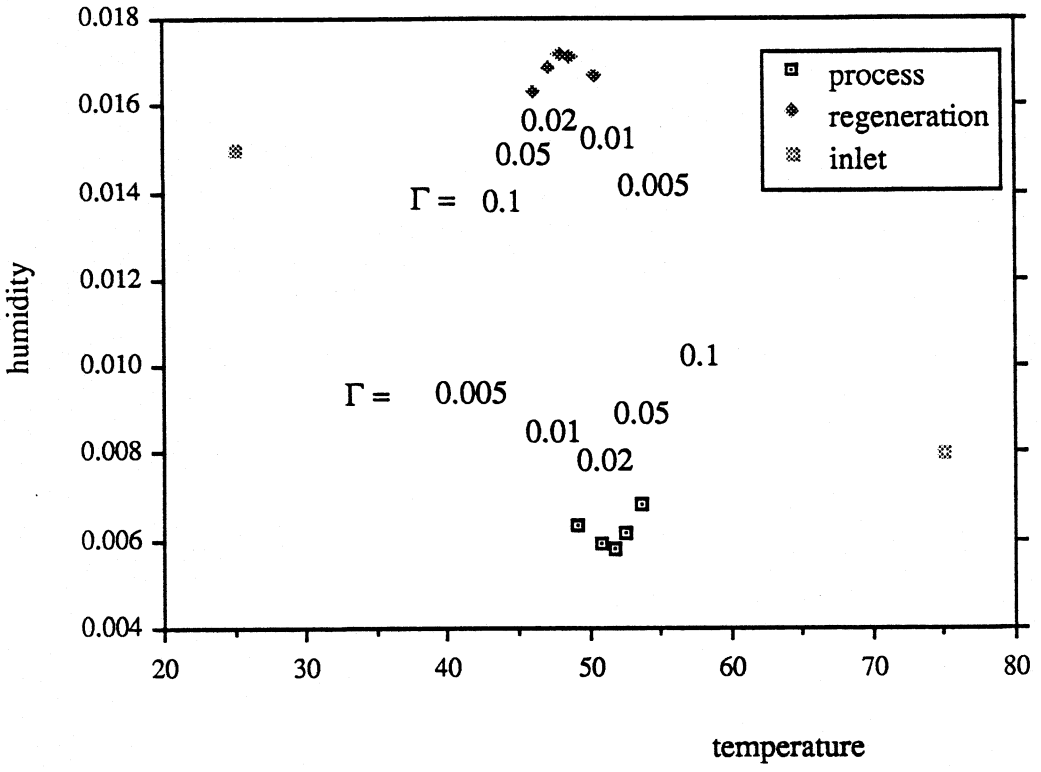

Fig. 5.21: The effect of Γ on the outlet states

COMBINED F-POTENTIALS FOR LITHIUM CHLORIDE

6.1 Definition of Combined F-Potentials

An approximate analytical solution to the governing equations (2.7) is available through an analogy to the sensible heat exchanger. This analogy is based on the introduction of two new dependent variables, the combined F-potentials, and the analogous capacitance ratios γ_i.

Let **X** be the matrix of the partial derivatives of the matrix properties with respect to the fluid properties [1]:

$$\mathbf{X} = \begin{bmatrix} \frac{\partial I}{\partial i} & \frac{\partial I}{\partial w} \\ \frac{\partial W}{\partial i} & \frac{\partial W}{\partial w} \end{bmatrix} \tag{6.1}$$

Thus **X** is a state property function. Then the analogous capacitance ratios are defined as eigenvalues of **X**:

[1] All the partial derivatives with respect to i are at constant w and vice versa

$$\det (\mathbf{X} - \gamma_i \mathbf{I}) = 0 \tag{6.2}$$

Equation (6.2) yields a quadratic expression in γ_i where γ_2 is taken to be the smaller root. The combined F-potentials are defined by the linearly independent eigenvectors of X as follows:

$$\mathbf{X}\left[\begin{array}{cc} \frac{\partial F_i}{\partial i} & \frac{\partial F_i}{\partial w} \end{array}\right]^T = \gamma_i \left[\begin{array}{cc} \frac{\partial F_i}{\partial i} & \frac{\partial F_i}{\partial w} \end{array}\right]^T \qquad i = 1,2 \tag{6.3}$$

The eigenvectors are normal to lines of constant F_i in the i,w-plane and define these lines. However they do not define the value of the F-potential itself. From equation (6.3) it is not even possible to evaluate $\frac{\partial F_i}{\partial i}$ and $\frac{\partial F_i}{\partial w}$ because the length of an eigenvector is not specified by the eigenvalue problem. The two equations for $\frac{\partial F_i}{\partial w}$ and $\frac{\partial F_i}{\partial i}$ that result from equation (6.3) are linearly dependent. Therefore it is also not possible to evaluate the F_i relative to a reference point. It can only be determined how the $\frac{\partial F_i}{\partial w}$ and $\frac{\partial F_i}{\partial i}$ relate to each other, i. e. the direction of the eigenvector. Hence the ratio of $\frac{\partial F_i}{\partial w}$ and $\frac{\partial F_i}{\partial i}$ can be evaluated by

$$\frac{\frac{\partial F_i}{\partial i}}{\frac{\partial F_i}{\partial w}} = \frac{\gamma_i - \frac{\partial W}{\partial w}}{\frac{\partial I}{\partial w}} \tag{6.4}$$

By replacing enthalpy i with temperature and by eliminating γ_i with equation (6.2) it is shown by Maclaine-cross that [2]

[2] Now all partial derivatives with respect to w are at constant t and vice versa

$$\frac{\frac{\partial F_i}{\partial t}}{\frac{\partial F_i}{\partial w}} = \frac{1}{2}\left\{ \left(\frac{\partial I}{\partial t} - \frac{\partial i}{\partial t}\frac{\partial W}{\partial w} - \frac{\partial i}{\partial w}\frac{\partial W}{\partial t}\right) + (-1)^i \sqrt{\left(\frac{\partial I}{\partial t} - \frac{\partial i}{\partial t}\frac{\partial W}{\partial w} - \frac{\partial i}{\partial w}\frac{\partial W}{\partial t}\right)^2 - 4\,\frac{\partial i}{\partial t}\frac{\partial W}{\partial t}\left(\frac{\partial W}{\partial w}\frac{\partial i}{\partial w} - \frac{\partial I}{\partial w}\right)} \right\} \left(\frac{\partial W}{\partial w}\frac{\partial i}{\partial w} - \frac{\partial I}{\partial w}\right)^{-1}$$

$$i = 1,2 \qquad (6.5)$$

This is equivalent to

$$-\left[\frac{\partial w}{\partial t}\right]_{F_i} = \frac{\frac{\partial F_i}{\partial t}}{\frac{\partial F_i}{\partial w}} = f(w,t)$$

where f(w,t) is the right hand side of equation (6.5). This equation can be numerically integrated by a 4th order Runge Kutta method to obtain lines of constant F_i in a psychrometric chart.

6.2 Transformation of the Governing Equations

The above definition of the F-potentials can be applied to the fluid state i,w or to the matrix state i_m,w_m where i_m and w_m are enthalpy and water content of air in equilibrium with the matrix at t_m,W. Therefore F_{if} and F_{im} have to be distinguished.

For unity Lewis number, the transfer equation for enthalpy in (2.3) can be written in a completely analogous form to the mass transfer equation. The enthalpy of air in equilibrium with the matrix state is (compare equation 3.1)

$$i_m = c_f t_m + h_{wv} w_m$$

The assumption of unity Lewis number is closely satisfied for air-water vapor mixtures. Then, the enthalpy transfer equation can be expressed as

$$\frac{\partial i}{\partial z} = h_{w,j} A \mu_j (i_f - i_m) \qquad (6.6)$$

For a set of conservation laws and transfer equations of this form, Maclaine-cross and Banks [9] derived the transformed equations by replacing the enthalpy and water content with F-potentials as dependent variables:

$$\mu_j \gamma_{im} \frac{\partial F_{im}}{\partial \Theta} + v_j \frac{\partial F_{im}}{\partial z} = 0$$

$$i = 1,2 \qquad (6.6)$$

$$v_j \frac{\partial F_{if}}{\partial z} = h_{w,j} A \mu_j (F_{if} - F_{im})$$

However, one important assumption has to be made:

$$\frac{\partial F_{i,m}}{\partial i_m} = \frac{\partial F_{i,f}}{\partial i_f} \quad ; \quad \frac{\partial F_{i,m}}{\partial w_m} = \frac{\partial F_{i,f}}{\partial w_f}$$

This assumption implies that the derivatives of the F_i are constant on a path between the fluid and matrix states. This is exactly true if the lines of constant F_i are linear and parallel or if there is complete equilibrium, i. e. the fluid and matrix states are the same. Therefore the error becomes smaller with increasing transfer coefficients. However, near the discontinuity, fluid and matrix states are never close. Also the F_i may change discontinuously at this point as shown below. Thus this assumption is very questionable for LiCl near its discontinuous phase changes.

Comparison to the governing equations of a sensible heat regenerator shows that the F-potentials correspond to temperature. Therefore the RHMX can be regarded as a superposition of two F_i exchangers. However the two F_i exchangers are only independent (or equations (6.6) are only uncoupled) if each $\gamma_{i,m}$ depends only on the corresponding $F_{i,m}$ and not on the other $F_{3-i,m}$. However this is a rather crude approximation for most desiccants.

The performance of each F_i regenerator may be characterized by an efficiency. An average $\bar{\gamma}_{ij}$ for each period j is determined [10] and used to evaluate the four dimensionless groups that are commonly employed to compute the regenerator efficiency [10].

However, the outlet states of the air streams cannot be directly calculated from the

efficiency for the F-potentials and the inlet states, since explicit values of the F-potentials as a function of air state are not known. The non-linear analogy method, proposed by Banks [20] uses invertible curve fits for the F_i as functions of t and w. An alternative approach was developed by Maclaine-cross and Banks [9] and is called the intersection point method. The two intersection point air states for a set of inlet conditions are defined as the air states with the F_i-potential of the inlet air of period i (or period 3-i) and the F_{3-i}-potential of the inlet of period 3-i (or i, respectively), thus the two points on a psychrometric chart, where the lines of constant F-potential through the inlet air states intersect. They can be obtained by integrating equation (6.5) along lines of constant F-potentials. The intersection points represent the maximum exchange of one F-potential and no exchange of the other one. Applying the efficiency to the intersection points, the outlet states can be predicted.

6.3 F_1, F_2-charts for LiCl

Psychrometric charts with lines of constant F-potential are called F_1, F_2-charts. Many publications [10] provide F_1, F_2-charts for silicagel. F_1, F_2-charts for LiCl in dilute solution are provided by Maclaine-cross [1]. For LiCl in saturated solution or in solid state, integration of equation (6.5) leads to some difficulties, because the partial derivatives of the matrix properties may become zero or infinite.

The partial derivatives of the matrix enthalpy can be replaced by partial derivatives of the water content according to equations (3.36) and (3.37). Then equation (6.5) can be rearranged to (also using equation (3.3)):

$$\left[\frac{\partial w}{\partial t}\right]_{F_i} = \frac{c_m}{2h_s\dfrac{\partial W}{\partial w}} - \frac{1}{2}\frac{\dfrac{\partial W}{\partial t}}{\dfrac{\partial W}{\partial w}} - \frac{1}{2\,h_s}\frac{\partial i}{\partial t} + (-1)^i \sqrt{\left\{\frac{c_m}{2h_s\dfrac{\partial W}{\partial w}} - \frac{1}{2}\frac{\dfrac{\partial W}{\partial t}}{\dfrac{\partial W}{\partial w}} - \frac{1}{2\,h_s}\frac{\partial i}{\partial t}\right\}^2 - \frac{1}{h_s}\frac{\partial i}{\partial t}\frac{\dfrac{\partial W}{\partial t}}{\dfrac{\partial W}{\partial w}}} \tag{6.6}$$

The critical terms in this equation are $\frac{\partial W}{\partial t}/\frac{\partial W}{\partial w}$ and $1/\frac{\partial W}{\partial w}$. Figure 6.1 shows a three dimensional plot of the equilibrium matrix water content as function of temperature t and humidity w. Lines of constant temperatures (isotherms) and lines of constant humidity (isopiestics) are drawn in this graph. At zero matrix water content, there is a horizontal plane for low humidities and high temperatures. This plane is bounded by the isostere for a

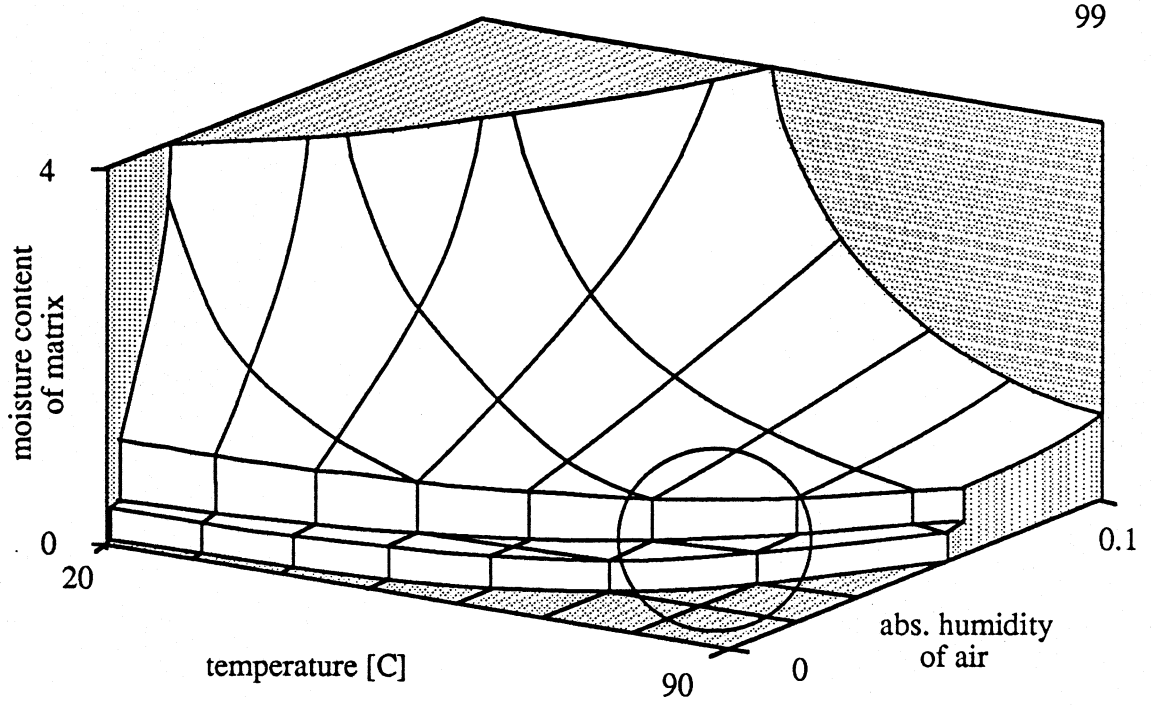

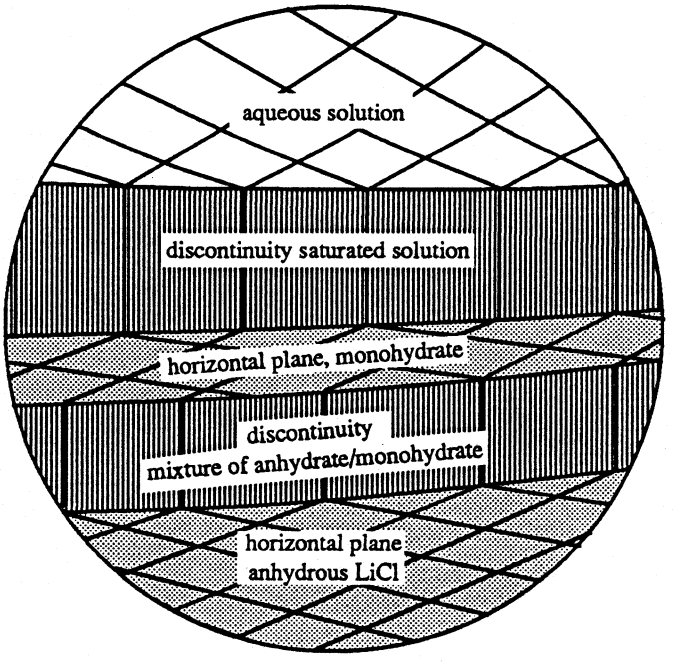

Fig. 6.1: Sorption equilibria for LiCl in 3 dimensions
Water content of matrix as function of temperature and humidity

system of anhydrous LiCl and monohydrate. At this line, the water content jumps from zero to W_{mono}, the water content of pure monohydrate, and therefore this line is a discontinuity line. Then for increasing humidity and decreasing temperature another horizontal plane follows that corresponds to monohydate LiCl, until with another discontinuous step change the LiCl turns into an aqueous solution. This second step change occurs at the solubility limit. Therefore, the solubility limit is another discontinuity line.

In the region of anhydrous LiCl or monohydrate, i.e. at the two horizontal planes, the two derivatives $\frac{\partial W}{\partial t}$ and $\frac{\partial W}{\partial w}$ are zero. At the discontinuity lines $\frac{\partial W}{\partial t}$ and $\frac{\partial W}{\partial w}$ are simultaneously infinite and in the region of dilute solution they are both finite. Since the ratio of the two derivatives can be replaced by

$$-\left[\frac{\partial w}{\partial t}\right]_W = \frac{\partial W}{\partial t} / \frac{\partial W}{\partial w} \tag{6.7}$$

it is shown by Figure 6.2 that this ratio is always finite because the isosteres w(t) at constant W are always continuous.

This leaves the term $1/\frac{\partial W}{\partial w}$ as the only troublemaker in equation (6.6). Three cases have to be distinguished: The first case corresponds to finite $\frac{\partial W}{\partial w}$, the second one corresponds to infinite $\frac{\partial W}{\partial w}$ and in the last case $\frac{\partial W}{\partial w}$ equals zero.

Case I: All derivatives are finite. Lines of constant F_i can be obtained by integrating equation (6.5) with the 4th order Runge Kutta method.

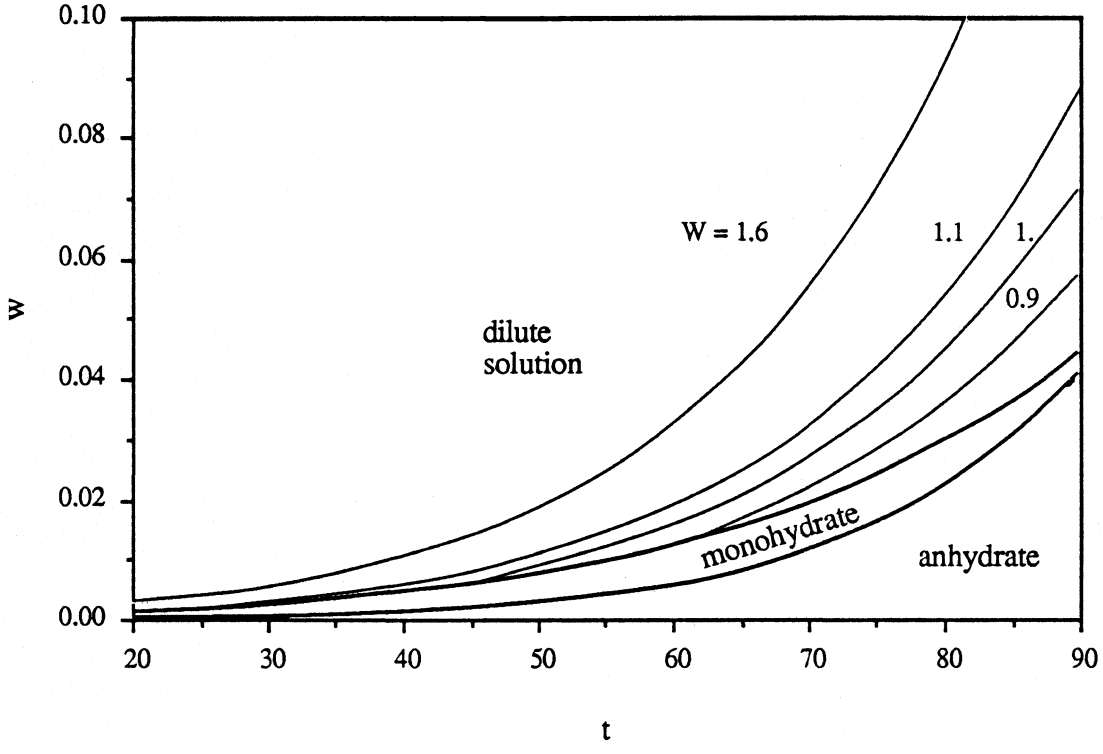

Fig. 6.2: LiCl isosteres w(t) at constant W

Case II: The matrix derivatives are infinite. Therefore $1/\frac{\partial W}{\partial w}$ equals zero and drops out of equation (6.6) which can be written as

$$\left[\frac{\partial w}{\partial t}\right]_{F_i} = \frac{1}{2}\left[\frac{\partial w}{\partial t}\right]_W - \frac{1}{2\,h_s}\frac{\partial i}{\partial t} + (-1)^i \sqrt{\left\{\frac{1}{2}\left[\frac{\partial w}{\partial t}\right]_W - \frac{1}{2\,h_s}\frac{\partial i}{\partial t}\right\}^2 - \frac{1}{h_s}\frac{\partial i}{\partial t}\left[\frac{\partial w}{\partial t}\right]_W} \qquad (6.8)$$

$$= \frac{1}{2}\left[\frac{\partial w}{\partial t}\right]_W - \frac{1}{2\,h_s}\frac{\partial i}{\partial t} + (-1)^i\left[\frac{1}{2}\left[\frac{\partial w}{\partial t}\right]_W + \frac{1}{2\,h_s}\frac{\partial i}{\partial t}\right]$$

Hence

$$\left[\frac{\partial w}{\partial t}\right]_{F_1} = -\frac{1}{h_s}\frac{\partial i}{\partial t} < 0 \qquad \text{for i=1} \qquad (6.9\ a)$$

$$\left[\frac{\partial w}{\partial t}\right]_{F_2} = \left[\frac{\partial w}{\partial t}\right]_{W} \qquad \text{for i=2} \qquad (6.9\ b)$$

The right hand side for i=1 is finite and negative for w,t values on the discontinuity lines . However, with an arbitrary small step, these lines can be crossed and case II is no longer valid, i. e. $\frac{\partial W}{\partial w}$ is no longer infinite. Hence there is no impact of the discontinuities on the shape of the lines of constant F_1-potential.

For i=2 the discontinuity lines, i. e. the solubility limit and the isostere for a system of anhydrous LiCl and monohydrate, are also lines of constant F_2.

Case III: For the horizontal planes in Figure 6.1, the derivative $\frac{\partial W}{\partial w}$ equals zero and the terms containing the inverse of this derivative become infinite. Therefore the other terms in the equation can be neglected and equation (6.6) can be written as

$$\left[\frac{\partial w}{\partial t}\right]_{F_i} = \frac{c_m}{2\,h_s\frac{\partial W}{\partial w}} + (-1)^i \sqrt{\left\{\frac{c_m}{2\,h_s\frac{\partial W}{\partial w}}\right\}^2}$$

Hence

$$\left[\frac{\partial w}{\partial t}\right]_{F_i} = 0 \qquad \text{for i=1} \qquad (6.10\ a)$$

$$\left[\frac{\partial w}{\partial t}\right]_{F_i} \rightarrow \infty \qquad \text{for i=2} \qquad (6.10\ b)$$

This results in horizontal lines for F_1 and in vertical lines for F_2.

Figure 6.3 shows the F-charts of LiCl for the entire temperature and humidity range of non-saturated air. The astonishing result is that the discontinuities cannot be seen in these charts. However, the fact that the lines of constant F-potential do not exhibit any discontinuity does not mean that the F-values do not change dramatically. The step change of the W(w,t) function in the 3d plot in Figure 6.1 cannot be seen in the lines of constant W,i. e. in the the isosteres in Figure 6.2, either. Thus the w,t - discontinuity lines for W may also be discontinuity lines for F_2.

The physical significance of these F-charts can be evaluated by plotting trajectories of the air outlet conditions of single blow simulations. In Chapter 5.1, three simulations for different initial matrix states are described. These initial states are either a dilute solution of LiCl, a saturated solution, or solid LiCl consisting of anhydrate and monohydrate. These initial states correspond to points in the F-chart that are in the region of dilute solution, on the solubility line or on the discontinuity line that separates the regions for anhydrate and monohydrate.

The outlet air in the very beginning will be in equilibirium with this initial point. Hence, the trajectory starts out at this point. At the end of the process when the matrix is completely exhausted the outlet air will be the same as the inlet air. Therefore, the

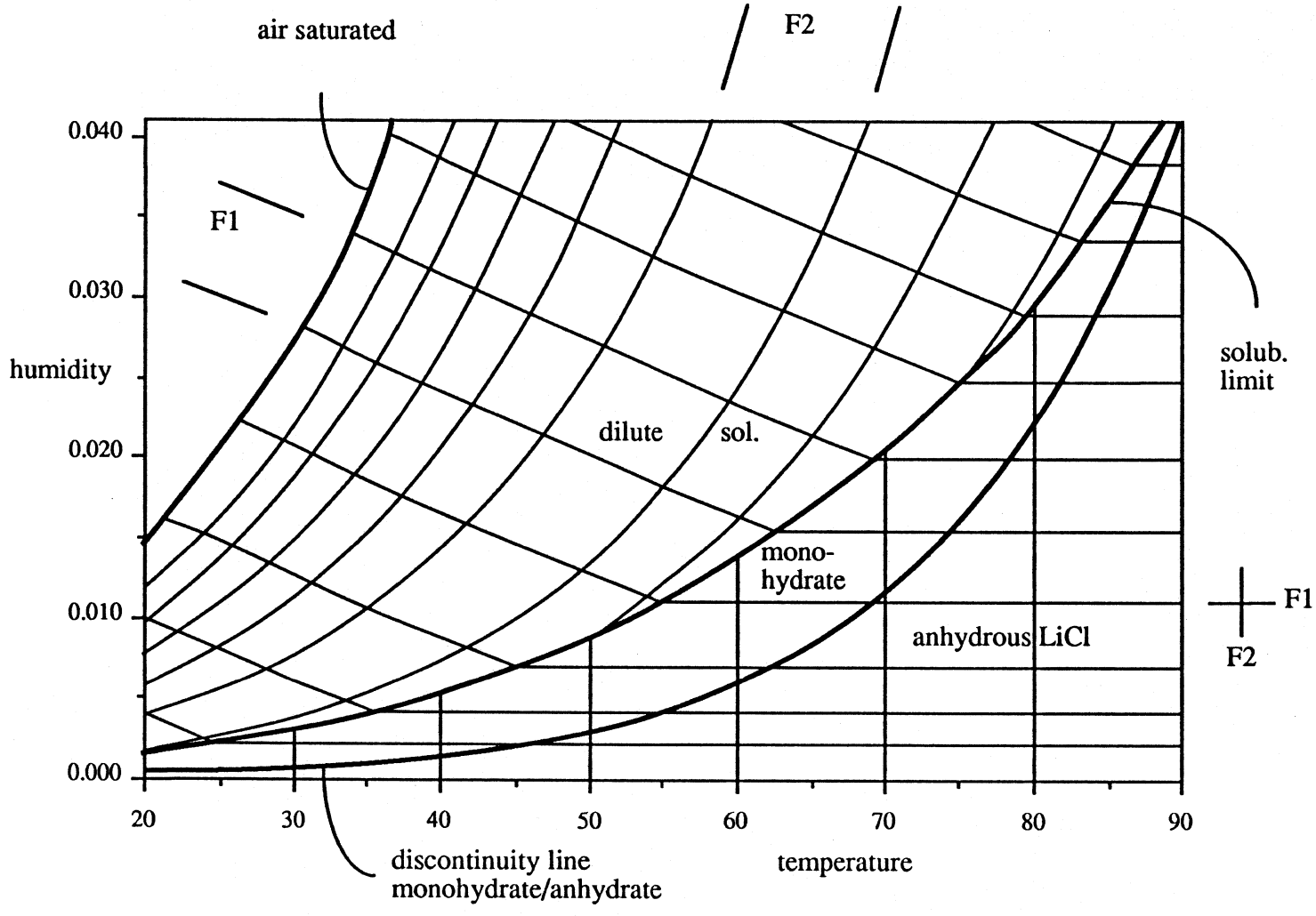

Fig. 6.3 F-charts for LiCl over the entire range of temperatures and humidities of non-saturated air

trajectories all end at the point of the inlet air state.

Figure 6.4 shows the trajectories of these simulations superimposed on the LiCl F-chart. For the first case where the matrix initially contains a dilute solution, the air outlet states move very fast down along the F_2-line. This corresponds to the initial fast wave that propagates to the matrix. Then the slow wave will shift the outlet states up the F_1-line until they reach the inlet state when the matrix is exhausted. Hence, the intersection point clearly represents the optimum dehumidification that can be obtained under these initial matrix and air inlet conditions.

The same holds for the matrix initially containing a saturated solution of LiCl except that the outlet states will stagnate at the intersection point until the wave front that corresponds to the change to dilute solution approaches the end of the dehumidifier and effects the outlet states. However, the point of inflexion in the air outlet state versus time graph (Fig. 5.10) that represents the break through of this wave front does not show on the trajectory. Finally the slow wave will move the outlet state up the F_1-line.

In the most complicated case, the matrix will change from solid LiCl to the saturated solution and then to the dilute solution. In this case the air outlet states will also stay constant after the fast wave passed through, but only for a very short time. Then the medium speed wave front that corresponds to the change to saturated solution will effect the outlet states and first lower the humidity before increasing it as shown in Chapter 5.1. Hence the air with the lowest humidity comes out of the dehumidifier while this wave front is still propagating through the matrix and not when it breaks through. This point of the trajectory is highly transitory compared to the air conditions after this wave front breaks through. Now the air outlet conditions will stay constant for a long time. They are close to

the solubility line. Finally, with the next wave front, the air outlet states move up along the F_1-line.

The problem in applying the analogy method for this last case is that the point with the lowest humidity cannot be identified from the F-chart alone. It lies on the F_2-line through the initial matrix state, but it cannot be shown that it has the same F_1 value. From this analysis it cannot be determined that this is the intersection point.

If the matrix at the beginning of the process period contains pure monohydrate or saturated solution, the regenerating air will be in the region of monohydrate. Then the intersection point is the intersection of the solubility line and the F_1 line through the process air inlet state.

For both inlet states being in the region of dilute solution, the analogy method can be applied as for continuous sorbents. If the F_2-line of the regenerating air inlet state hits the solubility limit before intersecting with the F_1-line of the process air inlet state, then the solubility line will continue the F_2-line and the intersection point of the solubility line and the F_1-line may also be used.

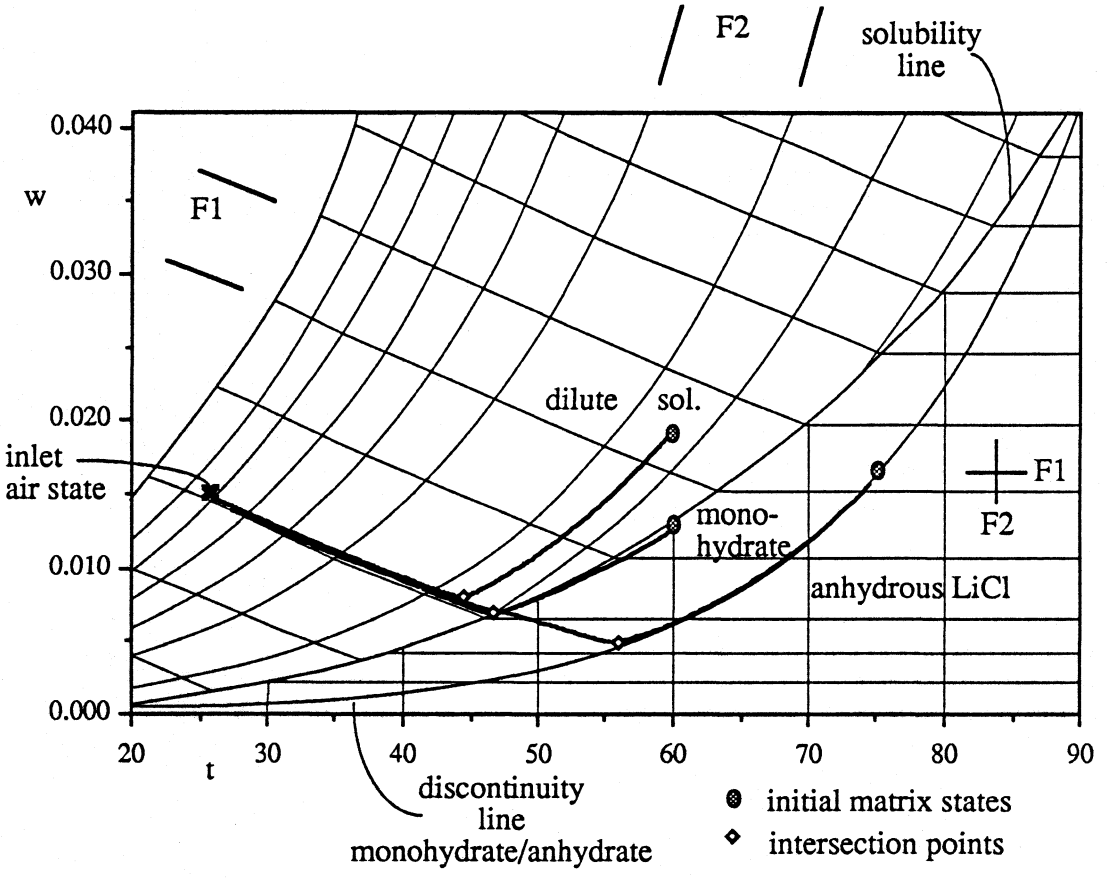

Fig. 6.4: Trajectories of air outlet states, superimposed on the LiCl F-chart

Chapter 7

Conclusions and Recommendations

The goal of this thesis was to develop a model that simulates RHMX that use LiCl as the desiccant. Two topics were involved in this: The thermodynamics of sorption processes on LiCl and the numerical analysis to accommodate discontinuities.

The thermodynamic behavior of the LiCl-water-air system was described by a set of equations and curve fits for the sorption equilibrium, the heat of sorption and the specific heat. The LiCl may be in solid state, i. e. a mixture of anhydrate and monohydrate, in saturated solution or in dilute solution. At water contents where LiCl changes its state of matter the equilibrium vapor pressure jumps discontinuously with respect to water content. At phase change temperatures such as 93.5 °C where monohydrate becomes instable, the enthalpy content of the matrix is discontinuous with temperature. It was assumed that a supporter does not influence the sorption equilibria.

To make use of the outstanding ability of LiCl to process very dry air, the regeneration period must reactivate the matrix such that anhydrous LiCl is obtained. Then, the reactivation temperature must be high enough such that the temperature dependent equilibrium humidity of solid LiCl is higher than the regenerating air humidity. That makes especially temperatures above 93.5 °C interesting since anhydrous LiCl can be obtained directly from the saturated solution. Therefore, such high regenerating temperatures allow higher

regenerating air humidities as they are usually inevitable.

The modified finite difference method is based on the model by Macclaine-cross [1]. In the case of continuous matrix properties the same finite difference equations are used. If the matrix is at the discontinuity a new model was derived. It was shown that for certain conditions where the matrix is at the discontinuity and the fluid humidity is in the humidity interval of the discontinuity, no sorption or desorption process is possible anymore. For this case second order accurate finite difference equations for heat exchange only were derived. The entire method is able to simulate dynamic single blow heat and mass exchange as well as RHMX in steady state. However, to converge to the steady state it requires many iterations and hence much computation. Water content and temperature of fluid and matrix can be determined at any time or axial position. The outlet states of the air streams can be predicted. The accuracy of the method still has to be determined by experiment.

Since enthalpies are replaced by temperatures, the finite difference model is not able to take the latent heat into account that is due to temperature dependent phase changes. Such a phase change occurs at 93.5 °C where the specific heat has to be considered infinite. A finite difference model that is analogous to the model in this thesis and that uses the enthalpies instead of replacing them by temperatures could be developed. It would require more computation since the temperature of the driving force of the heat exchange must be evaluated as function of the enthalpies, but it would avoid a specific heat term in the model. However, the same staggered mesh could be employed and the same methods to solve the implicit equations could be used.

The physical behavior of the RHMX may be described by an initial fast wave and slower subsequent wave fronts that represent the phase changes and propagate through the

matrix. These wave fronts have only a small effect on the water content profiles, but due to the large changes of the latent heat, they have a large effect on the temperature profiles. For the change from solid LiCl to saturated solution the water content profiles will exhibit a knee since the driving force for the mass transfer jumps discontinuously.

The fast wave shifts the temperature profiles up or down at the beginning of each period. Then the wave fronts move the temperature profiles back and forth during the two periods, while the water content profiles are shifted up and down. How far these wave fronts will move depends on the parameter Γ_j. For optimum dehumidification, the wave front where the matrix changes to saturated solution will come close to breaking through. The corresponding value for Γ_j was found to be approximately 0.02.

Psychrometric charts with lines of constant F-potential for LiCl in solid state, in saturated solution and in dilute solution were presented. It was shown that the discontinuity lines for the equilibrium water content are also F_2 lines. Trajectories of the outlet states of single blow simulations were used to identify possible intersection points. However, for the case where the matrix initially contains solid LiCl and will change across the discontinuity to saturated solution, the empirical point of lowest humidity of the trajectory cannot be found by intersecting the F-potential lines. Hence, the analogy method can only be applied for sorption processes on the saturated and dilute solution.

Appendix A

1. Derivation of the finite difference equations from system (4.7) for the continuous case:

System (4.7) is

$$\tilde{M}^{-1}\tilde{b} = \left[\begin{array}{cccc|c} \frac{1}{\Delta\xi}+\frac{Le}{2} & 0 & -\frac{Le}{2} & 0 & Le\left[t_{m\,i,k}-t_{f\,i,k}\right] \\ 0 & \frac{1}{\Delta\xi} & 0 & \frac{1}{\Delta\zeta} & 0 \\ 0 & \frac{1}{\Delta\xi}+\frac{1}{2} & -\frac{1}{2}\left[\frac{\partial w_m}{\partial t_m}\right]_w & -\frac{1}{2}\left[\frac{\partial w_m}{\partial W}\right]_{t_m} & w_{m\,i,k}-w_{f\,i,k} \\ \frac{c_f}{\Delta\xi} & \frac{h_{wv}}{\Delta\xi} & \frac{\partial I}{\partial t_m}\frac{1}{\Delta\zeta} & \frac{\partial I}{\partial W}\frac{1}{\Delta\zeta} & 0 \end{array}\right]$$

$$= \left[\begin{array}{cccc|c} 1 & 0 & A_{13} & 0 & A_{15} \\ 0 & 1 & 0 & A_{24} & 0 \\ 0 & A_{32} & A_{33} & A_{34} & A_{35} \\ A_{41} & A_{42} & A_{43} & A_{44} & 0 \end{array}\right]$$

where the coefficients are

$$A_{13} = \frac{-Le}{Le + 2/\Delta\xi} \qquad A_{15} = -2\,A_{13}\,(t_{m\,i,k}-t_{f\,i,k})$$

$$A_{24} = \Delta\xi/\Delta\zeta \qquad A_{32} = 1+2/\Delta\xi$$

$$A_{33} = -\left[\frac{\partial w_m}{\partial t_m}\right]_W \qquad A_{34} = -\left[\frac{\partial w_m}{\partial W}\right]_{t_m}$$

$$A_{35} = 2\,(w_{m\,\tilde{i},k} - w_{f\,\tilde{i},k}) \qquad A_{41} = c_f$$

$$A_{42} = h_{wv} \qquad A_{43} = A_{24}\frac{\partial I}{\partial t_m}$$

$$A_{44} = A_{24}\frac{\partial I}{\partial W}$$

Gauss elimination yields a triangular system:

$$\tilde{\tilde{M}}^{-1}\tilde{b} = \left[\begin{array}{cccc|c} 1 & 0 & B_{13} & 0 & B_{15} \\ 0 & 1 & 0 & B_{24} & 0 \\ 0 & 0 & 1 & B_{34} & B_{35} \\ 0 & 0 & 0 & B_{44} & B_{45} \end{array}\right]$$

where

$$B_{13} = A_{13} \qquad B_{15} = A_{15}$$

$$B_{24} = A_{24} \qquad B_{34} = A_{34} - A_{24}A_{32}/A_{33}$$

$$B_{35} = A_{35}/A_{33}$$

$$B_{44} = \frac{(A_{43}-A_{13}A_{41})(A_{34}-A_{24}A_{32})}{A_{33}} + A_{44} - A_{42}A_{24}$$

$$B_{45} = -A_{15}A_{41} - \frac{A_{35}}{A_{33}}(A_{43}-A_{13}A_{41})$$

This can be solved by back substitution:

$$\tilde{M}^{-1}\tilde{b} = \begin{bmatrix} B_{15} - B_{13}(B_{35} - B_{34}B_{45}/B_{44}) \\ - B_{24}B_{45}/B_{44} \\ B_{35} - B_{34}B_{45}/B_{44} \\ B_{45}/B_{44} \end{bmatrix}$$

2. Derivation of the finite difference equations from system (4.9) at the discontinuity:

System (4.9) has two more zeros in the matrix M. Also the element A_{35} needs to be slightly modified:

$$A_{33} = 0 \qquad A_{34} = 0$$

$$A_{35} = 2\,(w_{m\,\tilde{i},k} - w_{f\,\tilde{i},k}) + \Delta w_m = A_{35}(\text{old}) + \Delta w_m$$

Taking advantage of the zeros, it can be solved simply by back substitution:

$$\tilde{M}^{-1}\tilde{b} = \begin{bmatrix} A_{15} - A_{13}C_3 \\ A_{35}/A_{32} \\ C_3 \\ - A_{35}/A_{32}A_{24} \end{bmatrix}$$

where $$C_3 = \frac{- A_{41}A_{15} - A_{42}A_{35}/A_{32} + A_{35}/A_{32}A_{24}}{A_{43} - A_{13}A_{41}}$$

3. Derivation of the finite difference equation for heat exchange only:

Equation (4.10) is equivalent to

$$\begin{bmatrix} t_{f\,i+1,\tilde{k}} \\ t_{m\,\tilde{i},k+1} \end{bmatrix} = \begin{bmatrix} t_{f\,i,\tilde{k}} \\ t_{m\,\tilde{i},k} \end{bmatrix} + \begin{bmatrix} \frac{1}{\Delta\xi} + \frac{Le}{2} & -\frac{Le}{2} \\ \frac{c_f}{\Delta\xi} & \frac{\partial I}{\partial t_m}\frac{1}{\Delta\zeta} \end{bmatrix}^{-1} \begin{bmatrix} Le\,(t_{m\,\tilde{i},k} - t_{f\,i,\tilde{k}}) \\ 0 \end{bmatrix}$$

or

$$\begin{bmatrix} t_{f\,i+1,\tilde{k}} \\ t_{m\,\tilde{i},k+1} \end{bmatrix} = \begin{bmatrix} t_{f\,i,\tilde{k}} \\ t_{m\,\tilde{i},k} \end{bmatrix} + \begin{bmatrix} 1 & A_{13} \\ A_{41} & A_{43} \end{bmatrix}^{-1} \begin{bmatrix} A_{51} \\ 0 \end{bmatrix}$$

where the coefficients are the same as above

Gauss elimination and back substitution yields

$$\begin{bmatrix} t_{f\,i+1,\tilde{k}} \\ t_{m\,\tilde{i},k+1} \end{bmatrix} = \begin{bmatrix} t_{f\,i,\tilde{k}} \\ t_{m\,\tilde{i},k} \end{bmatrix} + \begin{bmatrix} A_{15} - A_{13}\,C_3 \\ C_3 \end{bmatrix}$$

where

$$C_3 = -\frac{A_{41}\,A_{15}}{A_{43} - A_{41}\,A_{13}}$$

References

[1] I.L. Maclaine-cross, "A Theory of Combined Heat and Mass Transfer in Regenerators", Ph.D. thesis, Monash University, Clayton, Victoria, Australia (1979)

[2] ASHRAE, *Handbook of Fundamentals*, American Society of Heating, Refrigeration and Air Conditioning Engineers, New York, (1985)

[3] E. Van den Bulck, "Convective Heat and Mass Transfer in Compact Regenerative Dehumidifiers", Ph.D. thesis, University of Wisconsin, Madison (1987)

[4] R. B. Holmberg, "Combined Heat and Mass Transfer in Regenerators with Hygroscopic Materials", *Journal of Heat Transfer, ASME transactions*, Vol. 101, (1979)

[5] M. J. Brandemuehl, "Analysis of Heat and Mass Regenerators with Time Varying or Spatially Non-Uniform Inlet Conditions", Ph.D. thesis, University of Wisconsin, Madison (1982)

[6] J. G. Van Leersum, "Heat and Mass Transfer in Regenerators", Ph.D. thesis, Monash University, Clayton, Victoria, Australia (1975)

[7] F. E. Pla-Barby, "Performance of Rotary Bed Silica Gel Solid Desiccant Dryers", ASME paper 78-HT-36, AIAA-ASME Thermophysical and Heat Transfer Conference (1987)

[8] B. Mathriprakasam, Lavan, "Performance Predictors for Adiabatic Desiccant Dehumidifiers Using Linear Solutions", *ASME J. Solar Energy Eng.* 102, p.73, (1987)

[9] I. L. Maclaine-cross, P. J. Banks, "Coupled Heat and Mass Transfer in Regenerators - Prediction Using an Analogy with Heat Transfer", *Int. J. Heat Mass Transfer* Vol 15, p. 1225, (1971)

[10] J. J. Jurinak, "Open Cycle Desiccant Cooling - Component Models and System Simulation", Ph.D. thesis, University of Wisconsin, Madison (1982)

[11] E. Van den Bulck, "Analysis of Solid Desiccant Rotary Dehumidifier", M.S. thesis, University of Wisconsin, Madison (1987)

[12] C. Chi, "Dynamics of fixed bed adsorbers", Ph.D. thesis, I.I.T., Chicago (1968)

[13] M.P. Appleby, Crawford, Gordon, "Vapour Pressure of Saturated Solutions. Lithium Chloride and Lithium Sulphate", *J. Chem. Soc.* 11, p.1665, (1934)

[14] Ch. Slonim, G.F. Hüttig, "Die Spezifischen Wärmen, Bildungswärmen der Lithiumhalogenidhydrate", *Z. Physik. Chem.* 141, p.55 (1929)

[15] M. Thakker, M.S. thesis, I.I.T., Chicago 1976

[16] N.A. Gokcen, "Vapor Pressure of Water above Saturated Lithium Chloride Solution", *J. Amer. Chem. Soc.* 73, p.3789, (1951)

[17] E.U. Schlünder, "Einfaches Verfahren zur Messung von Dampfdrucken über wäßrigen Salzlösungen", *Chemie-Ing.-Techn.* 35, p.482, (1963)

[18] E.F. Johnson, Molstad, "Thermodynamic Properties of Lithium Chloride Solutions", *J. Phys. Chem.* 55, Ithaca , p. 257 (1951)

[19] E. Lange, F. Dürr, "Lösungs- und Verdünnungswärmen von Salzen", *Z. Phys. Chem.* 121, p. 379, 1926